The Effect of Manipulation of the Phosphoinositide 3-kinase Pathway on Axon Regeneration *in vivo*

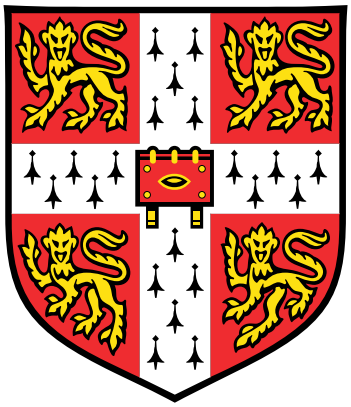

Rachel Shane Evans

Supervised by: Professor Keith R. Martin

John van Geest Centre for Brain Repair
Department of Clinical Neurosciences
University of Cambridge

This dissertation is submitted for the degree of
Doctor of Philosophy

Emmanuel College

September 2019

Declaration

This thesis is submitted for the degree of Doctor of Philosophy in Clinical Neurosciences at the University of Cambridge.

This thesis is the result of my own work and includes nothing which is the outcome of work done in collaboration except as declared at the beginning of each chapter, under the heading “Declaration,” and specified in the text.

It is not substantially the same as any that I have submitted, or, is being concurrently submitted for a degree or diploma or other qualification at the University of Cambridge or any other University or similar institution except as declared at the beginning of each chapter, under the heading "Declaration," and specified in the text. I further state that no substantial part of my dissertation has already been submitted, or, is being concurrently submitted for any such degree, diploma or other qualification at the University of Cambridge or any other University or similar institution except as declared at the beginning of each chapter, under the heading "Declaration," and specified in the text.

This thesis does not exceed the word limit specified by the Clinical Medicine and Clinical Veterinary Medicine Degree Committee.

Rachel Shane Evans
September 2019

Abstract

The Effect of Manipulation of the Phosphoinositide 3-kinase Pathway on Axon Regeneration *in vivo*

Rachel Shane Evans

Millions worldwide are visually impaired by optic nerve diseases, and glaucoma, the leading cause of irreversible blindness, is due to affect approximately 80 million people by 2020. The optic nerve is comprised of retinal ganglion cell (RGC) axons, and like all mammalian central nervous system axons, they fail to regenerate due to a combination of extrinsic and intrinsic factors. Current treatments have limited success preventing disease progression, and this failed regeneration presents a major barrier to restoring vision.

Previous research has demonstrated that manipulation of the phosphoinositide 3-kinase (PI3K) pathway by transgenic knockout of phosphatase and tensin homolog (PTEN) promotes survival and regeneration of murine RGC axons in an optic nerve crush (ONC) model. However, translation issues are yet to be addressed. PI3K converts phosphatidylinositol (3,4)-bis-phosphate (PIP2) lipids to phosphatidylinositol (3,4,5)-tris-phosphate (PIP3). PTEN acts as a pathway regulator, converting PIP3 back into PIP2. PIP3 is a second messenger molecule for several pathways, including the mammalian target of rapamycin (mTOR) pathway, which has been demonstrated to promote axon regeneration in RGCs, the spinal cord, and cortical neurons. The PI3K pathway is activated by growth factors, integrins and cytokine receptors. Integrins have also been shown to promote axon regeneration via the focal adhesion kinase pathway.

This thesis aimed to determine the effects on axon regeneration of manipulating the PI3K pathway in various ways. A transgenic approach was adopted to conditionally express the hyperactive p110α and p110δ PI3K isoforms using viral Cre recombination. Both survival and axon regeneration were significantly increased 4 weeks post-ONC injury in young and aged mice. No significant difference between the two isoforms was observed, except that p110α promoted RGC survival in aged mice whereas p110δ had no significant effect. This was developed further using viral vectors to upregulate PI3K and to knockdown PTEN for a more translational approach: AAV2.shPTEN.GFP and AAV2.PI3K(p110δ). PTEN

knockdown promoted both RGC survival and axon regeneration, while PI3K upregulation promoted axon regeneration. No significant difference in axon regeneration was seen between the two strategies. Where regeneration was seen, activation of the mTOR pathway was demonstrated.

It is becoming increasingly clear that strategies need to be combined to achieve long-distance, robust regeneration. In this thesis, PI3K upregulation was combined with PTEN knockdown and then with integrin activation using AAV2.Integrin.V5 and AAV2.Kindlin.GFP viruses. While PI3K upregulation and PTEN knockdown promoted RGC survival and axon regeneration compared to control, this was not significantly more than PI3K upregulation alone. The experiments involving integrin activation were unsuccessful and the viruses need to be investigated further.

While the field has achieved small numbers of regenerating axons up to the optic chiasm, key challenges for future work are reaching central targets in the brain and assessing axon regeneration in an aged model to better reflect the clinical setting, where neurodegenerative diseases predominately affect the aging population.

In summary, the work in this thesis investigated the pro-regenerative effects of potential gene therapy targets, advancing our knowledge for developing future clinical strategies.

Acknowledgements

I would like to thank Professor Keith R. Martin for providing me with this opportunity to work in his lab and for his guidance and supervision during the Ph.D. I would also like to thank Professor James Fawcett for being my second supervisor and especially for advising me during my thesis write up.

I'm grateful to Dr Amanda Barber for her supervision and mentorship during this Ph.D. I'd also like to thank Dr Andrew Osborne for his supervision, particularly when Amanda was away. I'd like to thank Dr Richard Eva for his advice and supervision for the PI3K work.

I would like to thank Dr Andrew Osborne, Dr Amanda Barber, Sam Hilton, Dr Tasneem Khatib, Raquel Conceição, and Dr Katie Hall for my *in vivo* training, and the staff at Phenomics for their contribution to making this *in vivo* work possible.

I would like to thank all members of the Martin-Fawcett group for their training and assistance in the lab, in particular Dr Andrew Osborne, Raquel Conceição, Dr Amanda Barber, Sarita Deshpande, Jennifer Jia, Dr Tasneem Khatib, Dr Katie Hall, Dr Craig Pearson, Dr Bart Nieuwenhuis, and Rob Watt. Specific contributions to the work in this thesis are acknowledged in the declaration section at the beginning of each chapter.

I acknowledge Cara Brodie for her support scanning samples at the fluorescent scanning service of the Cancer Research UK Cambridge (CRUK) Cambridge Institute.

I'm grateful for the funding I received to complete this Ph.D. My MRC and Sackler scholarship was funded by the UK Medical Research Council and the Sackler fund. The work itself has been funded by several grants written by Dr Amanda Barber and Prof Keith Martin: Wellcome Trust, Fight for Sight (The Eye Research Charity), Cambridge Eye Trust, International Glaucoma Association, and the National Eye Research Centre. During my Ph.D., I also received travel grants for conferences from the European Association for Vision and Eye Research (EVER), from Emmanuel College (Cambridge), and from the Guarantors of Brain.

I'd like to thank my family for always believing in me and supporting me.

Table of contents

List of figures

List of tables

List of Peer Reviewed Publications

Publications from work during this Ph.D.:

1. **Chapters 3 and 4:** *Barber, A.C., ***Evans, R.S.**, *Nieuwenhuis, B., Pearson, C.S., Fuchs, J., MacQueen, A.R., van Erp, S., Hänzi, B., Hulshof, L-A., Osborne, A., Conceição, R., Deshpande, S.S., Cave, J., ffrench-Constant, C., Smith, P.D., Okkenhaug, K., Eickholt, B.J., Martin, K.R., Fawcett, J.W., and Eva, R. (2020) PI3 kinase delta enhances axonal PIP3 to support axon regeneration in the adult CNS. (Manuscript submitted to *EMBO Molecular Medicine*, currently responding to reviewers comments). * = the authors contributed equally.

2. **Chapter 5: Evans, R.S.**, Deshpande, S.S., Conceição, R., Hänzi, B., Hulshof, L-A., Osborne, A., Fawcett, J.W., Martin, K.R., Eva, R., Barber, A.C. (2020) Translatable methods to stimulate mTOR mediated axon regeneration. (Manuscript in preparation).

3. Conceição, R., **Evans, R.S.**, Pearson, C.S., Hänzi, B., Osborne, A., Deshpande, S.S., Martin, K.R., and Barber, A.C. (2019) Expression of developmentally important axon guidance cues in the adult optic chiasm. *Invest Ophthalmol Vis Sci*, 60(14): 4727 - 4739. doi: https://doi.org/10.1167/iovs.19-26732

4. Khatib, T.Z., Osborne, A., Whitehead, M., Ali, Z., Ching, J., **Evans, R.S.**, Conceição, R., Martin, K.R. (2020) Optic nerve regeneration following glaucomatous injury in aged mice. (Manuscript in preparation).

5. Jia, J., **Evans, R.S.**, Khatib, T.Z., Martin, K.R., Káradóttir, R.T. (2020) Understanding myelination in the optic nerve. (Work still in progress).

Publications from work prior to this Ph.D.:

1. Wu, J., Bell, O.H., Copland, D.A., Young, A., Pooley, J., Maswood, R., **Evans, R.S.**, Khaw, P.T., Ali, R.R., Dick, A.D. and Chu, C.J.. (2020) Gene therapy for Glaucoma by

Ciliary Body Aquaporin 1 disruption using CRISPR-Cas9. *Molecular Therapy*, 28(3). doi: https://doi.org/10.1016/j.ymthe.2019.12.012

Nomenclature

Acronyms / Abbreviations

AAV Adeno-associated virus

Ab Antibody

BDNF Brain-derived neurotrophic factor

BLBP Brain lipid-binding protein

BSA Bovine serum albumin

cAMP Cyclic adenosine monophosphate

Catno. Catalogue number

CMV Cytomegalovirus

CNS Central nervous system

CNTF Ciliary neurotrophic factor

CRUK Cancer Research UK

CSPG Chondroitin sulfate proteoglycan

CTB Cholera toxin subunit-β

CTB – 555 Cholera toxin subunit-β with an Alexa Fluor 555 conjugate

DAPI 4,6-diamidino-2-phenylindole

DMEM Dulbecco's modified eagle medium

DRG Dorsal root ganglion

$EDTA$ Ethylenediaminetetraacetic acid

Ex Exon

FAK Focal adhesion kinase

$FGF2$ Fibroblast growth factor-2

flx Floxed

GC/mL Genome copies per mL

GFP Green fluorescent protein

HCl Hydrochloric acid

HEK Human embryonic kidney

Het Heterozygous

$Homo$ Homozygous

IGF Insulin-like growth factor

$IGF-R$ Insulin-like growth factor receptor

IHC Immunohistochemistry

ILK Integrin-linked kinase

$ITCN$ Image-Based Tool for Counting Nuclei

$JAK/STAT$ Janus kinase/signal transducers and activators transcription

MAG Myelin-associated glycoprotein

$mTOR$ Mammalian target of rapamycin

$NaOH$ Sodium hydroxide

NDS Normal donkey serum

NGS Normal goat serum

$OMgp$ Oligodendrocyte myelin glycoprotein

ONC Optic nerve crush

ooDSGCs ON-OFF direction-selective RGCs

*p*110α p110α isoform of PI3K

$p110\alpha^{H1047R}$ hyperactive p110α isoform of PI3K

*p*110δ p110δ isoform of PI3K

pAKT Phospho-AKT

*Pax*2 Pair box-containing gene

PBS Phosphate-buffered saline

PBST PBS-Tween20

PCR Polymerase chain reaction

PFA Paraformaldehyde

PI3K Phosphoinositide 3-kinase

PI3KCA Gene for PI3K(p110α)

PI3KCD Gene for PI3K(p110δ)

*PIP*2 Phosphatidylinositol(3,4)-bis-phosphate

*PIP*3 Phosphatidylinositol (3,4,5)-tris-phosphate

PNS Peripheral nervous system

PolyA Polyadenylation sequence

*pS*6 Phospho-S6 ribosomal protein

PTEN Phosphatase tensin homolog

PVDF Polyvinylidene difluoride

*RC*2 Radial glial cell marker 2

RGC Retinal ganglion cell

RGCL Retinal ganglion cell layer

RPM Revolutions per minute

RTK Receptor tyrosine kinase

RWM Retinal wholemount

*S*6*K*1 S6 kinase 1

SA Splice acceptor

SDS − *PAGE* Sodium dodecyl sulfate polyacrylamide gel electrophoresis

SEM Standard error of the mean

shRNA Short hairpin RNA

*Slit*1 Slit guidance ligand 1

*SOCS*3 Suppressor of cytokine signalling 3

TBE Tris/Borate/EDTA

TBS Tris-buffered saline

TBST Tris-buffered saline-Tween20

TrkB Tropomyosin receptor kinase B

*TSC*1 Tuberous sclerosis complex

*Tuj*1 βIII Tubulin

Chapter 1

Introduction

1.1 The Visual System: Anatomy and Pathology

1.1.1 The Retina

Within the visual system, the eyes detect light and convert it into electro-chemical impulses for processing in the brain. Light enters the eye through the cornea and is focused onto the retina, which is made up of six layers of five neuronal cell types: photoreceptors, horizontal cells, bipolar cells, amacrine cells, and ganglion cells, as illustrated in **Fig. 1.1A**[82]. The light passes through the retina to its most distal point, where it is absorbed by photopigment in the photoreceptors, known as rods and cones, altering their membrane potential. This signal is then transmitted to bipolar cells and on to ganglion cells. These three neuronal cell types are organised into distinct layers to facilitate the vertical flow of information, with the cell bodies of photoreceptors, bipolar cells, and ganglion cells found in the outer nuclear layer, the inner nuclear layer, and the ganglion cell layer respectively. The processes and synaptic contacts of the photoreceptors and bipolar cells are found in the outer plexiform layer, while those of the bipolar and ganglion cells are found in the inner plexiform layer.

In addition to the vertical flow of information, horizontal and amacrine cells mediate lateral interactions[82]. Their cell bodies are located in the inner nuclear layer with the bipolar cells. The processes of horizontal cells are found in the outer plexiform layer, while the processes of amacrine cells are found in the inner plexiform layer. At the most proximal point of the retina, the nerve fibre layer is made up of the ganglion cell axons, more commonly referred to as retinal ganglion cell (RGC) axons.

Several subtypes of each of these neuronal cell types exist, which accounts for the diversity and complexity of information conveyed to central targets in the brain. About 40

subtypes of RGCs have now been identified, with differences in morphology, localisation, function, susceptibility to degeneration, and regenerative capacity[86].

In addition to neuronal cells, the retina also contains three glial cell types: Müller cells, astrocytes, and microglia. These glial cells maintain neuronal health and homeostasis, including providing structural support and playing a role in metabolism, phagocytosis of debris, and release of certain transmitters[99]. Müller cells account for 90% of retinal glia. Their cell bodies reside in the inner nuclear layer and their processes project in either direction, ensheathing the cell bodies and processes of the retinal neurons. Müller cells have a range of functions related to development, survival, and information processing [85, 11]. Astrocytes are mainly found in the nerve fibre layer of the retina, ensheathing the axons, where they have several functions including providing neurotrophic support and enhanced mechanical support in degenerating axons[99]. Both Müller cells and astrocytes also surround blood vessels and are involved in the maintenance of the blood-retina barrier [84, 43]. Microglia are found throughout the retina and play a key role in the immune response[106], as well as tissue homeostasis[36].

1.1.2 The Central Targets of Retinal Ganglion Cells

RGC axons exit the retina and extend towards central targets in the brain, forming a bundle referred to as the optic nerve, as illustrated in **Fig. 1.1B**[82]. The two optic nerves converge at the optic chiasm, which is located behind the hypothalamus. In humans, approximately 60% of axons from each nerve exit the chiasm contralaterally and 40% exit ipsilaterally, forming the two optic tracts, which therefore contain input from both eyes[82]. Axons from the optic tracts have a few targets in the brain involved in circuitry for different functions, including vision, pupillary light reflex, regulation of the day/night cycle, and coordination of head and eye movements. The primary visual pathway is referred to as the retinogeniculostriate pathway. In this pathway, axons of the optic tracts connect to the lateral geniculate nuclei, located in the thalamus, from which they ultimately terminate at the primary visual cortex, where the initial light signal is perceived as sight[82].

1.1.3 Optic Nerve Pathology

According to data from 2015, approximately 1.3 billion people worldwide were visually impaired to varying degrees, due to several conditions, including uncorrected refractive errors, cataracts, diabetic retinopathy, and optic nerve disorders, like glaucoma[10]. Of these, 217 million people had moderate to severe impairment, and 36 million were blind. With an ever-increasing and aging population, these numbers are set to increase. Glaucoma, the

A. The retina

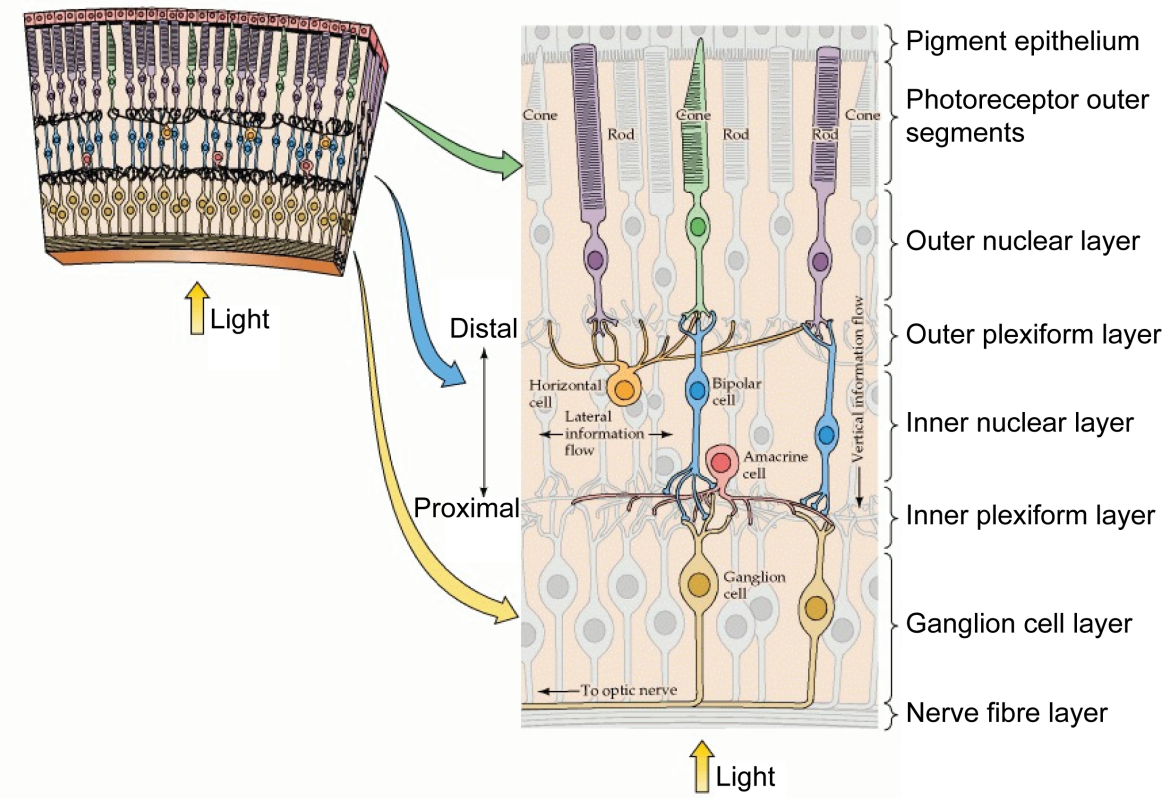

B. The visual pathway

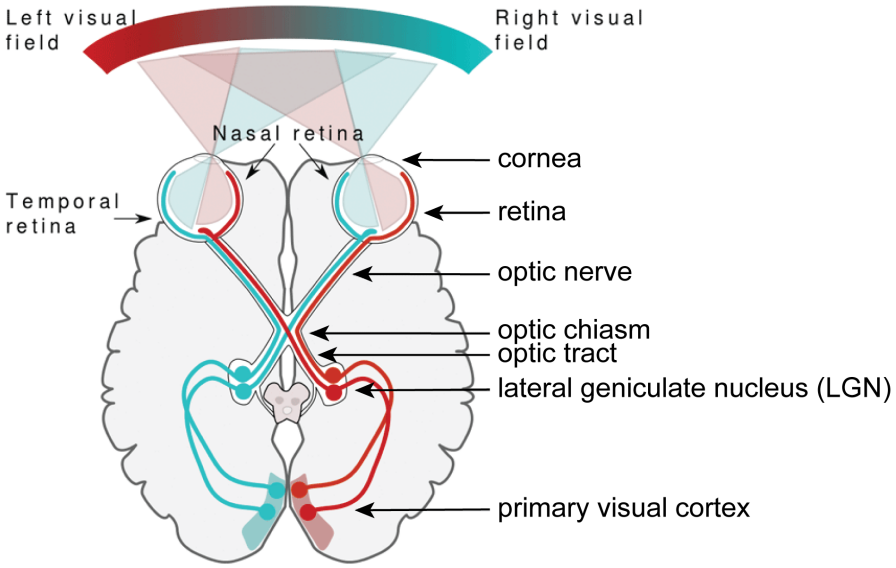

Fig. 1.1 **Anatomy of the Visual System.** In panel A, the neuronal cell types and their arrangement within the retina are illustrated (image from [82]). In panel B, the basic anatomy of the visual pathway is shown (image adapted from [98].)

leading cause of irreversible blindness, is due to affect approximately 80 million people by 2020, increasing from 6.9 million moderate to blind cases in 2015, up to a predicted 7.7 million moderate to blind cases in 2020[30].

Optic nerve disorders result in damage to the RGCs and their axons, which make up the optic nerves, resulting in vision loss. There are many optic nerve disorders, including glaucoma, optic neuritis, and optic nerve atrophy. The most prevalent is glaucoma, which is an umbrella term for a group of optic nerve diseases, often linked to a build-up of intraocular pressure[101]. Optic neuritis is inflammation of the optic nerve and can be caused by infections and autoimmune conditions, like multiple sclerosis[22]. Optic nerve atrophy can be hereditary or caused by environmental factors, like trauma and exposure to toxic substances[74].

In glaucoma, elevated intraocular pressure is often associated with optic nerve damage, although some patients with glaucoma never have eye pressures outside the statistically normal range and the full aetiology of the condition has not been elucidated[101]. Other risk factors include age, race, and family history. Current methods for diagnosis are visually examining the optic nerve for characteristic changes, monitoring intraocular pressure, and performing visual field tests. However, in the initial stages of disease, the majority of patients have no symptoms because the brain compensates for vision loss. It is only when a sufficient number of neurons have been lost, that loss of peripheral vision develops, followed by progressive blindness. This delays diagnosis and therefore, treatment. Regular opticians appointments are recommended to catch the disease early, but this is less feasible in the developing world.

Sustained reduction in pressure has been shown to slow glaucoma progression, preventing RGC death, optic nerve damage, and subsequent vision loss[32, 102, 14]. This forms the basis of current treatments, which are eye drops or surgery[67]. Eye drops can reduce the formation of fluid in the eye or increase its outflow. However, these daily drops require patient cooperation and can have side effects, including stinging, redness, and irritation[71, 91]. Laser surgery can be used to remove fluid blockage and increase the outflow of fluid from the eye. Trabeculectomy is a microsurgery which involves creating a new channel to drain the fluid from the eye. These surgeries carry risks of infection, and temporary, or even permanent, vision loss. They also require highly trained surgeons and medical care, so they are not easily accessible in the developing world[50, 52, 33]. Unfortunately, all these treatments have limited success in preventing disease and in many cases, the disease continues even after pressure returns to normal. At present, there are no treatments to restore vision loss due to the weak regenerative capacity of RGCs, as described in **Chapter 1.1.4**.

Future treatments aim to address these issues using gene therapy to both prevent disease progression and restore vision loss, with the advantage that a single injection can deliver long-term effects. This is particularly viable in the field of ophthalmology because the eye is easily accessible and is an immune-privileged site. Many genes have been associated with an increased risk of glaucoma, providing potential targets. However, focus on broader cell signalling pathways is a more feasible approach for maximising reach to patients. To date, such methods have focused on either reducing intraocular pressure[9, 73] or providing neuroprotection to RGCs[76, 64]. In Wu et al., I was involved in disrupting aquaporin 1, a gene involved in aqueous humour production, using the CRISPR-Cas9 system[104]. This approach resulted in a significant reduction in intraocular pressure in mice, with some promising *ex vivo* human data. In this thesis, I focus on promoting neuroprotective and pro-regenerative effects in RGCs, providing fundamental knowledge that may help guide clinical trials.

1.1.4 Injury to Retinal Ganglion Cells

The retina and optic nerve are an extension of the central nervous system (CNS), along with the brain and spinal cord. During development, CNS axons grow and are guided to form connections with their targets using numerous guidance cues, which can either be permissive or inhibitory. However, once matured, the intrinsic factors promoting growth become less abundant, and inhibitory extrinsic factors are switched on, preventing cellular overgrowth. As a result, axons in the adult mammalian CNS have a weak capacity for regeneration after injury. This creates a challenge for treatments for diseases involving vision impairment, spinal cord injury, and neurodegeneration.

In contrast, peripheral nervous system (PNS) axons maintain regenerative potential throughout adult life. The primary reasons for this are that PNS neurons can mount a regenerative response[83, 87, 92] and they support efficient transport of growth-promoting receptors[3, 44], both of which are downregulated in mature CNS axons. In addition, the glial environment of the mature CNS is different from that in the PNS and the embryonic nervous system, and this has been shown to play a role in inhibiting axon regeneration[108].

By two weeks post-ONC injury, approximately 80% of RGCs die and less than 1% of those that survive extend axons beyond the crush site [79, 62]. As mentioned above, about 40 RGC subtypes have now been identified, with differences in susceptibility to damage and ability to regenerate[86]. Duan et al. identified 11 different subtypes of RGCs using immunohistochemical and transgenic approaches and assessed their response to ONC injury[23].

Alpha RGCs (α-RGCs) are the largest RGCs, with at least three subsets, whilst W3-RGCs are the smallest and most numerous RGCs, with at least two subsets (W3B and W3D).

There are four groups of ON-OFF direction-selective RGCs (ooDSGCs), which are tuned into motion in a single direction: ventral, dorsal, nasal, and temporal. The listed RGCs were assessed, in addition to two subsets of intrinsically photosensitive RGCs (M1-RGCs and M2-RGCs). α-RGCs showed the highest survival rate at 2 weeks post-ONC, followed closely by M1-RGCs [23]. In contrast, M2-RGCs and ooDSGCs showed little, if any, survival. However, the RGC axons degenerated regardless of their retinal soma [17].

Duan et al. used phosphatase and tensin homolog (PTEN) knockdown to promote axon regeneration, a known pro-regenerative approach discussed in **Chapter 1.2**. Among survivors, α-RGCs accounted for nearly all axon regeneration, with little, if any, regeneration from M1-RGCs or the other subtypes [23]. The group then promoted regeneration by administering a combination of osteopontin and insulin-like growth factor 1 (IGF-1), an equally effective pro-regenerative approach discussed in **Chapter 1.2**. Again, α-RGCs accounted for nearly all regeneration seen. The group investigated this mechanistically and found that α-RGCs have high endogenous levels of mammalian target of rapamycin (mTOR) activity, a key pathway involved in the pro-regenerative effect of PTEN knockdown. α-RGCs also selectively express both osteopontin and IGF-1 receptors. This explains why α-RGCs respond favourably to these two pro-regenerative approaches. Future work needs to assess the regenerative ability of RGC subtypes using a variety of pro-regenerative approaches.

1.2 Targeting Extrinsic Factors to Promote Axon Regeneration

One approach for promoting CNS axon regeneration has been the targeting extrinsic factors that inhibit regeneration. These extrinsic factors can either be inhibitory guidance cues involved during development that persist in the mature CNS or components of the glial environment, including myelin-associated inhibitors and proteoglycans associated with astroglial scarring [108].

As the CNS matures, oligodendrocytes ensheath the axons with myelin to prevent aberrant sprouting and protect the neural networks formed. After injury, the myelin structure can become damaged, exposing severed axons to myelin-associated inhibitors, such as Nogo-A, myelin-associated glycoprotein (MAG), and oligodendrocyte myelin glycoprotein (OMgp)[108]. Both Nogo-A and MAG are expressed by CNS oligodendrocytes [38, 46, 89], whilst OMgp is enriched in membranes of oligodendroglia-like cells that encircle nodes of Ranvier [45]. Inhibitory axon guidance cues involved in pathway-finding during development have also been found in CNS myelin, including the transmembrane semaphorin

4D (Sema4D/CD100)[68] and Ephrin B3[7]. All these factors inhibit axon regeneration, although their respective contributions remain unclear.

Glial scar-derived inhibitors also limit axon regeneration. After CNS injury, microglia, oligodendrocyte precursors, meningeal cells, and astrocytes are recruited to the lesion site[108]. Whilst some astrocytes promote regeneration [28], others become reactive and release inhibitory extracellular matrix molecules known as chondroitin sulfate proteoglycans (CSPGs) [65]. During development, astrocytes express CSPGs to limit structural changes in the maturing CNS. When CSPG expression is upregulated by these reactive astrocytes after injury, it forms an inhibitory gradient and therefore prevents axon regeneration. The mechanisms by which CSPGs exert their inhibitory effects are not entirely clear.

Both genetic deletion and pharmacological interventions have been used to block these inhibitory pathways, targeting either myelin-associated inhibitors or glial scar-derived inhibitors [108]. Other studies have targeted the Nogo-66 receptor complex in an attempt to neutralise all three major myelin-associated inhibitors[37, 29, 55], based on findings that removal of the Nogo-66 receptor reduces neuronal responses to all three. Further studies have targeted intracellular pathways common to myelin-associated inhibitors and CSPGs, for example using C3 transferase to inhibit RhoA [20, 53]. Whilst these studies have shown some success promoting regeneration, this has been limited [108]. Therefore, focus has shifted to targeting intrinsic factors, like signalling molecules.

1.3 Targeting Intrinsic Factors to Promote Axon Regeneration: The PI3K Pathway

As mentioned, another approach for promoting CNS axon regeneration has been the targeting of intrinsic factors, with a focus on broader cell signalling pathways to maximise patient reach. One such pathway is the phosphoinositide 3-kinase (PI3K) pathway.

1.3.1 The PI3K Pathway

Phosphoinositide 3-kinases (PI3Ks) are a family of lipid kinases, which can be divided into three classes based on sequence similarity, substrate specificity, and mode of activation[94, 41, 42]. In this thesis, I was interested in the class I PI3Ks, which function as heterodimers with a catalytic subunit and a regulatory subunit. Activation of class I PI3Ks results in conversion of the membrane phospholipid, phosphatidylinositol(3,4)-bis-phosphate (PIP2), to phosphatidylinositol (3,4,5)-tris-phosphate (PIP3), as shown in **Fig. 1.2**. Phosphatase and tensin homolog (PTEN) is the primary regulator of this pathway, converting PIP3 back into

PIP2. PIP3 is a second messenger for several pathways, including the mTOR pathway, which is known to promote cell growth.

The class I PI3K catalytic subunit has four isoforms; class IA includes p110α (gene PI3KCA), p110β (gene PI3KCB), and p110δ (gene PI3KCD), and class IB includes p110γ (gene PI3KCG)[94]. The different isoforms have distinct functions and are found at different levels within different cell types[8]. For example, p110α and β have largely ubiquitous distribution, whereas p110δ and γ are mainly found in immune cells, like lymphocytes and neutrophils[42]. The exact role of these isoforms in neuronal cells had not been comprehensively studied but was investigated by R. Eva and B. Nieuwenhuis, as described in **Chapter 3.2**. In brief, p110α and δ were shown to be essential for axon growth and regeneration in both PNS and CNS neurons, whereas p110β and p110γ did not have significant roles in these processes[5].

PI3K mediates signalling through growth factor, integrin, and cytokine receptors[41]. The class IA PI3Ks are activated when growth factors bind to receptor tyrosine kinases (RTKs). The RTKs are a large family of receptors, including the insulin-like growth factor 1 (IGF-1) receptor (IGFR-1), which is activated by IGF-1, and the tropomyosin receptor kinase B (TrkB) receptor, which is activated by brain-derived neurotrophic factor (BDNF).

Integrins are heterodimeric cell-surface receptors, consisting of an α and a β subunit[70]. Through different combinations of the α and β subunits, about 24 unique integrin receptors are generated. When inactive, integrins have a bent conformation, which shifts into a straight conformation following activation, allowing the integrin receptor to bind ligands in the extracellular matrix. Integrins can be activated in several ways, including the binding of kindlins and talins to their β subunit. Focal adhesion kinase (FAK) is recruited to activated integrins, activating downstream proteins like paxillin and Src. Integrin-linked kinase (ILK) is also activated by integrins and phosphorylates several downstream proteins, including feeding into the PI3K pathway, as in **Fig. 1.3**.

The TrkB [105, 56, 59], IGF-1 [4, 77, 44] and integrin [81, 2] receptors all play an important role during development so are highly upregulated, but they are absent from the axons of mature corticospinal tract neurons to prevent uncontrolled cellular growth. Evidence suggests that these receptors are not present at useful levels on mature RGC axons either[90]. In Osborne et al., delivery of BDNF to RGCs had neuroprotective effects, but these were limited by the downregulation of TrkB receptors. Delivery of BDNF combined with TrkB receptor showed more robust neuroprotection[76]. In Dupraz et al., they demonstrated that IGFR is present at low levels in RGC cell bodies, but did not specifically assess levels on their axons. They found that re-expression and activation of IGFR-1 are required for

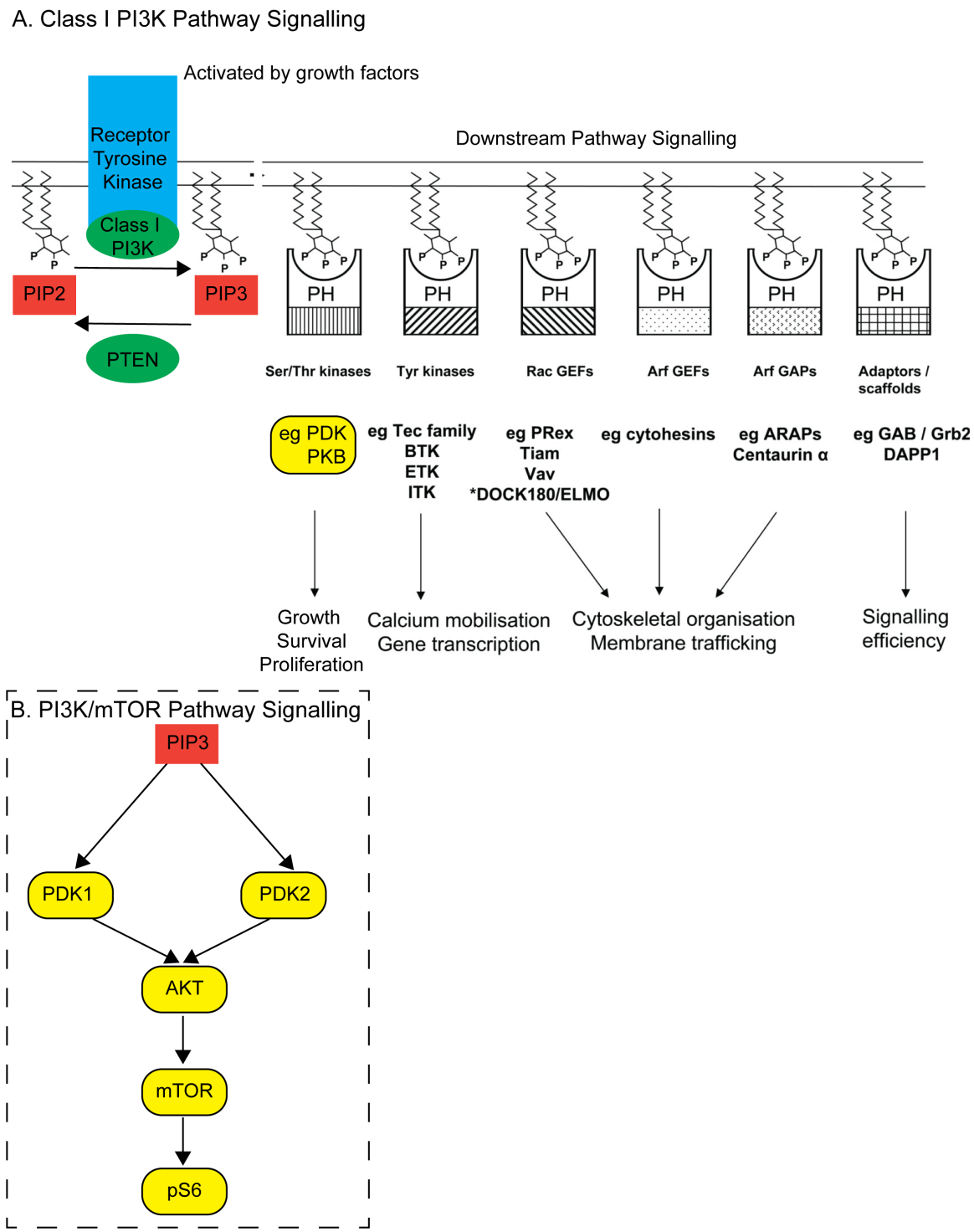

Fig. 1.2 **The PI3K Pathway** Class IA PI3Ks are activated by receptor tyrosine kinases. PI3K then converts the membrane phospholipid, PIP2, into PIP3. PTEN is the primary pathway regulator, converting PIP3 back into PIP2. PIP3 has several downstream signalling pathways, including the mTOR pathway (panel B), which are simplified in this diagram. Figure adapted from Hawkins et al. 2006 [41].

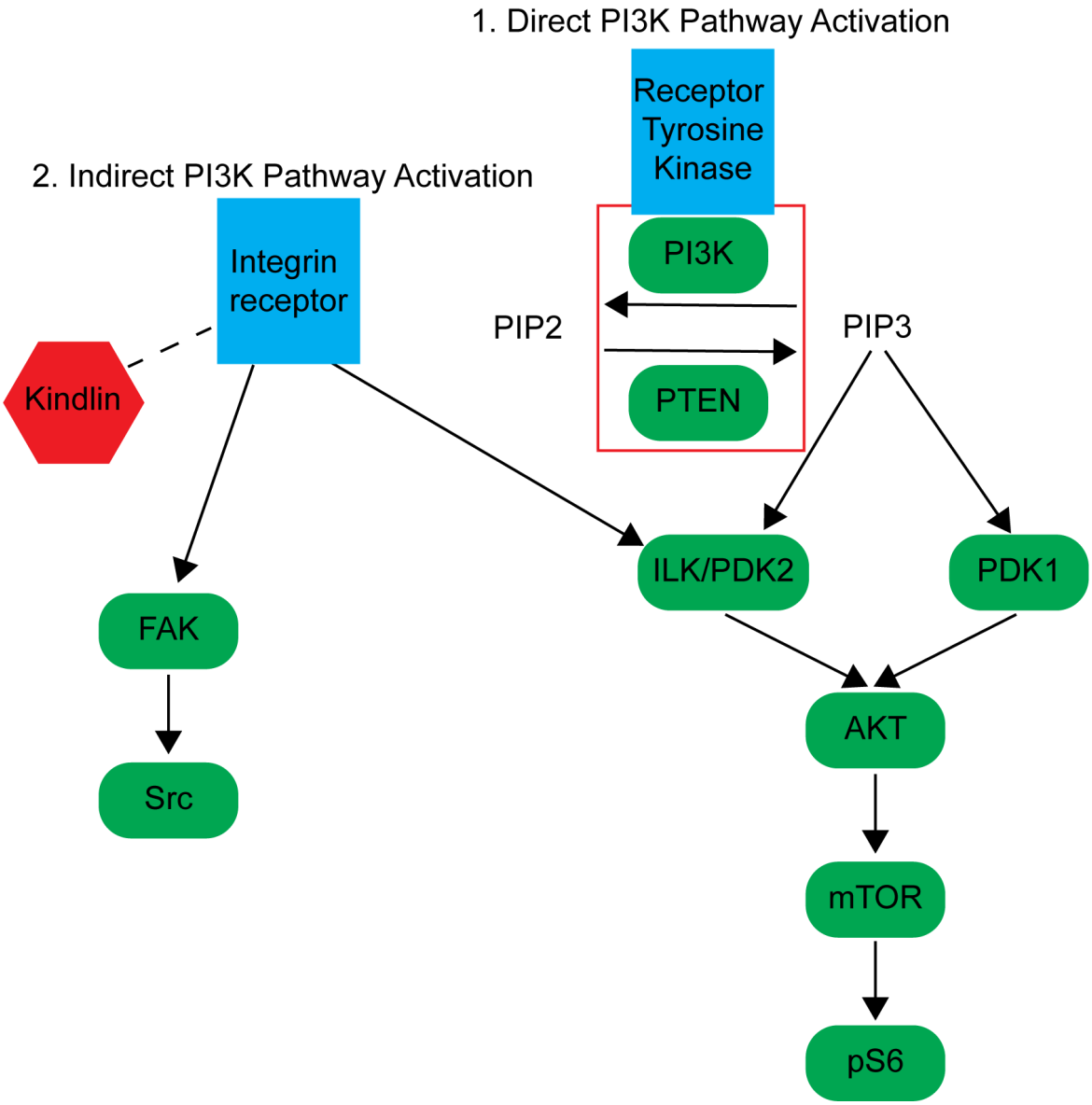

Fig. 1.3 **The PI3K Pathway and Integrin Activation** In addition to RTKs, the PI3K pathway can be also be activated by integrin and cytokine receptors. Integrin receptors activate the PI3K pathway just downstream of PIP3, as shown in the schematic, as well as other pathways including the FAK pathway. Integrin signalling is more complex but is highly simplified in this diagram.

axon regeneration[24]. Overall, these findings highlight the importance of the presence of receptors when manipulating intracellular pathways.

1.3.2 PTEN Deletion Promotes Axon Regeneration

In Park et al.[79], Zhigang He's lab compared the pro-regenerative effects of conditional knockout of different cell growth control genes using $Rb^{f/f}$[63], $P53^{f/f}$[63], $Smad4^{f/f}$[107], $Dicer^{f/f}$[40], $LKB1^{f/f}$[6] and $PTEN^{f/f}$[39] mice. Adult mice were intravitreally injected with an adeno-associated virus (AAV) expressing Cre (AAV.Cre), or AAV.GFP as a control, to induce knockout, and optic nerve crush (ONC) was performed 2 weeks later. The percentage survival of RGCs at 2 weeks post-ONC was estimated using immunostaining of retinal wholemounts (RWMs) with β-III tubulin (Tuj1) antibody, or by prelabelling with FluoroGold. Both techniques yielded similar results. The 20% RGC survival seen in the control group significantly increased to about 45% in the PTEN knockout mice. To assess axon regeneration, axonal fibres labelled with the anterograde tracer, cholera toxin subunit-β (CTB), were examined in optic nerve sections across the lesion site. Robust regeneration along the optic nerve was observed, with about 8 to 10% of the surviving RGCs in the PTEN knockout mice showing regeneration beyond 0.5mm distal to the lesion site, with some extending beyond 3mm. This was also seen at later time points, with some fibres reaching the optic chiasm at 4 weeks post-ONC. At 2 weeks post-ONC, approximately 1500 regenerating axons were observed at 0.5mm from the crush site, which increased to 1750 axons at 4 weeks post-ONC. Approximately 1000 regenerating axons were seen at 1.0mm for both time points. Of the targets investigated, only PTEN deletion and P53 deletion resulted in increased RGC survival, but only the PTEN deletion also increased axon regeneration. Therefore, PTEN deletion acts upon mechanisms promoting RGC survival and overcoming inhibition of axon regeneration after injury.

As mentioned above, PTEN is the primary regulator of the PI3K pathway, which has several downstream targets including the mTOR pathway. Therefore, PTEN deletion promotes PI3K/mTOR pathway signalling. Inhibition of the mTOR pathway by administering rapamycin largely neutralised both the survival and regeneration effects observed in the $PTEN^{f/f}$ mice, although not completely. Conversely, constitutive activation of the mTOR pathway by conditional knockout of a negative regulator of the mTOR pathway, tuberous sclerosis complex I (TSC1), resulted in significant RGC survival and regeneration. However, these effects were weaker than PTEN deletion. Both experiments demonstrated that mTOR pathway activation plays a major role in the pro-regenerative effects seen from PTEN deletion, but also indicate involvement from other pathways downstream of PTEN. The group also used immunohistochemistry (IHC) for phospho-S6 ribosomal protein (pS6), an mTOR

pathway marker, to confirm that mTOR pathway signalling is suppressed in mature adult RGC neurons and upregulated following PTEN deletion. Suppression of the mTOR pathway may limit protein synthesis, and reactivating this pathway would increase protein synthesis, which is necessary for axon regeneration.

Having shown a pro-regenerative effect from PTEN deletion in the optic nerve, He's group went on to investigate this in other CNS axons. In Liu et al., they demonstrated that transgenic PTEN deletion promotes regrowth, both due to sprouting and due to regeneration, in adult corticospinal tract axons. Such a robust regenerative response had never been seen before in the mammalian spinal cord[58].

While transgenic knockouts are useful for demonstrating proof of principle, non-genetic methods allow translation and more flexibility for combining strategies. In Zukor et al., He's lab used short hairpin RNA (shRNA) targeted against PTEN, packaged in an AAV, to knockdown PTEN and significantly enhance regeneration following a crush spinal cord injury[110]. It is worth noting that often RNA interference methods only partially suppress the expression of target genes, as opposed to complete suppression by genetic deletion. This shRNA was not assessed using the ONC model, so this was done as part of this thesis in **Chapter 4**.

1.3.3 The Pro-regenerative Role of PIP3

Deletion of PTEN, as described above, reduces the breakdown of PIP3 into PIP2, thereby increasing PIP3 levels and promoting its downstream effects, like mTOR pathway activation. In Al-Ali et al., inhibition of S6 kinase 1 (S6K1) promoted neurite outgrowth *in vitro* and stimulated corticospinal tract axon regeneration and locomotor recovery *in vivo*[1]. Like PTEN, S6K1 has a negative feedback effect on PI3K signalling. The group showed that inhibition of S6K1 promoted PI3K signalling, mediating the regenerative effect seen. Cosker et al. reviewed the literature, highlighting the critical role of PI3K signalling in neuronal development and axon growth[16]. These studies, as well as others, indicate a crucial role for PI3K signalling, and therefore PIP3, in axon growth and regeneration[26, 109, 66, 25].

RNASeq data and the literature indicate that PI3K is downregulated in mature CNS neurons, and that the receptors activating PI3K are also downregulated or absent in their axons. Both factors would result in low PIP3 levels in mature neurons, which was confirmed experimentally in **Chapter 3.2**[5]. Therefore, while deleting PTEN reduces the breakdown of PIP3, it should be noted that PIP3 levels are very low to begin with. PTEN deletion enhances regeneration through downstream signalling within the cell body, but it is not known whether it also has effects within the axon. It may not have effects within the axon, given the downregulation of PI3K-activating receptors in CNS axons. In this thesis, we

aimed to take the PTEN deletion work further by targeting PI3K directly, bypassing the lack of PI3K-activating receptors, and directly generating more PIP3 in both the cell body and axons.

1.3.4 Integrin Activation Promotes Regeneration

As mentioned, integrins are highly upregulated in neurons during development but are downregulated or completely absent in CNS axons once they mature. Integrins are involved in several cellular processes, including axon regeneration in the PNS[31, 27], which has made them targets for regeneration studies. Integrin $\alpha 9$ overexpression has been shown to promote regeneration both *in vitro* and *in vivo* in a spinal cord injury model [2, 3, 12]. There are three isoforms of kindlin, which is one of the factors that activates integrins. Kindlin-1 is not expressed in neurons, but its introduction into neurons has been shown to promote axon regeneration both *in vitro* and *in vivo* using a spinal cord injury model[96, 12, 70]. Combination of integrin-$\alpha 9$ and kindlin-1 leads to more robust axonal regeneration, exceeding that of either one individually[12].

1.4 Targeting Intrinsic Factors to Promote Axon Regeneration: Other Pathways

Beyond targeting the PI3K pathway, many other strategies have been shown to promote axon regeneration. Suppressor of cytokine signalling 3 (SOCS3), a negative regulator of the Janus kinase/signal transducers and activators of transcription (JAK/STAT) pathway, has been shown to promote regeneration[93]. Several polypeptide trophic factors have also been investigated, including BDNF[62], fibroblast growth factor 2 (FGF2)[88] and ciliary neurotrophic factor (CNTF)[69]. Of these, CNTF has been the most effective, and CNTF released by glial cells showed robust regeneration and neuronal survival[80]. Administration of either osteopontin or IGF-1 promoted regeneration in Duan et al.[23]. The pro-regenerative effects of inflammation have also been demonstrated and found to be promoted by factors like macrophage-derived growth factor, Oncomodulin, and zymosan, a glucan which induces an inflammatory response[51].

While single target strategies have shown moderate regeneration along the optic nerve, these have failed to provide robust long-distance regeneration into the brain. It has become increasingly clear that simultaneously administering different approaches is required. Several studies combining multiple strategies have shown long-distance regeneration, with some functional recovery. These include a combination of PTEN deletion and SOCS3

deletion[95], a combination of osteopontin and IGF-1[23], a combination of intraocular inflammation, PTEN deletion, and elevation of intracellular cyclic adenosine monophosphate (cAMP)[51], a combination of mTOR pathway activation and increased neural activity[57], and a combination of PTEN deletion, zymosan, and cAMP[19].

1.5 Further Challenges in Axon Regeneration

1.5.1 Axon Regeneration to Restore Visual Function

Optic nerve disorders arise when RGCs and their axons are damaged by a range of stimuli, resulting in vision loss. The ultimate aim for clinical intervention is to re-establish these axonal connections and restore visual function, replicating the route RGC axons travel to form the visual pathway during embryonic development. In brief, RGC axons extend from the eye to the optic chiasm, and on to central targets in the brain.

As described above, initial studies using the ONC model showed successful axon regeneration partway along the optic nerve from strategies like PTEN deletion. However, these axons failed to pass through the optic chiasm and into the brain[79]. In more recent studies, long-distance regeneration into the brain has been achieved, with some partial functional recovery [57, 51, 19, 80, 60]. For example, Lim et al. promoted regeneration using a combination of mTOR pathway activation and visual stimulation to increase neural activity[57]. Crucially, these studies have demonstrated target specificity, as RGC axons reconnected with their appropriate targets in the brain and avoided incorrect targets, as was shown using genetically-labelled RGCs in Lim et al.[57].

However, even in studies achieving longer distance regeneration, low numbers of axons make it through the optic chiasm, and path-finding errors are common, including frequent U-turns growing back towards the lesion site and misguidance into the contralateral optic nerve[80, 79, 57, 51, 19, 60]. The extracellular environment of the optic chiasm and axonal guidance have therefore come to the fore as key factors limiting the effects of pro-regenerative stimuli, and these need to be further studied.

During development, axons are guided by several guidance cues expressed in a highly organised spatiotemporal fashion. These guidance cues include glial markers, slits, CSPGs, neutrins, semaphorins, laminin and multiple members of the Ephrin/Eph families. Interestingly, the pathfinding errors of regenerating RGC axons are phenotypically similar to errors documented in RGC axon development when key guidance cues are absent or ectopically expressed[15].

In Conceição et al., we aimed to identify whether key developmental guidance cues were retained or lost in the adult optic chiasm and whether any of them were expressed following injury. The guidance cues studied were radial glial cell marker (RC2), brain lipid-binding protein (BLBP), and slit guidance ligand 1 (Slit1), which are three glial markers, CSPGs, which is an extracellular marker, and pair box-containing gene (Pax2), which is a developmental marker. In addition, the glial cell population of the optic chiasm was examined [15]. Overall the study found differences in key axonal guidance cue expression between embryonic and adult (uninjured) tissue and additional changes following injury. Despite some potentially reparative responses early on, this signal had disappeared by 6 weeks post-ONC, the point at which regenerating axons would reach the optic chiasm. This may be part of the reason for small numbers of regenerating axons reaching the optic chiasm and the misguidance seen in regeneration studies[51, 80, 19]. Future work should characterise more guidance cues at more time points, as well as under regenerating conditions.

1.5.2 Addressing Age in Axon Regeneration Studies

While studies of mammalian CNS axon regeneration have focused on younger animals, the majority of neurodegenerative diseases affect the aged population. However, the effect of aging on CNS axon regeneration is not well understood and this needs to be addressed to better match the clinical setting. Even PNS axons, which have a high regenerative potential, are subject to an age-associated decline in regeneration[100]. This has been shown to be due to neuron-extrinsic factors, including slower clearance of nerve and myelin debris[48, 78]. However, this has not been fully explained and neuron-intrinsic factors may also be involved.

Geoffroy et al. used a similar experimental model to Liu et al. to investigate the effects of aging on axon regeneration in corticospinal tract (CST) and rubrospinal tract (RST) axons. PTEN conditional knockout mice ($PTEN^{f/f}$) received an AAV.Cre injection at either P1, 4 to 6 weeks old, 10 weeks old, or 12 to 18 months old, and CST regeneration was assessed following injury. An age-dependent decline in axon regeneration was observed, with significantly less regeneration in the 10 week group and little, if any, in the 12 to 18 month group. RST regeneration was then assessed in ($PTEN^{f/f}$) mice that received an AAV.Cre injection at either 4 weeks old or 7 to 8 months old. A similarly diminished effect was seen. To understand the mechanisms behind this, Geoffroy et al. assessed mTOR activation by measuring pS6 levels and neuronal soma size. They found that PTEN deletion remained effective in promoting mTOR activity based on these readouts in both CST and RST axons, even in aged mice. As the neuron-intrinsic growth factors remain unaffected, this heavily implicates neuron-extrinsic factors for the age-dependent decline observed. However, it is

important to note that other aspects of the mTOR pathway or other intrinsic pathways were not studied and may be affected by age.

Potential extrinsic factors that may affect regeneration in aged animals include changes in the glial and fibrotic scar, inflammation, growth factor expression, and extracellular matrix components[35]. In Geoffroy et al., IHC showed that both the astroglial and macrophage response to injury were higher or more sustained in older mice compared to younger mice, although this needs to be characterised further[34].

Neuron-intrinsic factors may also contribute to the age-dependent decline in regeneration. For example, changes in receptor compositions and concentrations at the neuronal or axonal surface can result in an enhanced response to an inhibitory external environment. The intrinsic signalling and molecules in the cell can change as animals age, as epigenetics control the expression levels of genes and their corresponding proteins. As highlighted, whilst pS6 levels were unaffected in the Geoffroy et al. study, other aspects of PTEN-mTOR signalling may be compromised in older animals, which needs to be investigated. For example, decreased levels of p-Akt and p-GSK3β have been reported in the hippocampus of aged mice [75]. Other pathways known to promote regeneration, like IGF and SOCS/STAT3 signalling, may be altered in aged animals. Indeed, STAT3 levels are decreased in the aged human brain [13, 18]. Other intrinsic neuronal properties like neuronal viscosity, changes in axon transport, and reduced mitochondrial activity may also be involved.

It is likely both intrinsic and extrinsic factors play significant roles in the age-dependent decline of CNS axon regeneration and this needs to be further elucidated to better develop treatments.

1.6 Objectives

The primary aim of this thesis was to investigate the effects of manipulation of the PI3K pathway on axon regeneration.

The four PI3K isoforms were investigated *in vitro* by R. Eva and B. Nieuwenhuis. Building on this work, the most relevant isoforms, p110α and p110δ, were tested *in vivo* using a conditional transgenic approach and an ONC paradigm in **Chapter 3**. We hypothesised that p110α and p110δ would promote axon regeneration *in vivo*, with no significant difference between the two, as was seen *in vitro*.

In **Chapter 4**, a more translatable approach using viral PI3K(p110δ) was trialed. This was compared to viral PTEN knockdown, which had been tested with a spinal cord injury model but not with an ONC model. We hypothesised that viral PI3K(p110δ) would promote survival and axon regeneration to a greater extend than viral PTEN knockdown, based on the

fact that PI3K should increase PIP3 levels directly, whereas PTEN prevents the breakdown of already low PIP3 levels. We also expected that viral PI3K(p110δ) would be more effective than the transgenic approach because inserting a transgene at the Rosa26 locus only leads to moderate expression levels.

In **Chapter 5**, the PI3K(p110δ) virus was combined with other strategies, like PTEN knockdown and integrin activation. It was expected that combining strategies would have a summative effect, as seen from other studies in the literature, and would further promote regeneration than PI3K(p110δ) individually.

The ultimate aim of this work was to investigate potentially translational methods that may guide future clinical practice for optic nerve disorders.

Chapter 2

Methods

For each experimental chapter, a full set of methods is provided within that chapter, with references to **Chapter 2: Methods** for more detail where appropriate.

2.1 Cell Culture Work

Before being used for *in vivo* experiments, the viral vectors in this thesis were tested in human embryonic kidney (HEK) 293 cells.

2.1.1 Maintenance

HEK 293 cells were maintained using standard cell culture practice. The cells were grown in Dulbecco's modified eagle medium (DMEM) (Gibco, cat no. 41966-029) supplemented with 10% fetal calf serum, penicillin/streptomycin, and L-glutamate, and passaged every 2 or 3 days.

2.1.2 Preparing Cells for Transfection

Coverslips were sterilised in 100% ethanol and placed into a 24-well plate (one coverslip per well). 500μL of freshly prepared poly-L-lysine (10g/mL) (Sigma, cat no. p1274) was then added to each well and left to set for 30 minutes at room temperature. Coating the wells in poly-L-lysine enhances cell adhesion. Two quick washes with phosphate-buffered saline (PBS) were performed, and the plate was left to dry for 1 or 2 hours.

HEK 293 cells from a flask were harvested and resuspended in fresh medium. The viable cells were counted using trypan blue and a haemocytometer, and the concentration of cells in

Viral Construct	Source	Catalogue Number	Stock Titre
AAV2.Cre.GFP	Vector Biolabs	7016	1.00 x 10^{13}GC/mL
AAV2.Cre.GFP	SignaGen Labs	SL100814	1.45 x 10^{13}GC/mL
AAV2.GFP	Vigene Biosciences	CV10004	various
AAV2.shPTEN.GFP	gifted by He lab	N/A	3.94 x 10^{14}GC/mL
AAV2.shScram.GFP	SignaGen Labs	SL100815	1.17 x 10^{13}GC/mL
AAV2.shScram.GFP	Vigene Biosciences	P100042	1.20 x 10^{13}GC/mL
AAV2.PI3K(p110δ)	produced for project	N/A	2.04 x 10^{13}GC/mL
AAV2.GFP	Vigene Biosciences	CV17169-AV2	various
AAV2.Integrin.V5	produced for project	N/A	1.12 x 10^{13}GC/mL
AAV2.Kindlin.GFP	produced for project	N/A	1.19 x 10^{13}GC/mL

Table 2.1 Viral constructs used for transfection in HEK 293 cells

the medium was calculated. 150,000 cells were suspended in 500μL of medium for each well of the poly-L-lysine-coated 24-well plate.

2.1.3 Viral Transfection of HEK 293 Cells

The following day, the viral vectors listed in **Table 2.1** were diluted to a titre of 1.0 x 10^{13} genome copies per mL (GC/mL), using sterile PBS. The medium was removed from the wells and replaced with 2mL of plain DMEM with 2μL of diluted viral vector, giving a final titre of 1.0 x 10^{10}GC/mL in the wells. This titre was the optimal titre for viral transfection of HEK 293 cells found from dose-response experiments carried out by the Martin group. Schematics of the viral constructs are provided in **Chapter 2.3**. In addition, three wells were left untransfected (naive), and their medium was replaced with plain DMEM. The cells were left for 72 hours, after which they were fixed with chilled 4% paraformaldehyde (PFA) for 1 hour. The wells were washed twice with PBS and were stored in PBS at 4°C, ready for immunohistochemistry (IHC).

2.2 Ethics Statement

All animal research was conducted in accordance with UK Home Office regulations for the care and use of laboratory animals, the Animals (Scientific Procedures) Act (1986), and the University of Cambridge Animal Welfare and Ethical Review Body. Animals were housed in light- and temperature-controlled conditions with freely available food and water.

2.3 Intravitreal Injections

Mice were anaesthetised via intraperitoneal injection of ketamine (100mg/kg) and xylazine (10mg/kg). Topical analgesics were applied to the eyes being injected, and eyes not being injected were kept moist with viscotears. 2μL of solution was drawn up into a sterile 5μL Hamilton syringe with a 33-gauge removable needle, and the solution was slowly injected intravitreally. Before removing this needle, a sterile 33-gauge needle was used to puncture the cornea and drain the anterior chamber, to reduce intraocular pressure and prevent reflux of the injected solution. Between injections, the syringe was rinsed with 70% ethanol, followed by PBS.

2.3.1 Injection of Viral Vectors or PBS

For the validation work specified in **Chapters 3 to 5**, young adult (6 to 16 weeks old) mice received a 2μL intravitreal injection into the left eye of the treatment virus(es), and a 2μL intravitreal injection into the right eye of the control virus(es). The viral vectors were either commercially sourced, gifted, or produced in collaboration with Joost Verhaagen (Netherlands Institute for Neuroscience, Amsterdam), as specified in **Table 2.2**. A schematic of the viral constructs is shown in **Fig. 2.1**. All viruses for *in vivo* work were diluted to a titre of 1.0 x 10^{13}GC/mL with sterile PBS. This titre was the optimal titre for viral intravitreal injections in mice found from dose-response experiments carried out by Dr Barber. In **Chapter 3**, a few mice received a 2μL intravitreal injection of PBS into the left eye, while the right eye was left uninjected (naive).

For the regeneration studies specified in **Chapters 3 to 5**, young adult (6 to 8 weeks old) and aged adult (9 to 12 months old) mice received 2μL intravitreal injections into the left eye of the viral vectors.

Multiple injections were required in **Chapter 5**, and these were performed either 4 days or 1 week apart, as specified.

2.3.2 Injection of Cholera Toxin Subunit-β

In the regeneration studies in **Chapters 3 to 5**, 2 days before tissue collection, all mice received a 2μL intravitreal injection into the left eye of cholera toxin subunit-β (CTB) with an Alexa Fluor 555 conjugate (CTB-555) (Thermo Fisher Scientific, cat no. C22843). The CTB-555 was diluted to 1.0mg/mL using sterile PBS.

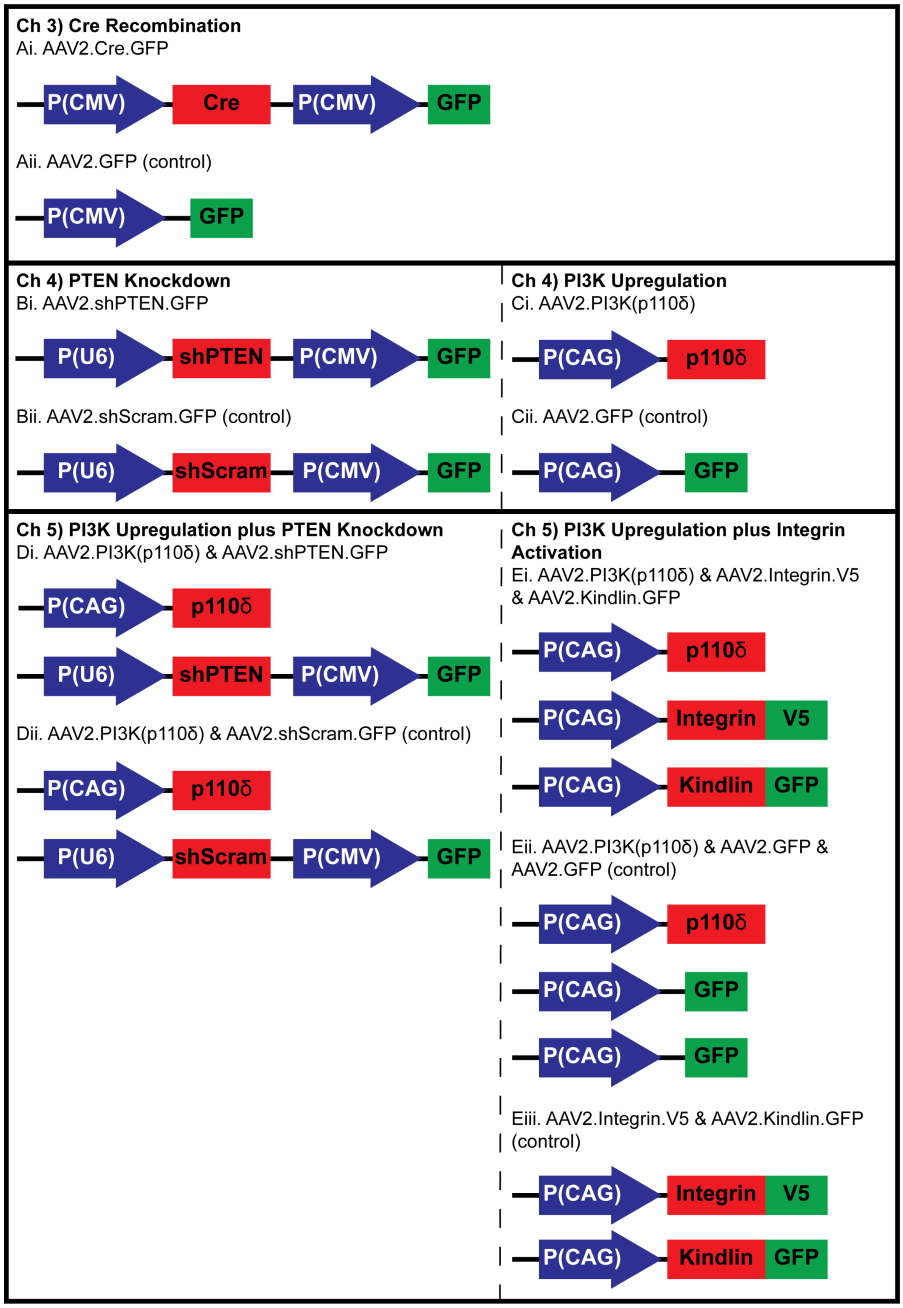

Fig. 2.1 **A schematic of the viral constructs used *in vivo*. A.** Cre recombination using Cre-recombinase was driven by a CMV promoter (Ai) and its corresponding control construct contained GFP (Aii). **B.** PTEN knockdown using shRNA (shPTEN) was driven by a U6 promoter (Bi) and its corresponding control construct contained a non-targeting scrambled sequence (shScram) (Bii). Both constructs also contained a GFP viral tag, driven by a CMV promoter. **C.** PI3K expression was driven by a CAG promoter (Ci), and its corresponding control construct contained GFP (Cii). **D.** The viruses from panel B and C were used. **E.** The viruses from panel C were used. Both integrin and kindlin expression were driven by a CAG promoter. The constructs also contained a V5 or GFP viral tag.

Viral Construct	Source	Stock Titre	Mouse Strain Injected
AAV2.Cre.GFP	Vector Biolabs	1.00 x 10^{13}GC/mL	p110α^{H1047R}, p110δ, Cre-reporter, C57BL/6J
AAV2.GFP	Vigene Biosciences	various	p110α^{H1047R}, p110δ, C57BL/6J
AAV2.shPTEN.GFP	gifted by He lab	3.94 x 10^{14}GC/mL	p110α^{H1047R}, p110δ, C57BL/6J
AAV2.shScram.GFP	SignaGen Labs	1.17 x 10^{13}GC/mL	p110α^{H1047R}, p110δ, C57BL/6J
AAV2.PI3K(p110δ)	produced in lab	2.04 x 10^{13}GC/mL	C57BL/6J
AAV2.GFP	Vigene Biosciences	various	C57BL/6J
AAV2.Integrin.V5	produced in lab	1.12 x 10^{13}GC/mL	C57BL/6J
AAV2.Kindlin.GFP	produced in lab	1.19 x 10^{13}GC/mL	C57BL/6J

Table 2.2 Viral constructs used for intravitreal injections *in vivo*

2.4 Optic Nerve Crush Injury

Mice were anaesthetised via intraperitoneal injection of ketamine (100mg/kg) and xylazine (10mg/kg) and received a subcutaneous injection of Carprieve as an analgesic. Both eyes were kept moist with viscotears during and after the procedure. Optic nerve crush (ONC) injury was performed as previously described[79]. In brief, the optic nerve was exposed intraorbitally and crushed for 10 seconds with curved forceps approximately 1mm from the eye so as not to cut off the retinal blood supply.

In the regeneration studies in **Chapters 3 to 5**, ONC injury was performed 2 weeks after the final intravitreal injection.

2.5 Cardiac Perfusion

Mice were intraperitoneally injected with a fatal dose of euthatol (sodium pentobarbitone, 0.3mL per mouse). Shortly after, the mice were transcardially perfused with PBS to flush out the blood and then with 4% PFA to fix the tissue. All tissue collection and dissections were performed on the day of perfusion.

In **Chapters 3 to 5**, mice from the regeneration studies were perfused 4 weeks post-ONC, and mice for the validation work were perfused 2 weeks after the final intravitreal injection, the point at which they would receive an ONC injury in regeneration studies.

2.6 Tissue Collection

2.6.1 Optic Nerves

In the regeneration studies in **Chapters 3 to 5**, mice were perfused, and the optic nerves were carefully dissected and laid flat on a strip of filter paper (Millipore, cat no. AABG01300) to help keep them straight. The nerves and filter paper were placed into a 1.5mL Eppendorf tube and post-fixed in 4% PFA at 4°C overnight. The nerves were then transferred to 30% sucrose for at least 24 hours for cryoprotection. The nerves were mounted onto a block of Tissue-Tek OCT compound and cryosectioned (14μm longitudinal sections) using a Leica cryostat (Leica Biosystems, CM 3050S Research Cryostat). Slides were dried for about 1 hour at room temperature and stored at -20°C.

2.6.2 Eyes: Retinal Sections

In the validation work in **Chapters 3 to 5**, mice were perfused, and whole eyes were collected, post-fixed in 4% PFA at room temperature for 2 hours, and then transferred to 20% sucrose overnight at 4°C for cryoprotection. The eyes were then embedded in Tissue-Tek OCT compound and cryosectioned (12μm thick) using a Leica cryostat (Leica Biosystems, CM 3050S Research Cryostat). Slides were dried for about 1 hour at room temperature and stored at -20°C.

2.6.3 Eyes: Retinal Wholemounts

In the regeneration studies in **Chapters 3 to 5** and in the validation work in the Cre-reporter mouse line in **Chapter 3**, mice were perfused, and whole eyes were collected. The retinas were extracted, and four small incisions were made to form retinal wholemounts (RWMs). RWMs were collected into a 24-well plate (one RWM per well) and post-fixed in 4% PFA for 2 hours. After this, the solution was replaced with PBS, and the plates were stored at 4°C.

2.6.4 Eyes: Retinas for Western Blots

In the validation work in **Chapter 3**, mice were culled by a rising concentration of carbon dioxide and cervical dislocation. Whole eyes were immediately removed, and the retinas were extracted, collected into 1.5mL Eppendorf tubes, and put on dry ice, ready for processing.

2.7 Immunohistochemistry

All antibodies mentioned below are summarised in **Table 2.3**. The IHC protocols and antibody concentrations used were found within the Martin group by trial and error to produce optimum results. For each antibody, a negative control using no primary antibody was performed, along with positive controls where appropriate.

2.7.1 Histology in HEK 293 Cells

Each of the viral vectors used in this thesis was tested in HEK 293 cells before being used *in vivo*. Viral-transfected HEK 293 cells were fixed in a 24-well plate and then counterstained with DAPI (1:10,000). Where appropriate, they were also immunostained for the viral tags, phosphoinositide 3-kinase (PI3K)(p110δ) or V5.

Keeping the HEK 293 cells in the 24-well plate, the cells were washed three times with PBS for 10 minutes each. For PI3K(p110δ) IHC, the cells were blocked in 2% bovine serum albumin (BSA), 5% normal goat serum (NGS) in 0.3% PBS-TritonX100 for 1 hour at room temperature. For V5 IHC, the cells were blocked in 3% BSA, 5% NGS in 0.4% PBS-TritonX100 for 2 hours at room temperature. Primary antibodies for PI3K(p110δ) (rabbit, 1:500, Abcam, cat no. ab1678) and V5 (mouse, 1:300, Invitrogen, cat no. R96025) were diluted in blocking solution for overnight incubation at 4°C.

The following day, the HEK 293 cells were washed three times with PBS for 10 minutes each, 20 minutes for V5. Goat anti-rabbit IgG (H+L) with Alexa Fluor-555 (1:1000, Invitrogen, cat no. A21428) and goat anti-mouse IgG (H+L) with Alexa Fluor-555 (1:1000, Invitrogen, cat no. A21424) were used as secondary antibodies for a 2 hour incubation period at room temperature, while counterstaining with DAPI (1:10,000). The HEK 293 cells were washed three times with PBS for 10 minutes each, 20 minutes for V5. Finally, the coverslips were carefully removed from the 24-well plates and mounted onto slides with Fluorsave reagent (Millipore, cat no. 345789).

2.7.2 Histology in Retinal Sections

In **Chapters 3 to 5**, IHC was used to identify viral tags, with antibodies against green fluorescent protein (GFP), PI3K(p110δ) or V5, or retinal ganglion cells (RGCs), with antibody against βIII tubulin (Tuj1). IHC was also used to quantify mammalian target of rapamycin (mTOR) pathway activity, with antibodies against phospho-AKT (pAKT) and phospho-S6 ribosomal protein (pS6). In **Chapter 4**, IHC was used to quantify phosphatase

and tensin homolog (PTEN) knockdown, with antibody against PTEN, and PI3K upregulation, with antibody against PI3K(p110δ).

All slides were washed three times with PBS for 10 minutes each, except for V5-stained slides, which were washed for 15 minutes each. For GFP, PI3K(p110δ), Tuj1, pAKT, and pS6 IHC, sections were blocked with 2% BSA, 5% NGS in 0.3% PBS-TritonX100 for 1 hour at room temperature. For V5 IHC, sections were blocked with 3% BSA, 5% NGS in 0.4% PBS-TritonX100 for 2 hours at room temperature. For PTEN IHC, sections were blocked with 2% BSA, 10% NGS in 0.3% PBS-TritonX100 for 1 hour at room temperature. The primary antibodies were diluted in blocking solution for incubation at 4°C overnight: GFP (rabbit, 1:500, Abcam, cat no. ab290), PI3K(p110δ) (rabbit, 1:500, Abcam, cat no. ab1678), V5 (mouse, 1:200, Invitrogen, cat no. R96025), Tuj1 (mouse, 1:400, Promega, cat no. G7121), pAKT (Thr308) (D25E6) XP (rabbit, 1:200, Cell Signaling Technology, cat no. 13038), pS6 (Ser235/236) (91B2) (rabbit, 1:200, Cell Signaling Technology, cat no. 4857), and PTEN (D4.3) XP (rabbit, 1:100, Cell Signaling Technology, cat no. 9188).

The next day, slides were washed three times with PBS for 10 minutes each, except for V5-stained slides, which were washed for 20 minutes each. Goat anti-rabbit IgG (H+L) with Alexa Fluor-488 (1:1000, Invitrogen, cat no. A11034), goat anti-rabbit with Alexa Fluor-555 (at double the primary antibody concentration, Invitrogen, cat no. A21428), goat anti-mouse IgG (H+L) with Alexa Fluor-488 (1:1000, Invitrogen, cat no. A32723), goat anti-mouse IgG (H+L) with Alexa Fluor-555 (1:500, Invitrogen, cat no. A21424), goat anti-mouse IgG (H+L) with Alexa Fluor-647 (1:1000, Invitrogen, cat no. A21235) were used as secondary antibodies for a 2 hour incubation period at room temperature, whilst also counterstaining with DAPI (1:10,000). The slides were washed three times with PBS for 10 minutes each, except for V5-stained slides, which were washed for 20 minutes each. Coverslips were placed over the tissue with Fluorsave reagent (Millipore, cat no. 345789) and the slides were stored at 4°C.

2.7.3 Histology in Retinal Wholemounts

In **Chapters 3 to 5**, IHC using an antibody against Brn3A, an RGC marker, was used to quantify RGC survival in RWMs following ONC injury. As described above, RWMs were collected into a 24-well plate and post-fixed in 4% PFA. The PFA was removed and replaced with PBS.

Keeping the samples in the 24-well plate, free-floating RWMs were washed four times with 0.5% PBS-TritonX100 for 10 minutes each. All steps were performed on a rocking plate at slow speed. In between the second and third wash, the retinas were frozen in 0.5% PBS-TritonX100 for 10 minutes at -70°C. The freezing permeates the nuclear membrane,

improving antibody penetration for Brn3A, which is a nuclear protein. The washes were resumed after thawing. The RWMs were then blocked with 2% BSA, 10% normal donkey serum (NDS) in 2% PBS-TritonX100 for 1 hour at room temperature. Brn3A (C-20) (goat, 1:200, Santa Cruz Biotechnology, cat no. sc-31984) was diluted in blocking solution for a 2 hour incubation at room temperature, followed by overnight incubation at 4°C.

The next day, the RWMs were washed once with 2% PBS-TritonX100 for 5 minutes and three times with 0.5% PBS-TritonX100 for 30 minutes each. Donkey anti-goat IgG (H+L) with an Alexa Fluor-647 (1:500, Invitrogen, cat no. A21447) was used as secondary antibody, diluted in 2% PBS-TritonX100 for a 2 hour incubation period at room temperature. Samples were then washed three times for 30 minutes in PBS and counterstained with DAPI (1:10,000). Finally, the RWMs were mounted onto slides using Fluorsave reagent (Millipore, cat no. 345789), with the RGC layer facing upward, and stored at 4°C.

2.8 Western Blots

Western blots of whole retinal lysate were used to confirm successful viral transduction, using antibody against GFP, and to quantify mTOR pathway activity, using antibodies against pAKT, mTOR, and pS6. The protocols and antibody concentrations used were found within the Martin group by trial and error to produce optimum results.

2.8.1 Sample Preparation

As mentioned above, fresh retinal tissue was collected and stored on dry ice, ready for processing. 100μL of freshly prepared lysis buffer, made using cOmplete™ Lysis-M EDTA-free (Roche, cat no. 04719964001), was added to each tube. The tissue was homogenised using a sterile pestle, and the samples were kept on ice for 15 minutes, before spinning them down to separate the dissolved protein from insoluble components (13,000 revolutions per minute (rpm) for 10 minutes at 4°C). The supernatant was collected from each sample, and its protein concentration was quantified using a Pierce BCA Protein Assay Kit (Thermo Scientific, cat no. 23227). Samples were stored at -20°C.

2.8.2 Electrophoresis

Western blots were performed using standard western blot protocol.

For each sample, 8μg of protein was made up to a total volume of 15μL, with 10% NuPAGE Sample Reducing Agent (10x) (Invitrogen, cat no. NP0009) and 25% NuPAGE LDS Sample Buffer (4x) (Invitrogen, cat no. NP0007) in water. A positive control for pS6

Primary Antibody (Ab)	Secondary Ab	Specificity	Species	Type	Company	Ab Dilution Factor
GFP	Goat α-rabbit, AF555+488	GFP	Rabbit	Polyclonal	Abcam	1:500
V5	Goat α-mouse, AF555	V5-tag	Mouse	Monoclonal	Invitrogen	1:200
Tuj1	Goat α-mouse, AF488+647	neuronal cells (including RGCs)	Mouse	Monoclonal	Promega	1:400
PI3K(p110δ)	Goat α-rabbit, AF555	PI3K(p110δ)	Rabbit	Polyclonal	Abcam	1:500
PTEN	Goat α-rabbit, AF555	PTEN	Rabbit	Monoclonal	Cell Signaling Tech	1:100
phospho-AKT (Thr308) (D25E6) XP	Goat α-rabbit, AF555	pAKT	Rabbit	Monoclonal	Cell Signaling Tech	1:200
phospho-S6 (Ser235/236) (91B2)	Goat α-rabbit, AF555	pS6	Rabbit	Monoclonal	Cell Signaling Tech	1:200
Brn3A	Donkey α-goat, AF647	RGCs	Goat	Polyclonal	Santa Cruz Biotech	1:200

Table 2.3 Antibodies used for immunohistochemistry

was prepared in the same way, using viral-transfected HEK 293 cells known to show strong pS6 signal.

The samples were denatured at 70°C for 10 minutes, and proteins were separated by sodium dodecyl sulfate polyacrylamide gel electrophoresis (SDS-PAGE) under reducing conditions. For GFP, pS6, PTEN, and PI3K(p110δ), NuPAGE 4-12% Bis-Tris gels (1.5mm x 15 well) (Invitrogen, cat no. NP0336) were used in NuPAGE MOPS SDS Running Buffer (20x) (Invitrogen, cat no. NP0001) and water. For pAKT and mTOR, NuPAGE 3-8% Tris-Acetate gels (1.0mm x 15 well) (Invitrogen, cat no. EA03755) were used in Tris-Acetate SDS Running Buffer (20x) (Invitrogen, cat no. LA0041) and water. The inner chamber was filled with running buffer plus 0.25% NuPAGE Antioxidant (Invitrogen, cat no. NP0005). 15μL of each sample was loaded, alongside 10μL of Precision Plus Protein Kaleidoscope (Bio-Rad, cat no. 1610375) for GFP, pS6, PTEN, and PI3K(p110δ), or alongside 10μL of HiMark Pre-Stained HMW Protein Standard (Invitrogen, cat no. LC5699) for pAKT and mTOR. The gels were run at 150V and 420A.

The gels were then transferred to a 0.45μm polyvinylidene difluoride (PVDF) membrane (Invitrogen, cat no. LC2005), using a solution made from 5% NuPAGE Transfer Buffer (Invitrogen, cat no. NP0006-1), 10% methanol and 0.1% antioxidant in water. The transfers were run at 30V and 420A on ice.

Immunoblotting

All antibodies mentioned below are summarised in **Table 2.4**. Antibody concentrations were found within the Martin group by trial and error to produce optimum results.

After transfer, the membranes were washed twice with PBS for 5 minutes each. All steps were performed on a rocking plate at slow speed. Membranes were then incubated for 1 hour at room temperature in blocking solution, made from 5% milk in 0.2% PBS-Tween20 (PBST). For *in vivo* work, primary antibodies for GFP (rabbit, 1:1000, Abcam, cat no. ab290), pAKT (T308) (D25E6) XP(R) (rabbit, 1:300, Cell Signaling Technology, cat no. 13038), mTOR (7C10) (rabbit, 1:800, Cell Signaling Technology, cat no. 2983), pS6 (S235/236) (91B2) (rabbit, 1:200, Cell Signaling Technology, cat no. 4857) and β-actin (rabbit, 1:1000, Cell Signaling Technology, cat no. 4967) were diluted in blocking solution for overnight incubation at 4°C. For *in vitro* work, primary antibodies for PTEN (D4.3) XP (rabbit, 1:1000, Cell Signaling Technology, cat no. 9188), PI3K(p110δ) (rabbit, 1:1000, Abcam, cat no. ab1678) and β-actin (rabbit, 1:1000, Cell Signaling Technology, cat no. 4967) were diluted in blocking solution for overnight incubation at 4°C.

The next day, membranes were washed three times with blocking solution for 10 minutes each. The membrane was incubated with the secondary antibody, peroxidase-labelled goat

anti-rabbit IgG (1:10000, Vector laboratories, cat no. PI-1000), in blocking solution for 2 hours at room temperature. The membrane was washed twice with blocking solution for 10 minutes each and once with 0.2% PBST for 10 minutes. ECL Prime western blotting detection reagent (GE Healthcare Amersham, cat no. RPN2232) was added to the membranes for 5 minutes before imaging.

The immunoblotting method for pS6 had been used successfully in the lab for HEK 293 cells, and in my experiments, pS6 signal was detected from the HEK 293 cell-positive control. However, pS6 signal was not detected in whole retinal lysate. In an attempt to see signal, I tried an alternative protocol using tris-buffered saline (TBS) instead of PBS.

After transfer, membranes were washed with TBS twice for 5 minutes each. Membranes were blocked in 5% milk in 0.1% TBS-Tween20 (TBST) for 1 hour at room temperature. The membrane was washed three times with 0.1% TBST for 5 minutes each. The primary antibodies for pS6 (S235/236) (91B2) (rabbit, 1:200, Cell Signaling Technology, cat no. 4857) and β-actin (rabbit, 1:1000, Cell Signaling Technology, cat no. 4967) were diluted in 5% BSA in 0.1% TBST for overnight incubation at 4°C.

The next day, membranes were washed three times with TBST for 5 minutes each. The membranes were incubated with the secondary antibody, peroxidase-labelled goat anti-rabbit IgG (1:10000, Vector laboratories, cat no. PI-1000), in 5% BSA in 0.1% TBST for 2 hours at room temperature. The membrane was washed three times with 0.1% TBST for 5 minutes each.

2.9 Microscopy and Quantification

Immunofluorescence was analysed using fluorescence microscopy (Leica, DM6000 and DMi8) and confocal microscopy (Leica, SPE and Sp5). Where stated, some images were taken using a Zeiss AxioScan Z1 by the Histopathology/ISH core facility at the Cancer Research UK (CRUK) Cambridge Institute.

2.9.1 Viral Transfection *In Vitro*

HEK 293 cells transfected with each viral vector were counterstained with DAPI, and where appropriate, were immunostained for the viral tag markers, PI3K(p110δ) and V5. These were imaged by confocal microscopy at x40 magnification. The images were used to confirm that the appropriate viral tag was observed and that this signal was not seen in untransfected cells.

Primary Antibody (Ab)	Species	Type	Company	Ab Dilution Factor	Molecular Weight (kDa)
GFP	Rabbit	Polyclonal	Abcam	1:1000	27
β-actin	Rabbit	Polyclonal	Cell Signaling Technology	1:1000	45
phospho-AKT (Thr308) (D25E6) XP	Rabbit	Monoclonal	Cell Signaling Technology	1:200	60
mTOR	Rabbit	Monoclonal	Cell Signaling Technology	1:800	289
phospho-S6 (Ser235/236) (91B2)	Rabbit	Monoclonal	Cell Signaling Tech	1:200	32
PTEN	Rabbit	Monoclonal	Cell Signaling Technology	1:1000	54
PI3K(p110δ)	Rabbit	Polyclonal	Abcam	1:1000	110

Table 2.4 Antibodies used for immunoblotting

2.9.2 Viral Transduction *In Vivo*

Successful viral transduction *in vivo* of AAV2.Cre.GFP and AAV2.GFP was confirmed in western blots of whole retinal lysate by the presence of the viral tag, GFP.

Successful transduction of all viral vectors was confirmed in retinal sections injected with each viral vector, immunostained for viral tag markers, GFP, PI3K(p110δ), and V5, and counterstained with DAPI. The presence of viral tag was confirmed, and eye cups were imaged using a Zeiss AxioScan Z1 at x20 magnification (0.22μm/pixel) by the team at the Histopathology/ISH core facility at the CRUK Cambridge Institute. Retinal sections were imaged using confocal microscopy at x40 magnification.

2.9.3 RGC Survival

In **Chapters 3 to 5**, images of Brn3A-labelled RWMs were taken at x20 magnification using fluorescence microscopy, sampling both the more central and more peripheral regions of each of the four quadrants (eight images total). These images were analysed in Image J Fiji (Fiji-win64) using The Image-Based Tool for Counting Nuclei (ITCN) Plugin (University of California, Santa Barbara, CA, USA) for automated counting of Brn3A-positive cells with the following settings: width 22, minimum distance 5 and threshold 0.1. Two custom programs written by S. S. Deshpande were used to expedite the ImageJ analysis.

J. Cave calculated the retinal surface area of several images and found that on average, 21.5% of the total retinal surface area was sampled by taking eight images. Therefore, the sum of the RGC counts from the eight images was multiplied by 4.65 to calculate the estimated total RGC count of the retina. The total RGC count in each ONC-injured (left) eye was divided by the mean RGC count from all the uninjured contralateral control (right) eyes. This value was then expressed as a percentage, referred to as percentage RGC survival.

2.9.4 Axon Regeneration

Prior to tissue collection, CTB-555 was intravitreally injected into eyes that had received an ONC injury. This anterograde tracer was used to label regenerating axons for quantification. The optic nerves were then collected and sectioned longitudinally (14μm thick) (**t = thickness of each section**). Four nerve sections were analysed per animal.

The CTB-555-labelled axons were visualised using fluorescence microscopy at x40 magnification. Axon regeneration was quantified by counting the number of CTB-labelled axons extending from the end of the crush site at 0.5mm increments (ie. 0.5mm, 1.0mm, 1.5mm, 2.0mm...), as illustrated in **Fig. 2.2**. The crush site was identified using the characteristic autofluorescent scar material of glia and macrophages. The cross-sectional width of the nerve was also measured at each point at which the counts were taken and was used to calculate the number of axons per millimeter of nerve width (**n = number of axons counted/mm**). In addition, the maximum radius recorded across all four nerve sections at each 0.5mm increment was noted (**r = maximum radius**).

Modelling the nerve as a cylinder, the total number of regenerating axons per nerve was calculated for each nerve section at each distance from the end of the crush site using a previously developed formula[54, 79]:

$$N = \frac{n\pi r^2}{t} \tag{2.1}$$

N = total number of regenerating axons per nerve
n = the number of axons counted/mm (eg. 10axons/mm)
r = the maximum radius recorded at that distance from the crush site (eg. 0.15mm)
t = thickness of each section (eg. 14μm = 0.014mm)

For each 0.5mm increment, the total number of regenerating axons per nerve was then averaged from the four sections to give one result per animal.

Axonal sections were imaged using a Zeiss AxioScan Z1 at x40 magnification (0.11μm/pixel) by the Histopathology/ISH core facility at the CRUK Cambridge Institute.

A. A nerve section

Nerves were sectioned longitudinally, ***t = thickness of each section (14μm thick)***

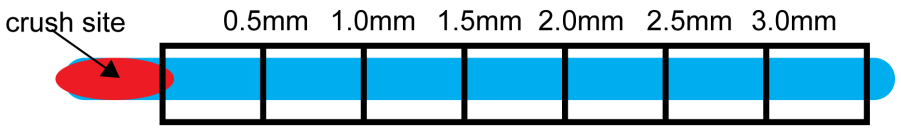

B. Zoom in of a nerve section at 0.5mm

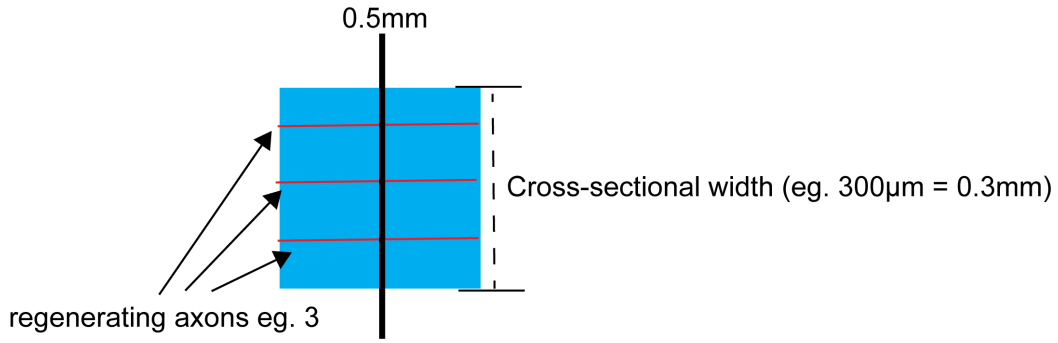

n = number of axons per mm (eg. 3 axons/0.3mm = 10 axons/mm)

C. Modelling the nerve as a cylinder at 0.5mm

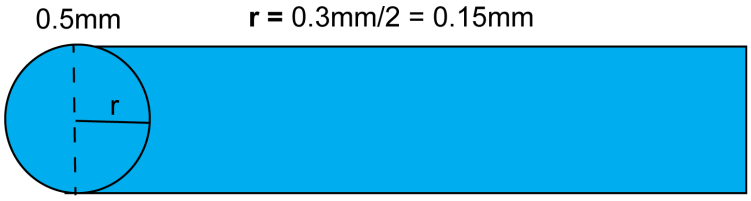

r = maximum radius at each distance from the crush site (from the 4 sections) (eg. 0.15mm)

Fig. 2.2 **A diagram to illustrate quantification of axon regeneration.**

2.9.5 mTOR Pathway Activation in Retinal Sections

The RGC layer of retinal sections injected with each virus, immunostained for pAKT or pS6, and counterstained with DAPI, was examined at x40 magnification by fluorescence microscopy. 100 GFP-positive RGCs (identified using DAPI and GFP signal from the viral vector(s)) were counted from retinal sections immunostained with pAKT and were identified as either positive or negative for pAKT. This method was repeated for retinal sections immunostained with pS6. Four mice were counted for each group (100 RGCs per mouse), and the average was expressed as a percentage of GFP-positive cells co-localised with pAKT or pS6. AAV2.PI3K(p110δ) lacked a clear viral tag, so the total number of pS6-positive RGCs was counted across the retina from 12 retinal sections sampled sequentially throughout the whole eye, using Tuj1 as a marker of RGCs. This method was repeated for AAV2.GFP-transduced retinal sections for comparison. The pAKT signal was not clear enough to count in this way. Representative images were taken at x80 magnification by confocal microscopy.

2.10 Statistics

All statistical tests were performed using GraphPad Prism 7.0 (GraphPad Software, La Jolla, CA). Unpaired one-tailed T-tests were used to compare the effects of two groups which were control versus treatment. Unpaired two-tailed T-tests were used to compare the effects of two groups. One-way ANOVA with Tukey's post-hoc analysis was used to compare the effects of multiple groups. Two-way ANOVA with Tukey's post-hoc analysis was used to compare the effects of multiple groups with two variables (ie. axon regeneration). Asterisks indicate significance levels on graphs: NS = no significance ($p>0.05$), * = $p<0.05$, ** = $p<0.01$, *** = $p<0.001$, **** = $p<0.0001$. Data are presented as mean±standard deviation unless otherwise stated. The statistical tests used, n values and error bars are specified on all graphs.

Chapter 3

Transgenic Manipulation of the PI3K Pathway and its Effects on Axon Regeneration

3.1 Declaration

The work presented in **Chapters 3 and 4** of this thesis has been submitted to EMBO Molecular Medicine for publication. At the time of thesis submission, we are responding to reviewers' comments. This work is cited in the thesis as: *Barber, A.C., ***Evans, R.S.**, *Nieuwenhuis, B., Pearson, C.S., Fuchs, J., MacQueen, A.R., van Erp, S., Hänzi, B., Hulshof, L-A., Osborne, A., Conceição, R., Deshpande, S.S., Cave, J., ffrench-Constant, C., Smith, P.D., Okkenhaug, K., Eickholt, B.J., Martin, K.R., Fawcett, J.W., and Eva, R. (2020), PI3 kinase delta enhances axonal PIP3 to support axon regeneration in the adult CNS (not yet published)[5]. * = the authors contributed equally.

The phosphoinositide 3-kinase (PI3K) *in vitro* data from this paper is summarised in the introduction of this chapter, with appropriate referencing. The majority of the data investigating the effects of the PI3K isoforms was generated by R. Eva and B. Nieuwenhuis. Phospholipid fixation and labelling procedures were developed and performed by J. Fuchs and R. Eva. S. van Erp performed laser axotomy procedures in human embryonic stem cell neurons, supervised by C. ffrench-Constant.

The viral PI3K *in vivo* data from this paper is presented in the results section of **Chapter 4**, and acknowledgments are covered in that chapter's declaration.

The transgenic PI3K *in vivo* data from this paper is presented in the results section of this chapter. The data in this chapter was generated by me, under the supervision of A.C. Barber, with contributions from others declared below.

Transgenic mouse lines: A.R. MacQueen generated the conditional knock-in PI3K mouse lines, supervised by K. Okkenhaug, and these were kindly donated to the Martin-Fawcett group. At the time of thesis submission, these lines have not yet been published. The hyperactive p110α (p110α^{H1047R}) mouse line was derived and established from donated founder mice by P.D. Smith and then maintained by C.S. Pearson. The p110δ mouse line was derived and established from donated founder mice by R. Conceição and me. The isolated p110δ mouse line was derived and established by me. From October 2016, all mouse lines were maintained by me. Four Cre-reporter mice were kindly donated by C. Kapeni (University of Cambridge).

p110α^{H1047R} regeneration data (Part of Fig3.10, 3.11, 3.12 and 3.13): The p110α^{H1047R} regeneration data was generated by A.C. Barber, P.D. Smith, C.S. Pearson, J. Cave, and R. Conceição. While I was not involved in the p110α^{H1047R} regeneration study, the data is presented in the results section of this chapter alongside my data for completeness, with appropriate referencing in the text.

p110δ regeneration data: The p110δ regeneration data was generated by me under the supervision of A.C. Barber. While I was learning the techniques, A.C. Barber performed the initial ONC surgeries and taught me how to collect and analyse tissue for RGC survival and axon regeneration. A.C. Barber also counted axon regeneration alongside me and we compared values for accuracy and to check my counting technique. S.S. Deshpande created a program to speed up RGC survival analysis and did some manual counting to compare with data generated by the program. R. Conceição assisted with some retinal wholemounts during tissue collection.

Validation data: All validation data, including testing the viral vectors *in vitro* and *in vivo*, and quantifying mTOR pathway activity, was generated by me.

R. Eva wrote the manuscript. R. Eva, J.W. Fawcett, B.J. Eickholt, K. Okkenhaug, B. Nieuwenhuis, S. van Erp, A.C. Barber and I edited the manuscript.

3.2 Introduction

3.2.1 The PI3K Pathway and Axon Regeneration

Key points from **Chapter 1** are summarised below.

The regenerative ability of central nervous system (CNS) neurons, including cortical neurons, declines as they mature. However, this capacity is maintained throughout life by peripheral nervous system (PNS) neurons, including dorsal root ganglion (DRG) neurons.

Phosphoinositide 3-kinase (PI3K) converts phosphatidylinositol(3,4)-bis-phosphate (PIP2) to phosphatidylinositol (3,4,5)-tris-phosphate (PIP3). In the reverse, phosphatase and tensin homolog (PTEN), converts PIP3 back into PIP2. PI3K is made up of a catalytic subunit (p110) and a regulatory subunit, and there are four catalytic subunit isoforms: p110α, β, δ and γ. The contribution of these isoforms to neuronal function had not been comprehensively studied.

In the literature, PI3K has been implicated to play a role in the regulation of axon growth and regeneration. Transgenic knockout of PTEN has been shown to have significant effects on retinal ganglion cell (RGC) survival and axon regeneration in CNS neurons *in vivo*, using optic nerve crush (ONC)[79] and spinal cord crush models[58]. This was demonstrated to be primarily due to PI3K/AKT/mammalian target of rapamycin (mTOR) pathway activation.

PTEN knockout reduces the breakdown of PIP3, which is thought to be at low levels in mature CNS neurons. In Barber et al., we hypothesised that upregulating PI3K directly would lead to increased PIP3 production, and therefore a greater increase in PIP3 levels than that seen from PTEN knockout. We expected this would lead to greater axon regeneration in CNS neurons. The effects of the different PI3K isoforms on axon regeneration in PNS and CNS neurons were compared *in vitro*, as described below, and then these were tested *in vivo* using the ONC model.

3.2.2 The Effects of the Different PI3K Isoforms on Axon Regeneration *In Vitro*

In Barber et al., R. Eva and B. Nieuwenhuis investigated the effects of the different PI3K isoforms on axon regeneration *in vitro*, with some input from others as detailed in the declaration section. Their data is summarised under this heading.

The p110α and p110δ isoforms of PI3K are required for axon regeneration in adult DRG neurons *in vitro*

Consulting RNASeq databases, it was found that p110α, β and δ are expressed at all stages in DRG neurons *in vitro*, while p110γ is at very low levels. Previous literature has shown that p110δ is involved in axon regeneration in DRG neurons[25].

In Barber et al. (manuscript submitted, not yet published), the effects of the different p110 isoforms of PI3K on axon regeneration were compared in rat adult DRG neurons. The

following small molecule inhibitors against the different isoforms were used: A66 (inhibitor of p110α), TGX221 (inhibitor of p110β), IC-87114 (inhibitor of p110δ), Idelalisib (inhibitor of p110δ), LY294002 (inhibitor of p110α, β and δ, referred to as pan-PI3K), and XL147 (inhibitor of p110α and δ). The axons of adult DRG neurons were severed using laser axotomy, under the effect of each of these inhibitors or dimethyl sulfoxide as a control. Pan-PI3K inhibition reduced the rate of growth cone regeneration in severed axons and the extension rate of uncut axons, as did inhibition of p110α and of p110α and p110δ combined. Inhibition of p110δ affected growth cone regeneration in severed axons but had no effect on uncut axons, whereas p110β had no effect on either.

Microfluidic compartmentalised chambers, in which axons extend through microchannels into a separate compartment from the cell bodies, were used to investigate the localisation of these effects. Inhibition of p110α in both the axonal and somatic compartments reduced axon regeneration and increased the time taken to generate a new growth cone. Inhibition of p110δ also reduced regeneration in the axonal compartment but interestingly had no effect in the somatic chamber nor on the time to generate a new growth cone. Therefore, both the p110α and p110δ isoforms of PI3K are necessary for efficient axon regeneration in adult DRG neurons, whereas p110β is not. p110α is required throughout the neuron whereas p110δ is specifically required within the axon.

The p110α and p110δ isoforms of PI3K promote axon growth in developing cortical neurons *in vitro*

In Barber et al. (manuscript submitted, not yet published), the effects of overexpression of p110α and p110δ on regulation of axon growth were compared in rat embryonic day 18 (E18) cortical neurons developing *in vitro*, as well as overexpression of a hyperactive p110α H1047R mutant (p110α^{H1047R}). p110α^{H1047R} is an oncogenic point mutation, which has been shown to enhance PIP3 production[61]. p110δ is rarely mutated in cancer. Previous work has shown that p110α^{H1047R} and p110δ can sustain downstream AKT activation on overexpression in fibroblasts, while native p110α does not[49]. Overexpression of p110α^{H1047R} or p110δ led to an increase in axon length, dendrite length, the axon/dendrite length ratio and the number of dendritic branches compared to green fluorescent protein (GFP)-transfected controls. Downstream signalling through the PI3K/AKT/mTOR pathway was confirmed by an increase in cell body size and increased levels of phospho-S6 ribosomal protein (pS6) compared to GFP controls. Overexpression of native p110α had no effect. Therefore, both p110α^{H1047R} and p110δ behave similarly and enhance axonal and dendritic growth.

The p110α and p110δ isoforms of PI3K promote axon regeneration in mature cortical neurons *in vitro*

In Barber et al. (manuscript submitted, not yet published), the effects of p110α, p110α^{H1047R} and p110δ on axon regeneration were compared in E18 cortical neurons using an *in vitro* model of mature CNS regeneration. Laser axotomy was used to sever axons of cortical neurons at a stage at which they have limited capacity for regeneration. Overexpression of p110α^{H1047R} or p110δ led to an increased percentage of regenerating axons, an increase in length of regenerated axons, and a shorter time of onset to regeneration compared to controls. Native p110α had no effect. Therefore, both p110α^{H1047R} and p110δ behave similarly in both developing and mature CNS neurons *in vitro*.

Overexpression of p110δ was also investigated in human neurons maturing *in vitro* (human embryonic stem cells). This fully restored regenerative ability to that of young neurons.

PIP3 levels are high in DRG neurons and immature cortical neurons, but are downregulated as cortical neurons develop. Both the p110α^{H1047R} and p110δ isoforms of PI3K increase PIP3 levels in cortical neurons.

Having investigated the effects of PI3K isoforms on axon regeneration, PIP3 levels were assessed. In Barber et al. (manuscript submitted, not yet published), PIP3 immunostaining was optimised and used to examine endogenous PIP3 levels in rat adult DRG neurons and in rat E18 cortical neurons. High levels of PIP3 were detected in DRG growth cones and in cortical neurons at day 3 *in vitro*. However, PIP3 levels were downregulated as the cortical neurons developed, first in the cell body and then in the axon, which coincided with the loss of regenerative ability. Therefore, PI3K and PIP3 are developmentally downregulated in cortical neurons but remain present in mature DRG neurons.

The effects of overexpression of p110α, p110α^{H1047R} and p110δ on PIP3 levels were compared in rat E18 cortical neurons at 16 days *in vitro*. Overexpression of p110α^{H1047R} or p110δ led to a significant increase in PIP3 levels in the cell body, and an even greater increase at the axon growth cones compared to GFP-transfected controls. Overexpression of native p110α had no effect on PIP3 levels. Therefore, p110α^{H1047R} and p110δ function in a hyperactive fashion to generate PIP3 in cortical neurons.

3.2.3 The Effects of PI3K on Axon Regeneration *In Vivo*

The *in vitro* data demonstrated the pro-regenerative effects of PI3K, specifically the p110α^{H1047R} and p110δ isoforms. The next step was to test whether these results were translatable to *in vivo* models. This data is presented in this thesis chapter.

Two conditional knock-in PI3K mouse lines were created in the K. Okkenhaug lab, making use of Cre-lox recombination technology to allow conditional expression of the transgenes. A few of these mice were kindly donated to the Martin-Fawcett lab, from which three mouse lines were then derived and established.

Hyperactive p110α (p110α^{H1047R}) mice

The first mouse line used in this thesis is referred to as the "hyperactive p110α (p110α^{H1047R})" mouse line (currently unpublished). The p110α^{H1047R} mice have a knock-in fragment containing the human PI3KCA gene, which encodes PI3K(p110α), with an H1047R point mutation. This fragment was inserted at the Rosa26 locus, which results in transgene expression at moderate levels[72]. The genotype is illustrated in the schematic diagram in **Fig. 3.1**. A stop sequence is in front of the transgene, flanked by two loxP sites, preventing gene expression. Following Cre-mediated recombination, the stop sequence is removed, and the transgene is expressed. Therefore, these mice overexpress human p110α^{H1047R} in the presence of endogenous p110α and p110δ.

p110δ mice and isolated p110δ Mice

One mouse line donated by K. Okkenhaug had a knock-in fragment containing the human PI3KCD gene, which encodes PI3K(p110δ), inserted at the Rosa26 locus. The genotype is illustrated in the schematic diagram in **Fig. 3.2**. Following Cre-mediated recombination, the stop sequence is removed, and the transgene is expressed. Therefore, these mice overexpress human PI3K(p110δ). In addition, the mice have floxed mouse PI3KCA and floxed mouse PI3KCD genes. The mouse PI3KCA gene is flanked by two loxP sites, as is the mouse PI3KCD gene. Following Cre-mediated recombination, the genes are removed. Therefore, these mice do not express endogenous mouse p110α and p110δ.

The second mouse line used in this thesis, referred to as the "p110δ" mouse line (currently unpublished), carries the human PI3KCD gene but the floxed PI3KCA and PI3KCD were bred out. Therefore, these mice overexpress PI3K(p110δ) in the presence of endogenous p110α and p110δ.

The third mouse line used in this thesis, referred to as the "isolated p110δ" mouse line (currently unpublished), carries the human PI3KCD gene and kept the floxed mouse PI3KCA

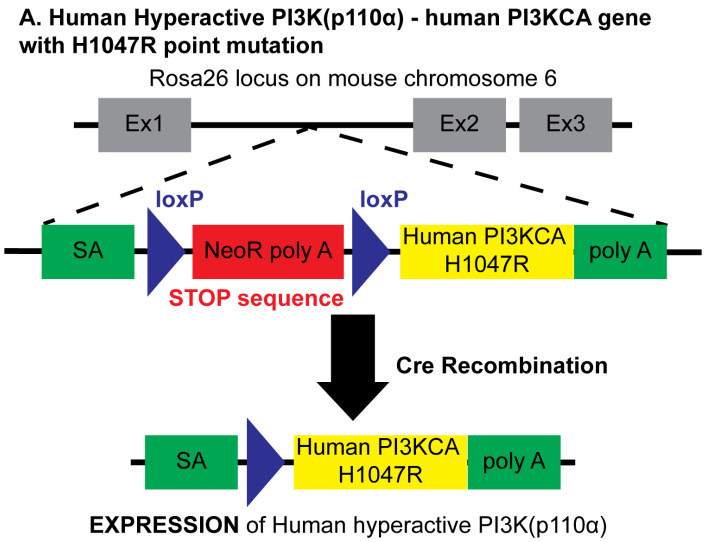

Fig. 3.1 **Hyperactive p110α (p110α^{H1047R}) mice** The genotype of the p110α^{H1047R} mice is illustrated in this schematic. A knock-in fragment containing the human PI3KCA gene with an H1047R point mutation was inserted at the Rosa26 locus. A stop sequence in front of the transgene, flanked by two loxP sites, prevents expression of the gene. However, following Cre recombination, the stop sequence is removed, and human p110α^{H1047R} is expressed. Ex = exon, SA = splice acceptor, poly A = polyadenylation sequence

and floxed mouse PI3KCD genes. Therefore, these mice overexpress PI3K(p110δ) in the absence of endogenous p110α and endogenous p110δ.

3.2.4 Aim

As summarised above, the *in vitro* data from Barber et al. showed that the p110α^{H1047R} and p110δ isoforms of PI3K promote axon regeneration and behave in a similar way. In the results section of this chapter, this was tested *in vivo* using ONC injury in a conditional knock-in p110α^{H1047R} mouse line and a conditional knock-in p110δ mouse line. We hypothesised that both isoforms would promote RGC survival and axon regeneration, behaving in the same way.

3.3 Methods

Any references to **Chapter 2** are clearly stated in the text.

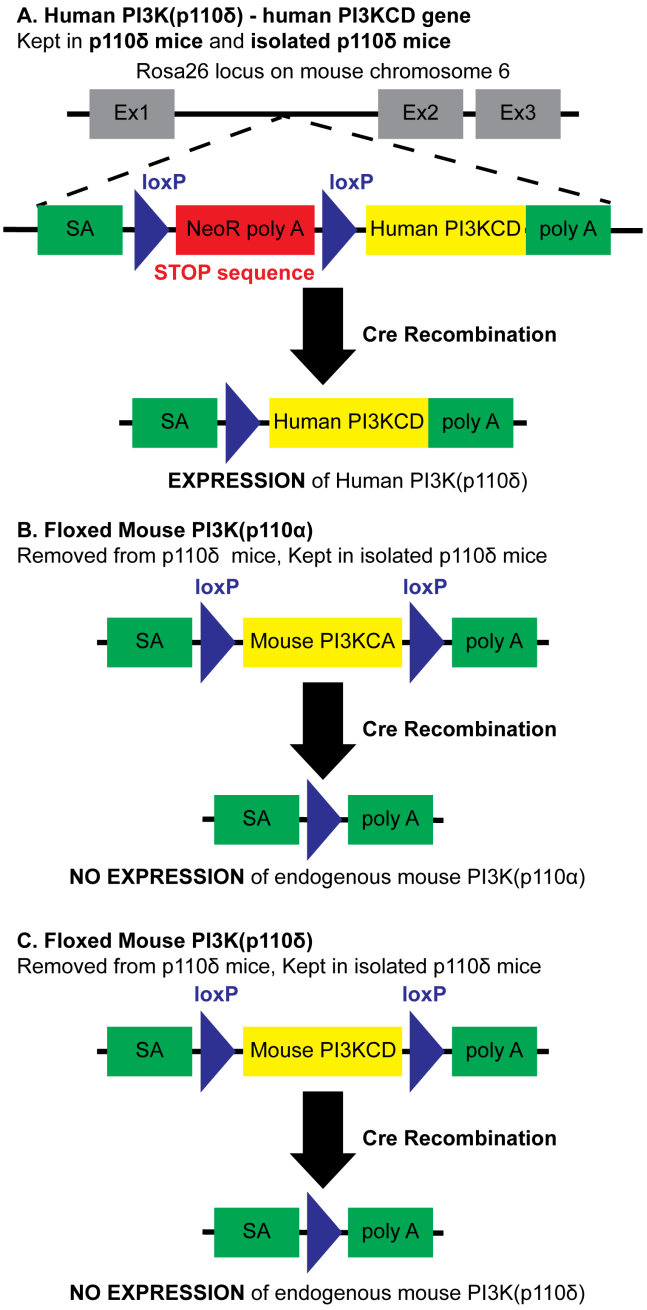

Fig. 3.2 **p110δ and isolated p110δ mice** The genotypes of the donated PI3K(p110δ) mice, the p110δ mice and isolated p110δ mice are illustrated in this schematic. In panel A, loxP sites surround a stop sequence in front of the human PI3KCD gene, which prevents gene expression. Following Cre recombination, this results in human PI3K(p110δ) expression. This is found in both the p110δ and isolated p110δ mice. LoxP sites also surround both the mouse PI3KCA (panel B) and mouse PI3KCD (panel C) genes. Following Cre recombination, this removes expression of endogenous PI3K(p110α) and PI3K(p110δ). This was bred out of the p110δ mice but kept in the isolated p110δ mice. Ex = exon, SA = splice acceptor, poly A = polyadenylation sequence

3.3.1 Breeding Strategy for p110δ Mice and Isolated p110δ Mice

Two conditional knock-in PI3K(p110δ) males were kindly donated by the K. Okkenhaug lab to the Martin-Fawcett lab. As described in more detail in **Chapter 3.2.3**, these males were heterozygous for the human PI3KCD gene, which encodes PI3K(p110δ), and homozygous for mouse PI3KCA flx, which encodes floxed PI3K(p110α), and homozygous for mouse PI3KCD flx, which encodes floxed PI3K(p110δ). A breeding strategy was devised to establish the conditional knock-in p110δ and isolated p110δ mouse lines in this thesis, as laid out in **Fig. 3.3**.

The two founder males were crossed with C57BL/6J females. 1 in 2 of the offspring were "intermediate heterozygotes" and these were crossed with C57BL/6J mice. From these matings, 1 in 8 of the offspring were heterozygous p110δ mice, and 1 in 8 were heterozygous isolated p110δ mice. To derive the p110δ mice, heterozygous p110δ mice from separate litters were crossed. 1 in 4 of the offspring were then the desired homozygous p110δ mice. To derive the isolated p110δ mice, heterozygous isolated p110δ mice from separate litters were crossed. 1 in 64 of the offspring were then the desired homozygous isolated p110δ mice. Once the lines were derived, breeding pairs were set up to maintain the colony.

3.3.2 Genotyping of Conditional Knock-in Mice

DNA Extraction

Ear clips were obtained from the conditional knock-in PI3K mice, collected into Eppendorf tubes, and flash-frozen in liquid nitrogen. 50μL of alkaline lysis buffer (200mg NaOH, 14.88mg EDTA, 200ml water) was added to each sample. The tubes were heated at 95°C for 1 hour, after which 50μL of neutralisation buffer (1.3g Tris HCl and 200ml water) was added. Samples were stored at -20°C.

PCR

Three sets of primers were designed by the K. Okkenhaug lab to detect specific sequences in each of the three transgenes of the PI3K mice, as listed in **Table 3.1**. One set of primers was designed to detect the p110 subunit of PI3K, regardless of isoform, inserted at the Rosa26 locus: Rosa26 F1 AMQ, Rosa26 R2 AMG and Rosa26 loxP R1 AMG. A second set of primers was designed to detect floxed mouse PI3KCA (PI3KCA flx): Ma50 and Ma51. A third set of primers was designed to detect floxed mouse PI3KCD (PI3KCD flx): Delta flox F2, Delta flox R2 and Delta flox R4.

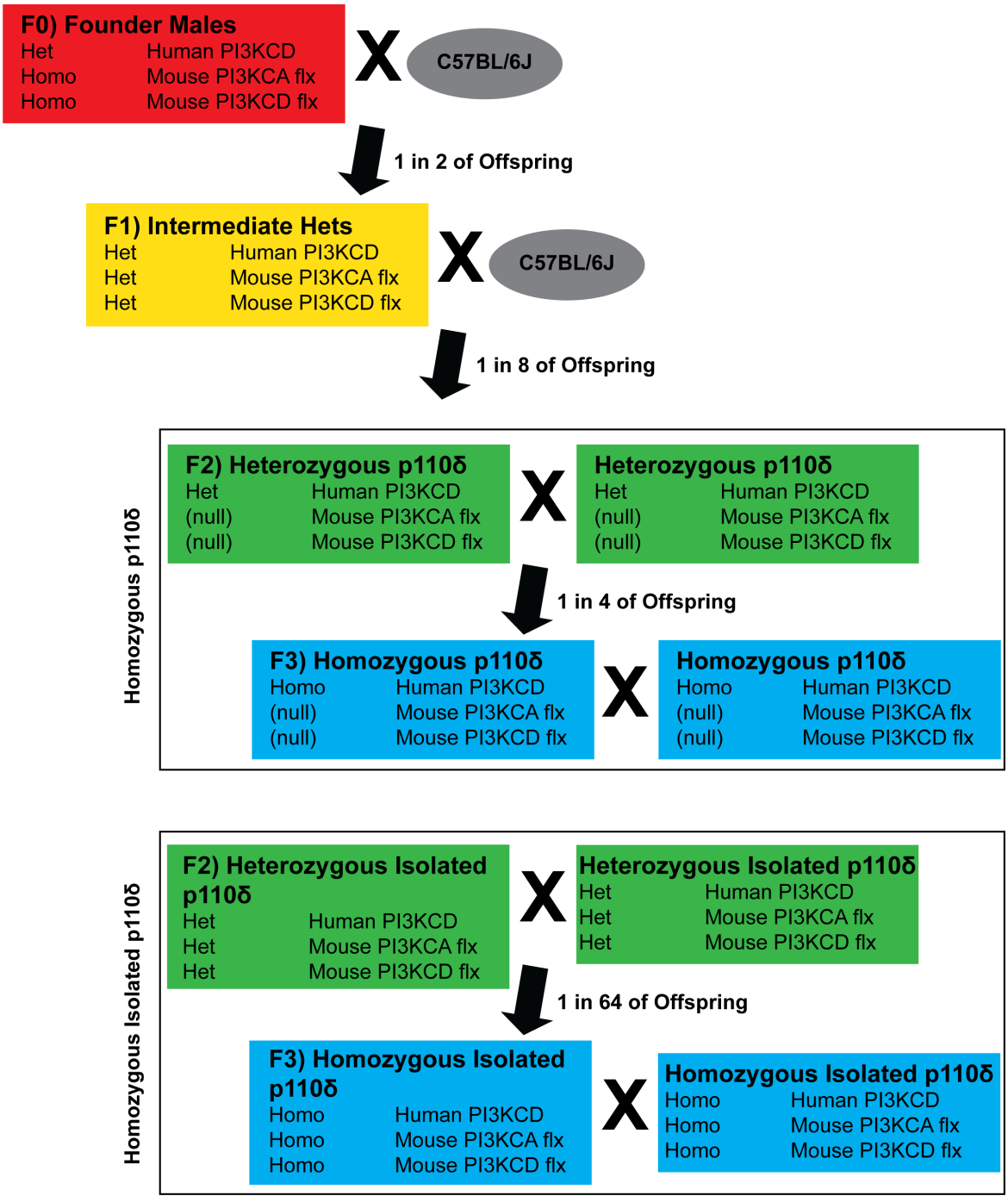

Fig. 3.3 **Breeding strategy for p110δ and isolated p110δ mice.** p110δ mice and isolated p110δ mice were derived from 2 founder males, which were donated by K. Okkenhaug, as shown in the diagram. The breeding strategy had multiple steps, which diverged to produce the two different strains. Het = heterozygous. Homo = homozygous.

Transgene	Primer ID	Primer Sequence
Rosa26 PI3K(p110)	Rosa26 F1 AMQ	GGCTCAGTTGGGCTGTTTTG
	Rosa26 R2 AMQ	TCTGTGGGAAGTCTTGTCCC
	Rosa26 loxP AMQ	GTGGATGTGGAATGTGTGCG
PI3KCA flx	Ma50	CTAAGCCCTTAAAGCCTTAC
	Ma51	CAGCTCCCATCTCAGTTCA
PI3KCD flx	Delta flox F2	CATGCCTACAGTTGATTAAGT
	Delta flox R2	AAGTTCAAAACCAGCTTGATG
	Delta flox R4	TCAGGCCCCAAAGCAGGAAG

Table 3.1 Primers for genotyping PCR reaction

Cycle Step	Temperature	Duration
1. Initial denaturation	94°C	2min
2. Denaturation	94°C	30sec
3. Annealing	65 - 55°C (reducing 0.5°C per cycle)	90sec
4. Extension	72°C	90sec
	repeat steps 2-4	*20 cycles*
5. Denaturation	94°C	30sec
6. Annealing	55°C	90sec
7. Extension	72°C	90sec
	repeat steps 5-7	*20 cycles*
8. Final extension	72°C	5min
9. Hold	4°C	hold

Table 3.2 PCR reaction protocol for genotyping

For each transgene, a separate polymerase chain reaction (PCR) reaction mixture was prepared with 0.5μL of DNA, 12.5μL of GoTaq Hot Start Green Master Mix 2x (Promega, cat no. M512B), 0.5μL of each appropriate primer, and either 6.0μL or 6.5μL of nuclease-free water to give a total volume of 25μL. The PCR reaction protocol is detailed in **Table 3.2**.

10μL of each PCR product was run on a 1% agarose gel, made using Tris/Borate/EDTA (TBE) buffer with 0.01% ethidium bromide, immersed in TBE buffer. 5μL of O'generuler 100bp DNA ladder (Thermo Scientific, cat no. SM1143) was run alongside. Electrophoresis was performed at 100V for 35 minutes. Bands were imaged under ultraviolet light to confirm the presence or absence of the transgenes based on band size.

3.3.3 *In Vitro* Work

Before injecting the viruses *in vivo*, they were tested *in vitro*. Human embryonic kidney (HEK) 293 cells were transfected with AAV2.Cre.GFP (Vector Biolabs, cat no. 7016), AAV2.Cre.GFP (SignaGen Labs, cat no. SL100814), and AAV2.GFP (Vigene Biosciences, cat no. CV10004), as described in **Chapter 2.1**. Two AAV2.Cre.GFP viruses were trialled to see which gave the most GFP signal.

3.3.4 *In Vivo* Work

Viral Validation Work: Retinal Sections

For viral validation work *in vivo*, young adult (6 to 16 weeks old) p110α^{H1047R} mice and p110δ mice received a 2μL intravitreal injection of AAV2.Cre.GFP (Vector Biolabs, cat no. 7016) into the left eye and 2μL of AAV2.GFP (Vigene Biosciences, cat no. CV10004) into the right eye, as described in **Chapter 2.3**. Young adult (6 to 16 weeks old) B6;129S6-Gt(ROSA)26Sor$^{tm14(CAG-tdTomato)Hze}$/J (The Jackson Laboratory, strain no. 007908[97]), referred to in this thesis as "Cre-reporter" mice, received a 2μL intravitreal injection into the left eye of AAV2.Cre.GFP (Vector Biolabs, cat no. 7016). All viruses were injected at a titre of 1.0 x 10^{13}GC/mL, a preoptimised titre for viral intravitreal injections. 2 weeks after injection, the mice were perfused, as described in **Chapter 2.5**.

Whole eyes were collected, post-fixed in 4% paraformaldehyde (PFA) at room temperature for 2 hours, and then transferred to 20% sucrose overnight at 4°C for cryoprotection, as described in **Chapter 2.6.2**. The eyes were then embedded in Tissue-Tek OCT compound and cryosectioned (12μm thick) using a Leica cryostat (Leica Biosystems, CM 3050S Research Cryostat).

For some eyes from the Cre-reporter mice, the retinas were extracted and made into retinal wholemounts (RWMs). These were post-fixed in 4% PFA at room temperature for 2 hours and stored in phosphate-buffered saline (PBS) at 4°C, as described in **Chapter 2.6.3**.

Viral Validation Work: Western Blots

For viral validation work *in vivo*, young adult (6 to 16 weeks old) p110α^{H1047R} mice and p110δ mice received a 2μL intravitreal injection into the left eye of AAV2.Cre.GFP (Vector Biolabs, cat no. 7016) and a 2μL intravitreal injection into the right eye of AAV2.GFP (Vigene Biosciences, cat no. CV10004), as described in **Chapter 2.3**. All viruses were injected at a titre of 1.0 x 10^{13}GC/mL, a preoptimised titre for viral intravitreal injections. A few mice received a 2μL intravitreal injection of PBS into the left eye, while the right

eye was left uninjected (naive). 2 weeks after injection, the mice were culled by a rising concentration of carbon dioxide and cervical dislocation.

Whole eyes were immediately removed, and the retinas were extracted, collected into 1.5mL Eppendorf tubes, and put on dry ice, ready for processing.

Regeneration Studies

For the regeneration work, young adult (6 to 8 weeks old) and aged adult (9 to 12 months old) p110α^{H1047R} mice, p110δ mice, and C57BL/6J mice received a 2μL intravitreal injection of AAV2.Cre.GFP (Vector Biolabs, cat no. 7016) into the left eye, as described in **Chapter 2.3**. 2 weeks after injection, the mice received an ONC injury behind the left eye, as described in **Chapter 2.4**. At 26 days post-ONC, the mice were intravitreally injected with cholera toxin subunit-β with an Alexa Fluor 555 conjugate (CTB-555) (Thermo Fisher Scientific, cat no. C22843), as described in **Chapter 2.3**. At 4 weeks post-ONC, the mice were perfused, as described in **Chapter 2.5**.

The optic nerves were collected, post-fixed in 4% PFA at 4°C overnight, and transferred to 30% sucrose for at least 24 hours for cryoprotection, as described in **Chapter 2.6.1**. The nerves were then cryosectioned (14μm longitudinal sections) using a Leica cryostat (Leica Biosystems, CM 3050S Research Cryostat).

The retinas were collected, and four small incisions were made to form RWMs as described in **Chapter 2.6.3**. RWMs were post-fixed in 4% PFA for 2 hours at room temperature, and then the solution was changed to PBS, ready for immunohistochemistry (IHC).

3.3.5 Immunohistochemistry

IHC in HEK 293 Cells

Having been fixed in 4% PFA, HEK 293 cells were counterstained with DAPI as described in **Chapter 2.7.1**.

Retinal Section Histology

Having been fixed in 4% PFA and sectioned, IHC was performed as described in **Chapter 2.7.2**. IHC against GFP was used to identify the viral tags. IHC against phospho-AKT (pAKT) and pS6 was used to quantify PI3K/AKT/mTOR pathway activity.

Retinal Wholemount Histology

Having been fixed in 4% PFA, RWMs were then stored in PBS at 4°C. IHC against Brn3A, an RGC marker, was performed on RWMs as described in **Chapter 2.7.3**.

3.3.6 Western Blots

Western blots of whole retinal lysate were performed. Immunoblotting against the viral tag, GFP, was used to confirm successful viral transduction and immunoblotting against mTOR pathway markers (pAKT, mTOR and pS6) was used to quantify PI3K/AKT/mTOR pathway activity, as described in **Chapter 2.8**.

3.3.7 Microscopy and Quantification

Viral Validation *In Vitro*

HEK 293 cells transfected with either AAV2.Cre.GFP or AAV2.GFP were counterstained with DAPI. These were imaged by confocal microscopy at x40 magnification. The images were used to confirm that the GFP viral tag was observed and that this signal was not seen in untransfected (naive) cells.

Viral Validation *In Vivo*

Successful viral transduction was confirmed in retinal sections injected with AAV2.Cre.GFP and AAV2.GFP, immunostained for GFP and counterstained with DAPI. The presence of viral tag, GFP, was confirmed, and eye cups were imaged using a Zeiss AxioScan Z1 at x20 magnification (0.22μm/pixel) by the team at the Histopathology/ISH core facility at the Cancer Research UK (CRUK) Cambridge Institute. The RGC layer of retinal sections was imaged using confocal microscopy at x40 magnification.

Viral Validation: Cre-mediated Recombination

The Cre recombinase activity of the AAV2.Cre.GFP virus was validated by injecting the virus in a Cre-reporter mouse line. The RGC layer of retinal sections was imaged by confocal microscopy at x80 magnification, and co-localisation of the tdTomato fluorescence, a result of Cre-mediated recombination, with the GFP viral tag was observed. RWMs were imaged at x20 magnification, and the images were stitched together to show the spread across the retina.

RGC Survival

Percentage RGC survival was calculated as described in **Chapter 2.9.4**. In brief, Brn3A-stained RWMs were imaged at x20 magnification using fluorescence microscopy. For each image, the number of RGCs was quantified using a counting program in Image J Fiji (Fiji-win64). The number of surviving RGCs in the ONC (left) eye was expressed as a percentage relative to the number of RGCs in the uninjured contralateral control (right) eye.

Axon Regeneration

Axon regeneration was calculated as described in **Chapter 2.9.5**. In brief, the CTB-555-labelled axons were visualised using fluorescence microscopy at x40 magnification, counting the number of axons at 0.5mm increments from the crush site. Modelling the nerve as a cylinder, the number of regenerating axons per nerve was calculated at each increment using a previously developed formula. Four sections were counted per nerve and used to average the total number of regenerating axons per nerve.

Axonal sections were imaged using a Zeiss AxioScan Z1 at x40 magnification (0.11μm/pixel) by the Histopathology/ISH core facility at the CRUK Cambridge Institute.

Viral Validation: PI3K/AKT/mTOR Pathway Activation

Western Blots of Whole Retinal Lysate

Whole retinal lysate from eyes injected with either AAV2.Cre.GFP or AAV2.GFP was analysed by immunoblotting. Successful viral transduction from AAV2.Cre.GFP and AAV2.GFP was confirmed by the presence of the viral tag, GFP. Then immunoblotting for PI3K/AKT/mTOR pathway markers (pAKT, mTOR, and pS6) was performed. PBS-injected eyes and naive eyes were also analysed as a control. The pAKT and mTOR signal was quantified using Image J Fiji and expressed relative to the β-actin signal per sample. The average signal relative to β-actin for untransfected (naive) retinas was calculated. All values were then expressed relative to the average for naive eyes.

IHC in Retinal Sections

Retinal sections injected with either AAV2.Cre.GFP or AAV2.GFP and immunostained with either pAKT or pS6 were examined at x40 magnification by fluorescence microscopy, as described in **Chapter 2.9.3**. In brief, 100 GFP-positive RGCs, identified using DAPI and GFP signal from the viral vector, were counted and identified as either positive or negative for pAKT. This was repeated for retinal sections immunostained with pS6. Four mice were counted for each group (100 RGCs per mouse), and the average was expressed as

a percentage of GFP-positive cells co-localised with pAKT or pS6. Representative images were taken at x80 magnification by confocal microscopy.

3.4 Results

3.4.1 ONC Validation

As part of my Ph.D., I spent time mastering several *in vivo* techniques: ear notching, intravitreal injections, optic nerve crush (ONC) injury, cardiac perfusion, intraperitoneal injections, subcutaneous injections, and surgery support for ketamine anaesthesia.

To confirm that I had mastered the ONC injury technique, I performed ONC behind the left eyes of eight C57BL/6J mice. The mice were perfused, and RWMs were collected at 4 weeks post-ONC. IHC against Brn3A, an RGC marker, was used to quantify RGCs. The number of surviving RGCs in the ONC (left) eye was expressed as a percentage relative to the uninjured contralateral control (right) eye. As shown in **Fig. 3.4**, my ONC injury resulted in 4.61%±1.08 (n=8 retinas) RGC survival at 4 weeks post-ONC, which fits with the 5% survival typically seen at this time point.

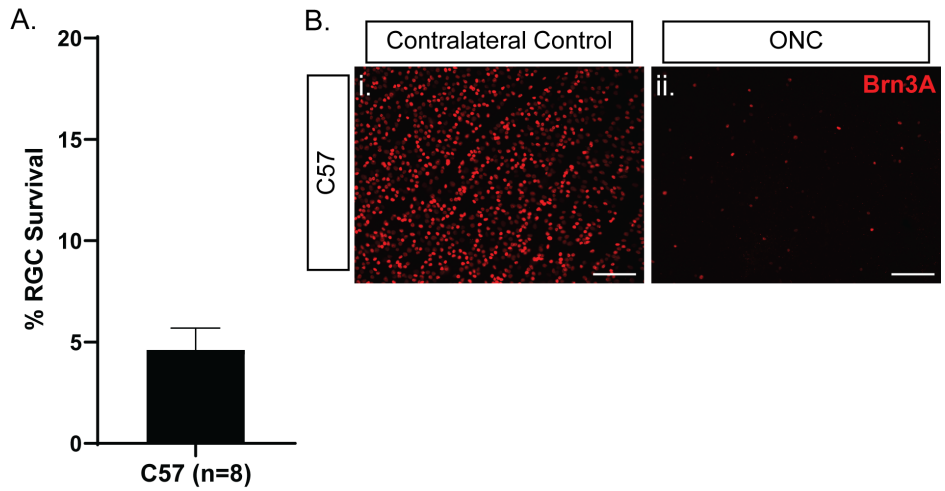

Fig. 3.4 **Validating my ONC injury technique.** Mice received an ONC injury behind the left eye. RWMs were stained with Brn3A (red), which was used to quantify RGCs. The number of RGCs in the ONC (left) eye (panel Bii) was expressed as a percentage survival relative to the uninjured contralateral control (right) eye (panel Bi). My RGC survival of 4.61% at 4 weeks post-ONC fits with the 5% survival typically seen at this time point. n = 8, error bar = SD. Scale bar = 100μm.

3.4.2 Three conditional knock-in PI3K mouse lines were established and maintained

A.R. MacQueen of the K. Okkenhaug lab generated a conditional knock-in PI3K(hyperactive p110α (p110α^{H1047R})) mouse line and a conditional knock-in PI3K(p110δ) mouse line. At the time of thesis submission, neither of these lines had been published. A few of these mice were kindly donated to the Martin-Fawcett lab, from which three conditional knock-in PI3K mouse lines were established and maintained: a hyperactive p110α (p110α^{H1047R}) mouse line, a p110δ mouse line, and an isolated p110δ mouse line. These mice are described in more detail in **Chapter 3.2.3**.

Establishing the conditional knock-in PI3K mouse lines involved genotyping the mice for three transgenes: human Rosa26 p110, mouse PI3KCA flx, which encodes floxed PI3K(p110α), and mouse PI3KCD flx, which encodes floxed PI3K(p110δ). Genomic DNA was extracted from mice by ear notching, and the transgenes were confirmed by PCR, using primers designed by A.R. MacQueen to detect specific sequences within each transgene.

The genotypes of the mouse lines are summarised in **Table 3.3**. PCR for human Rosa26 p110 was performed with the following three primers: GGCTCAGTTGGGCTGTTTTG, TCTGTGGGAAGTCTTGTCCC, and GTGGATGTGGAATGTGTGCG. The homozygous knock-in allele is 606 base pairs (bp), and the homozygous wildtype allele is 359 bp. All three mouse lines are homozygous for the knock-in allele and mice with the expected 606bp band were selected.

PCR for mouse PI3KCA flx was performed with the following primer pair: CTAAGCCCTTAAAGCCTTAC and CAGCTCCCATCTCAGTTCA. The homozygous knock-in allele is 591 bp, and the homozygous wildtype allele is 527 bp. PCR for mouse PI3KCD flx was performed with the following three primers: CATGCCTACAGTTGATTAAGT, AAGTTCAAAACCAGCTTGATG, and TCAGGCCCCAAAGCAGGAAG. The homozygous knock-in allele is 477 bp, and the homozygous wildtype allele is 361 bp. The isolated p110δ mice are homozygous for both knock-in alleles and mice with the expected 591bp and 477bp bands were selected. Mouse PI3KCA flx and mouse PI3KCD flx were bred out of the p110δ mice, making them homozygous for the wildtype allele, and mice with the expected 527bp and 361bp bands were selected.

Examples of DNA gels showing the products of the genotyping PCR reactions are shown in **Fig. 3.5**. Mice with the desired genotype were identified and bred to maintain a colony.

Transgene	Knock-in (KI) allele band size	Wildtype (WT) allele band size	p110α^{H1047R} mice	p110δ mice	isolated p110δ mice
Human Rosa26 p110	603bp	359bp	KI	KI	KI
Mouse PI3KCA flx	591bp	527bp	WT	WT	KI
Mouse PI3KCD flx	477bp	361bp	WT	WT	KI

Table 3.3 Genotypes of conditional knock-in PI3K mice

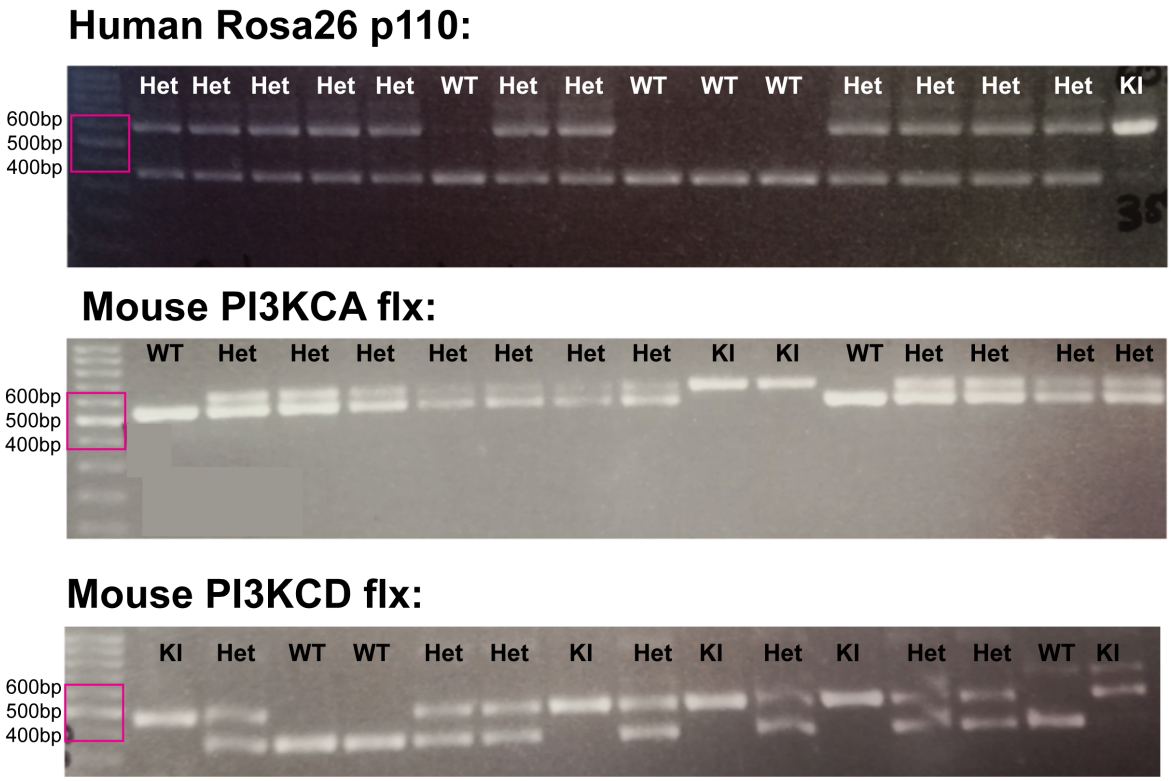

Fig. 3.5 **Genotyping to establish three conditional knock-in PI3K mouse lines.** DNA gels are shown with the products of the genotyping PCR reactions, which were designed to detect specific sequences from each of the three transgenes: human Rosa26 p110, mouse PI3KCA flx and mouse PI3KCD flx. KI denotes homozygous for knock-in allele, WT denotes homozygous for wildtype allele, Het denotes heterozygous.

3.4.3 Viral Validation

AAV2.Cre.GFP and AAV2.GFP successfully transfected HEK 293 cells *in vitro*

Before using the AAV2.Cre.GFP and AAV2.GFP viruses *in vivo*, successful viral transfection was confirmed *in vitro* using HEK 293 cells, as shown in **Fig. 3.6**. Signal from the viral tag, GFP, was detected from all viruses. AAV2.Cre.GFP (Vector Biolabs, cat no. 7016) gave noticeably stronger GFP signal than AAV2.Cre.GFP (SignaGen Labs, cat no. SL100814) so this virus was used *in vivo*.

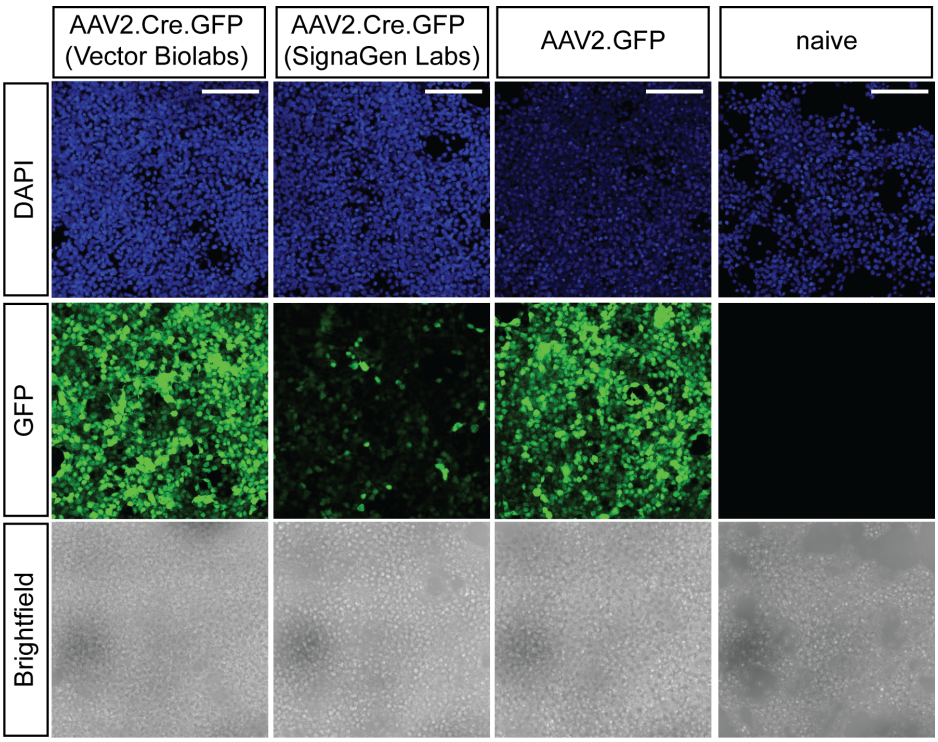

Fig. 3.6 **AAV2.Cre.GFP and AAV2.GFP were tested *in vitro*.** Two AAV2.Cre.GFP viruses and one AAV2.GFP virus were tested in HEK 293 cells prior to *in vivo* work. The presence of GFP signal indicates successful transfection. AAV2.Cre.GFP from Vector Biolabs gave a stronger signal than AAV2.Cre.GFP from SignaGen Labs. Scale bar = 100μm.

AAV2.Cre.GFP and AAV2.GFP successfully transduced RGCs *in vivo*

Viral transduction of RGCs was tested *in vivo*. Young adult (6 to 16 weeks old) p110α^{H1047R} mice and p110δ mice were injected intravitreally with 2μL of AAV2.Cre.GFP in the left eye and 2μL of AAV2.GFP in the right eye. The eyes were collected 2 weeks later, and 12μm retinal sections were produced.

Successful viral transduction of AAV2.Cre.GFP and AAV2.GFP *in vivo* was confirmed by signal from the viral tag, GFP, in the RGC layer. Eye cup images showed signal throughout the retina, and closer inspection of the retinal sections confirmed that this signal was in the RGC layer, as shown in **Fig. 3.7** where staining was indicative of RGCs.

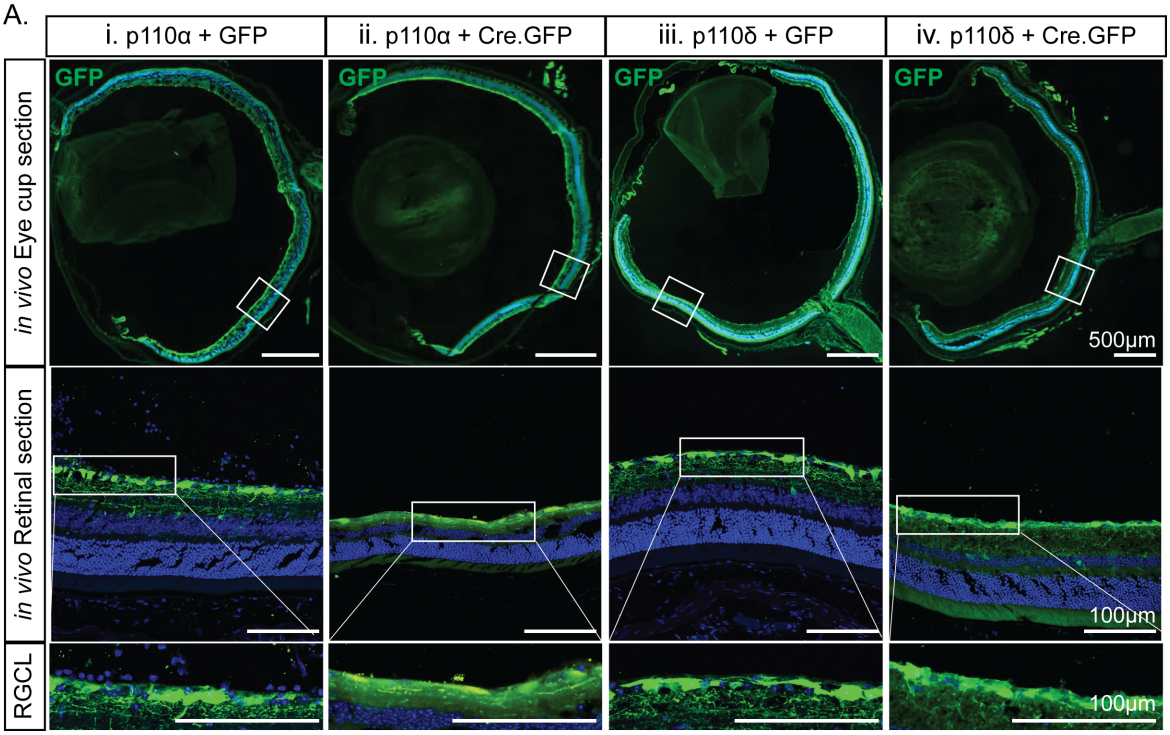

Fig. 3.7 **Successful viral transduction of AAV2.Cre.GFP and AAV2.GFP was confirmed *in vivo***. In panel A, eye cups and zoomed in images of the RGC layer showed GFP signal in the RGC layer throughout the retina for AAV2.Cre.GFP (Aii and iv) and AAV2.GFP (Ai and Aiii) in both p110α^{H1047R} and p110δ mice. Staining was indicative of RGCs. Scale bar = 500μm for eye cups, 100μm for retinal sections.

The Cre recombinase activity of AAV2.Cre.GFP was confirmed in RGCs *in vivo*

The Cre recombinase activity of AAV2.Cre.GFP was tested in RGCs *in vivo* using a tdTomato Cre-reporter mouse line. Young adult (6 to 16 weeks old) Cre-reporter mice were injected intravitreally with 2μL of AAV2.Cre.GFP in the left eye. The eyes were collected 2 weeks later, and both RWMs and 12μm retinal sections were produced.

The tdTomato fluorescence produced as a result of Cre-mediated recombination was seen throughout the retina in RWMs, as shown in **Fig. 3.8**. On closer inspection of the RGC layer in retinal sections, co-localisation of tdTomato fluorescence (red) with GFP signal from the virus (green) was confirmed. Staining in the RGC layer was indicative of RGCs.

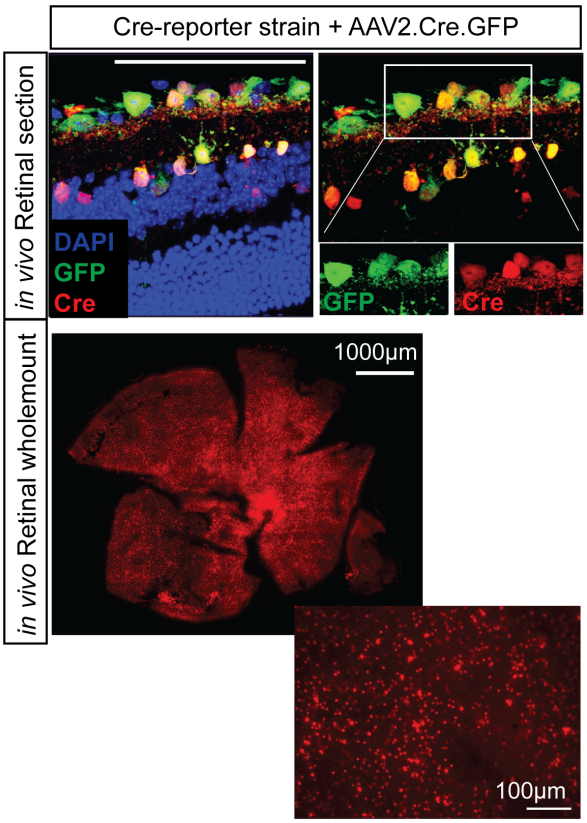

Fig. 3.8 **The Cre recombinase activity of AAV2.Cre.GFP was confirmed *in vivo*.** The Cre recombinase activity of AAV2.Cre.GFP was confirmed using a Cre-reporter mouse line. tdTomato fluorescence, resulting from Cre-mediated recombination, was seen throughout the retina in RWMs and within RGCs in retinal sections. Staining in the RGC layer was indicative of RGCs. Scale bar = 100μm, and 1000μm for full RWM.

3.4.4 RGC Survival and Axon Regeneration

Young adult (6 to 8 weeks old) and aged adult (9 to 12 months old) p110α^{H1047R} mice, p110δ mice, and C57BL/6J mice were intravitreally injected with 2μL of AAV2.Cre.GFP into the left eye. 2 weeks later, ONC surgery was performed. At 26 days post-ONC, 2μL of cholera toxin subunit-β with an Alexa Fluor 555 conjugate (CTB-555) was intravitreally injected into the left eye. At 4 weeks post-ONC, the eyes and optic nerves were collected, as summarised in **Fig. 3.9**.

Please note that all regeneration experiments in the p110α^{H1047R} mice were not carried out as part of this thesis, but the results have been provided here for completeness (credit to A.C. Barber, C.S. Pearson, and J. Cave).

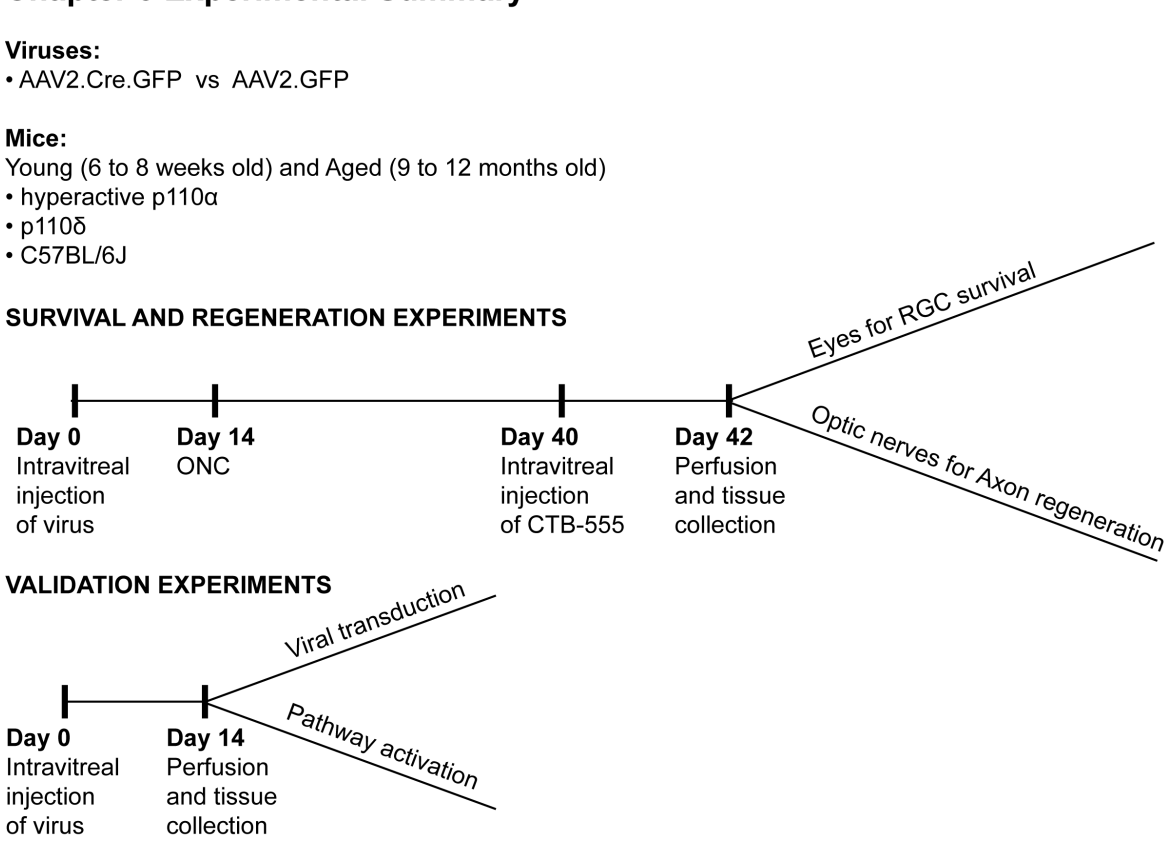

Fig. 3.9 **Chapter 3 Experimental Summary**

Transgenic PI3K upregulation via activation of p110α^{H1047R} or of p110δ promoted RGC survival in young adult (6 to 8 weeks old) mice. p110α^{H1047R} also promoted survival in aged adult (9 to 12 months old) mice.

The retinas were collected at 4 weeks post-ONC and IHC against Brn3A, an RGC marker, was used to quantify RGCs. The number of surviving RGCs in the ONC (left) eye was expressed as a percentage relative to the uninjured contralateral control (right) eye.

In the young adults (6 to 8 weeks old), the AAV2.Cre.GFP-treated p110α^{H1047R} mice showed 10.7%±4.5 (n=10 retinas) RGC survival at 4 weeks post-ONC and the AAV2.Cre.GFP-treated p110δ mice showed 11.4%±5.8 (n=6 retinas) RGC survival. Both groups were significantly higher than the AAV2.Cre.GFP-treated C57BL/6J mice, which showed 5.6%±2.1 (n=7 retinas) RGC survival (see **Fig. 3.10**, one-way ANOVA with Tukey's post-hoc analysis, p=0.0464 for p110α^{H1047R} and p=0.0478 for p110δ). There was no significant difference between the two mouse lines. Therefore, transgenic PI3K upregulation via activation of p110α^{H1047R} or of p110δ promoted RGC survival at 4 weeks post-ONC.

In the aged adults (9 to 12 months old), the AAV2.Cre.GFP-treated C57BL/6J mice showed 4.5%±2.7 (n=6 retinas) RGC survival, which was not significantly different from the 5.6%±2.1 (n=7 retinas) seen in young mice, as shown in **Fig. 3.11**.

The AAV2.Cre.GFP-treated p110α^{H1047R} mice showed 12.8%±4.8 (n=4 retinas) RGC survival at 4 weeks post-ONC and the AAV2.Cre.GFP-treated p110δ mice showed 4.5%±2.3 (n=7 retinas) RGC survival. The p110α^{H1047R} mice were significantly higher than the AAV2.Cre.GFP-treated C57BL/6J mice, which showed 4.5%±2.7 (n=6 retinas) RGC survival (one-way ANOVA with Tukey's post-hoc analysis, $p < 0.0001$), whereas the p110δ mice were not (see **Fig. 3.11**). In addition, the p110α^{H1047R} mice showed significantly higher survival than the p110δ mice (one-way ANOVA with Tukey's post-hoc analysis, $p < 0.0001$). No significant difference was found between young and aged p110α^{H1047R} mice. Therefore, transgenic PI3K upregulation via activation of p110α^{H1047R} promoted RGC survival in both young and aged adult mice at 4 weeks post-ONC. While activation of p110δ promoted RGC survival in young adult mice, it had no significant effect in aged mice.

Transgenic PI3K upregulation via activation of p110α^{H1047R} or of p110δ promoted axon regeneration in young adult (6 to 8 weeks old) and aged (9 to 12 months old) mice

2 days before tissue collection, the left eyes were intravitreally injected with 2μL of CTB-555. At 4 weeks post-ONC, the optic nerves were dissected, and 14μm longitudinal sections were produced. Axons were counted using the CTB-555 fluorescence at 0.5mm increments.

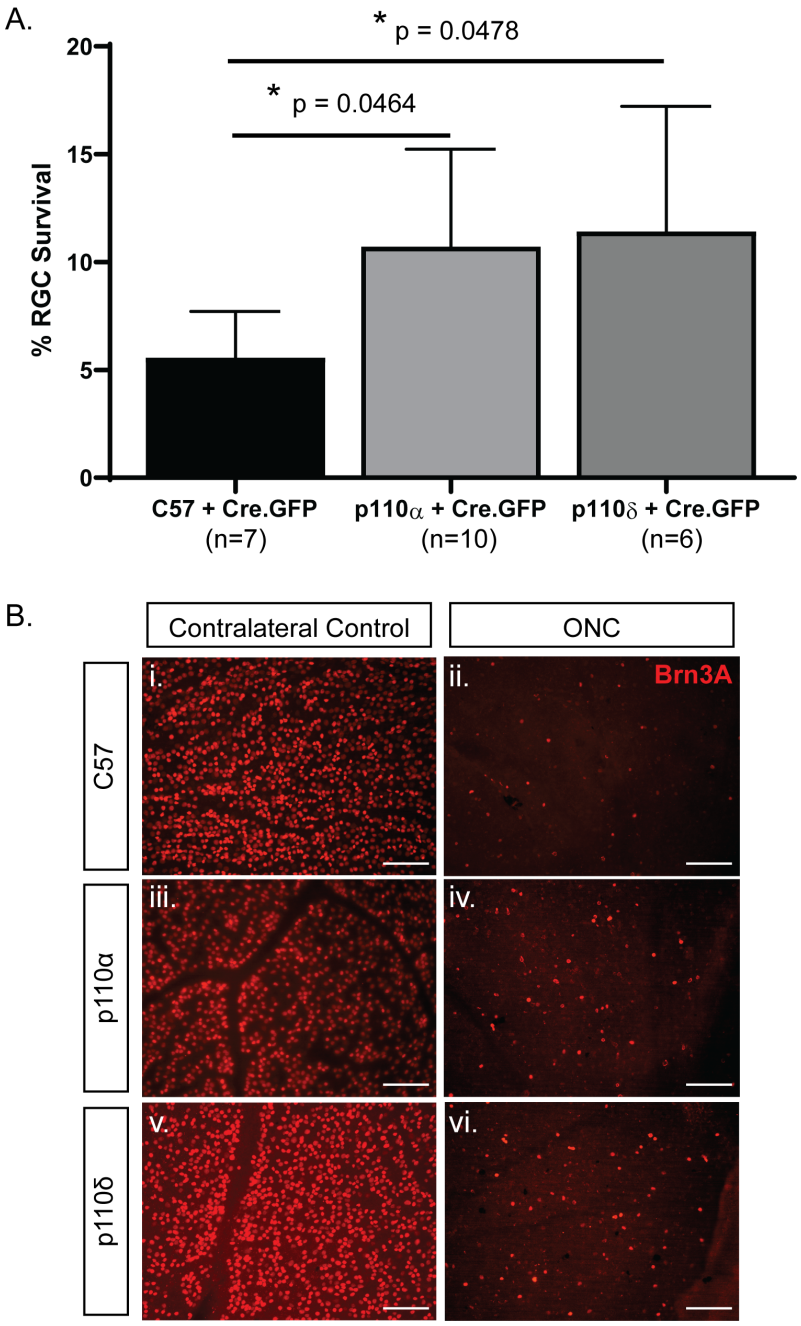

Fig. 3.10 **Transgenic PI3K upregulation via activation of p110α^{H1047R} or of p110δ promoted RGC survival in young mice.** As seen in panel A, activation of p110α^{H1047R} or p110δ using AAV2.Cre.GFP promoted RGC survival 4 weeks post-ONC injury. RWMs were stained with Brn3A (red), which was used to quantify RGCs. The number of RGCs in the ONC (left) eye (panels Bii, Biv, and Bvi) was expressed as a percentage survival relative to the uninjured contralateral control (right) eye (Bi, Biii, and Bv). p values measured by one-way ANOVA with Tukey's post-hoc analysis, n = 6 to 10 as specified, error bars = SD. Scale bar = 100μm. p110α^{H1047R} data provided by A.C. Barber, C.S. Pearson, J. Cave.

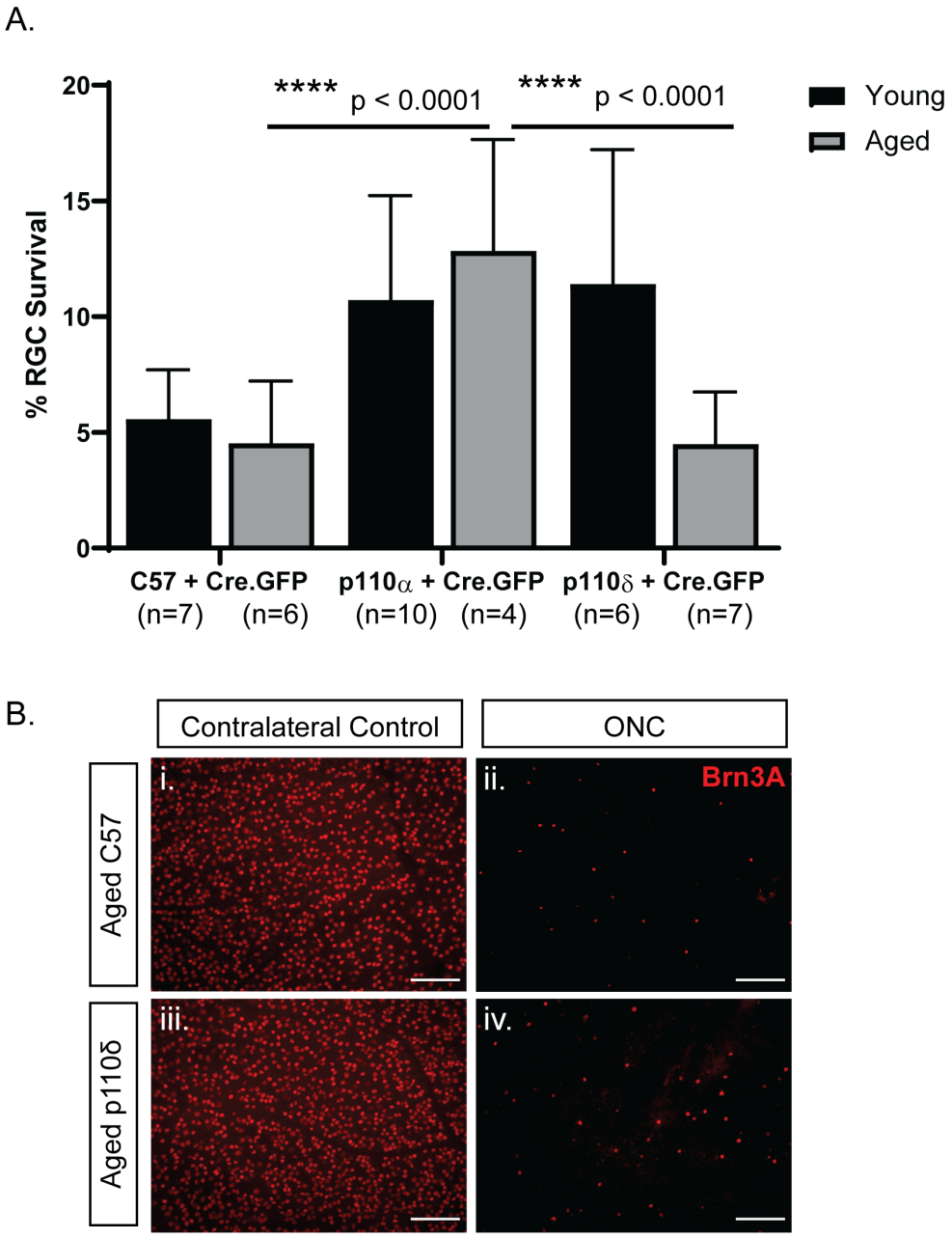

Fig. 3.11 **Transgenic PI3K upregulation via activation of p110α^{H1047R} promoted RGC survival in aged mice, but p110δ had no significant effect.** As seen in panel A, activation of p110α^{H1047R} using AAV2.Cre.GFP promoted RGC survival 4 weeks post-ONC injury in aged mice, but p110δ had no significant effect. RWMs were stained with Brn3A (red), which was used to quantify RGCs. The number of RGCs in the ONC (left) eye (panels Bii and Biv) was expressed as a percentage survival relative to the uninjured contralateral control (right) eye (Bi and Biii). p values measured by one-way ANOVA with Tukey's post-hoc analysis to compare aged data, n = 4 to 10 as specified, error bars = SD. Scale bar = 100μm. p110α^{H1047R} data provided by A.C. Barber, C.S. Pearson, J. Cave.

In the young adults (6 to 8 weeks old), the AAV2.Cre.GFP-treated p110α^{H1047R} mice showed 72±45 regenerating axons (n=11 nerves) at 0.5mm from the crush site, and the p110δ mice showed 61±35 axons (n=6 nerves), as shown in **Fig. 3.12**. This was a significant increase compared to 19±23 axons (n=15 nerves) in the control (two-way ANOVA with Tukey's post-hoc analysis, $p < 0.0001$ for p110α^{H1047R} and $p < 0.0001$ for p110δ). No significant differences were seen between the two mouse lines. Therefore, transgenic PI3K upregulation via activation of p110α^{H1047R} or of p110δ promoted axon regeneration at 4 weeks post-ONC.

In the aged adults (9 to 12 months old), the AAV2.Cre.GFP-treated C57BL/6J mice showed 3±2 regenerating axons (n=17 nerves), which was significantly less than the 19±23 axons (n=15 nerves) in the young mice (two-tailed T-test, $p<0.0001$) as shown in **Fig. 3.13**. Therefore, aged C57BL/6J mice have lower regenerative potential than young mice, as has previously been shown in the literature.

The AAV2.Cre.GFP-treated p110α^{H1047R} mice showed 19±9 regenerating axons (n=4 nerves) at 0.5mm from the crush site, which was significantly less than the 72±45 axons in the young mice (two-tailed T-test, p=0.0248), but more than the 3±2 axons (n=17 nerves) in the aged control (one-way ANOVA with Tukey's post-hoc analysis, p=0.0106). The AAV2.Cre.GFP-treated p110δ mice showed 20±17 axons (n=7 nerves) at 0.5mm from the crush site, which was significantly less than the 61±35 axons in the young mice (two-tailed T-test, p=0.0200), but more than the 3±2 axons (n=17 nerves) in the aged control (one-way ANOVA with Tukey's post-hoc analysis, p=0.0007). This difference between young and aged adult mice fits with our data from the C57BL/6J mice and the literature, showing significantly less regeneration. No significant difference was found between the two mouse lines. Therefore, transgenic PI3K upregulation via activation of p110α^{H1047R} or of p110δ promoted axon regeneration in aged mice at 4 weeks post-ONC, but to a lesser extent than in young adult mice.

3.4.5 mTOR Pathway Activation

The regeneration data showed that activation of p110α^{H1047R} and p110δ by Cre-mediated recombination promoted both RGC survival and axon regeneration. To validate that this was due to activation of PI3K, PI3K/AKT/mTOR pathway activity was assessed.

RGCs could not be successfully isolated

In mice, RGCs account for less than 1% of total retinal cells[47, 103]. Therefore, we planned to isolate RGCs from the retina to more accurately assess their mTOR pathway activation.

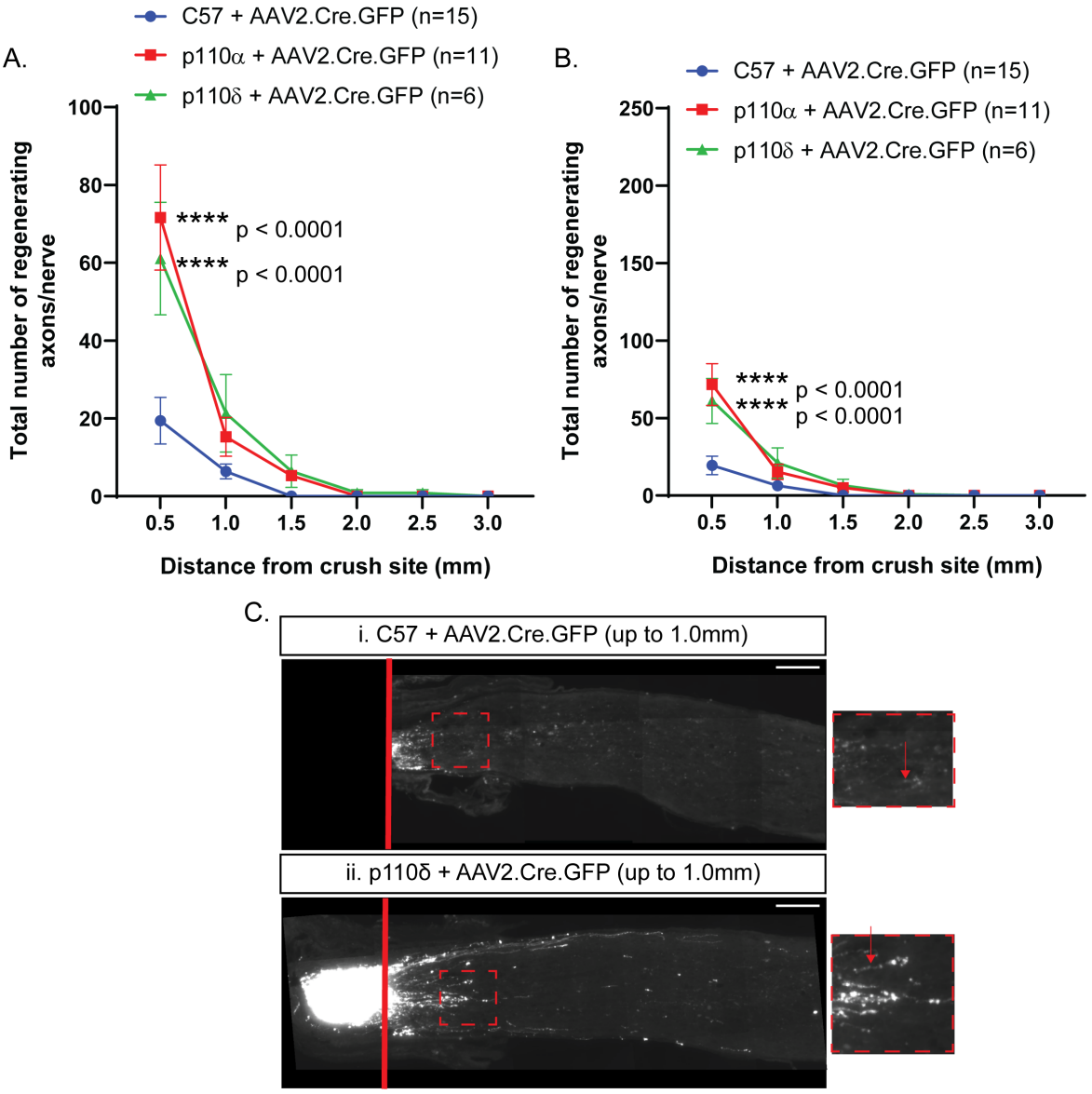

Fig. 3.12 **Transgenic PI3K upregulation via activation of p110α^{H1047R} or of p110δ promoted axon regeneration.** As shown in panel A, transgenic PI3K upregulation via activation of p110α^{H1047R} or of p110δ promoted axon regeneration following ONC injury. The same graph but with a different scale for comparison to other chapters is shown in panel B. Images of crushed nerves are shown in panel C for AAV2.Cre.GFP in C57BL/6J (Ci) and AAV2.Cre.GFP in p110δ (Cii). p values measured by two-way ANOVA with Tukey's post-hoc analysis, n = 6 to 15 as specified, error bars = SEM. Scale bar = 100μm. p110α^{H1047R} data provided by A.C. Barber, C.S. Pearson, J. Cave.

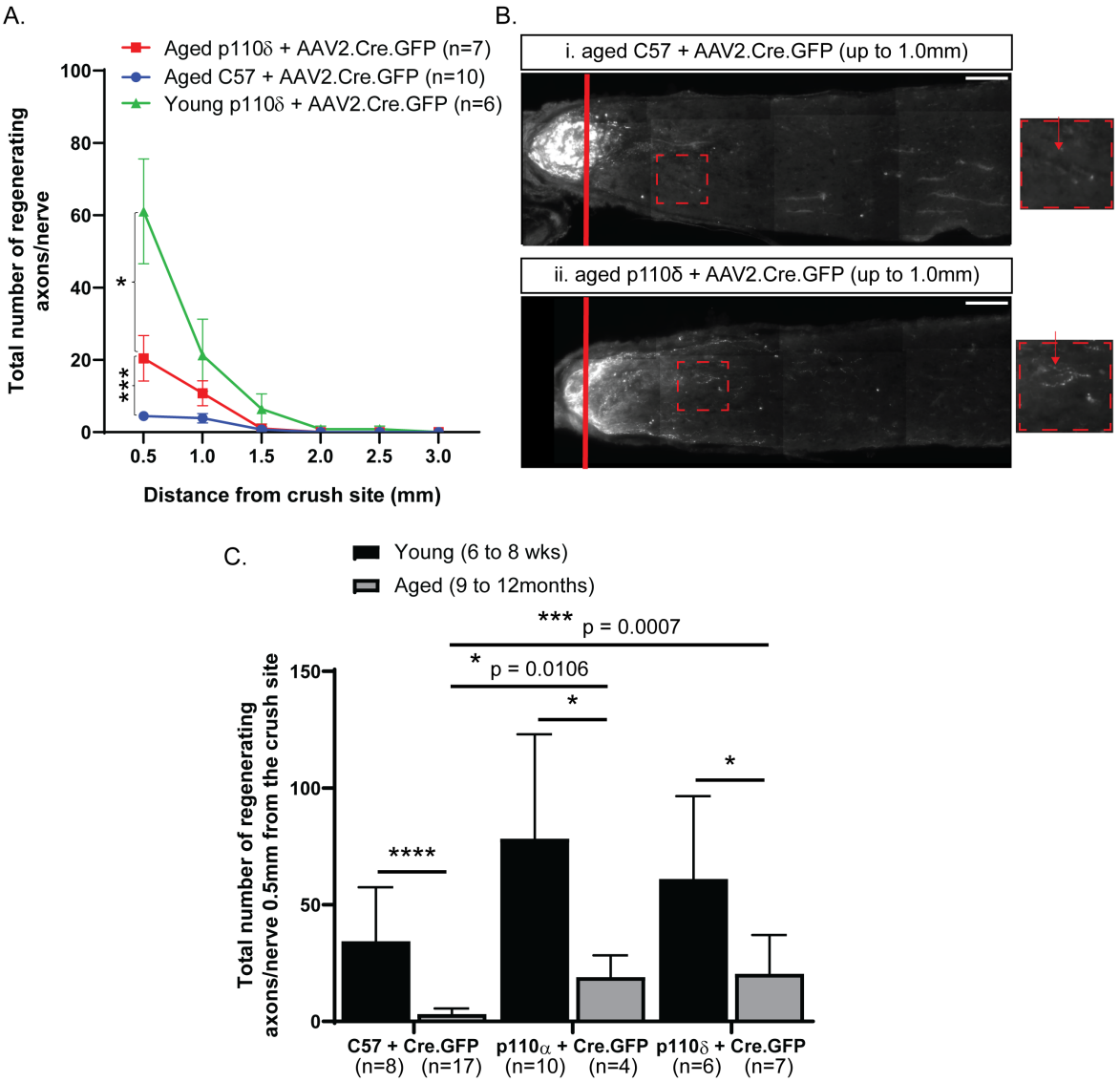

Fig. 3.13 **Transgenic PI3K upregulation via activation of p110α^{H1047R} or of p110δ promoted axon regeneration in aged mice, although less so than young mice.** As shown in panel A, aged p110δ mice promote axon regeneration following ONC injury compared to aged controls, but less so than young p110δ mice. Images of crushed nerves are shown in panel B for AAV2.Cre.GFP in aged C57BL/6J (Bi) and AAV2.Cre.GFP in aged p110δ mice (Bii). Summary data in panel C shows that transgenic PI3K upregulation via activation of p110α^{H1047R} or of p110δ promoted axon regeneration in aged mice, but to a lesser extent than in young mice. p values measured by two-way ANOVA (graph A) and one-way ANOVA (graph C: comparing aged data) with Tukey's post-hoc analysis and two-tailed T-test (graph C: comparing young and aged data within each strain), n = 4 to 17 as specified, error bars = SEM (graph A) and SD (graph C). Scale bar = 100μm. p110α^{H1047R} data provided by A.C. Barber, C.S. Pearson, J. Cave.

Within the lab, immunopanning, microbead isolation, fluorescence-activated cell sorting, and laser capture microdissection were tried. However, a reliable RGC isolation method with enough yield to analyse was not found, so whole retinal tissue had to be assessed.

mTOR pathway activation could not be confirmed using western blots of whole retinal lysate

Immunoblotting against the viral tag, GFP, and against mTOR pathway markers (pAKT, mTOR, and pS6) was performed on whole retinal lysate using the western blot technique, as seen in **Fig. 3.14**. As expected, GFP signal was seen from the AAV2.Cre.GFP and AAV2.GFP viruses, but not from PBS-injected or naive eyes. This confirmed successful viral transduction. The GFP signal of AAV2.Cre.GFP was fainter than that of the AAV2.GFP. This was not a surprise because the GFP of AAV2.Cre.GFP is under the control of a second promoter, which can result in lower expression levels.

pS6 was detected in the positive control, which was HEK 293 cells transfected with a virus known to increase pS6 levels. However, this could not be detected in the whole retinal lysate, even with increasing antibody concentration and exposure times. pAKT and mTOR were detected, but the signal was variable, and no clear pattern was seen. As mentioned, RGCs only make up less than 1% of retinal cells, so any potential changes in mTOR pathway marker proteins were too diluted to detect.

mTOR pathway activation was confirmed in retinal sections using IHC

IHC against mTOR pathway markers (pAKT and pS6) was performed on the retinal sections used for viral validation, as shown in **Fig. 3.15**. The percentage of GFP-labelled cells in the RGC layer co-localised with either pAKT or pS6 was quantified and compared to control injection. Staining was indicative of RGCs.

In p110α^{H1047R} mice, eyes injected with AAV2.GFP showed 23.8%±4.2 pAKT-GFP-labelled cells, which increased to 62.3%±5.3 in AAV2.Cre.GFP-injected eyes (one-tailed T-test, $p<0.0001$). The average fold change in pAKT was 2.70±0.63. Eyes injected with AAV2.GFP showed 45.3%±6.8 pS6-GFP-labelled cells, which increased to 80.0%±5.4 in AAV2.Cre.GFP-injected eyes (one-tailed T-test, $p=0.0010$). The average fold change in pS6 was 1.79±0.21.

In p110δ mice, eyes injected with AAV2.GFP showed 21.5%±3.9 pAKT-GFP-labelled cells, which increased to 53.3%±8.7 in AAV2.Cre.GFP-injected eyes (one-tailed T-test, $p=0.0003$). The average fold change in pAKT was 2.49±0.22. Eyes injected with AAV2.GFP

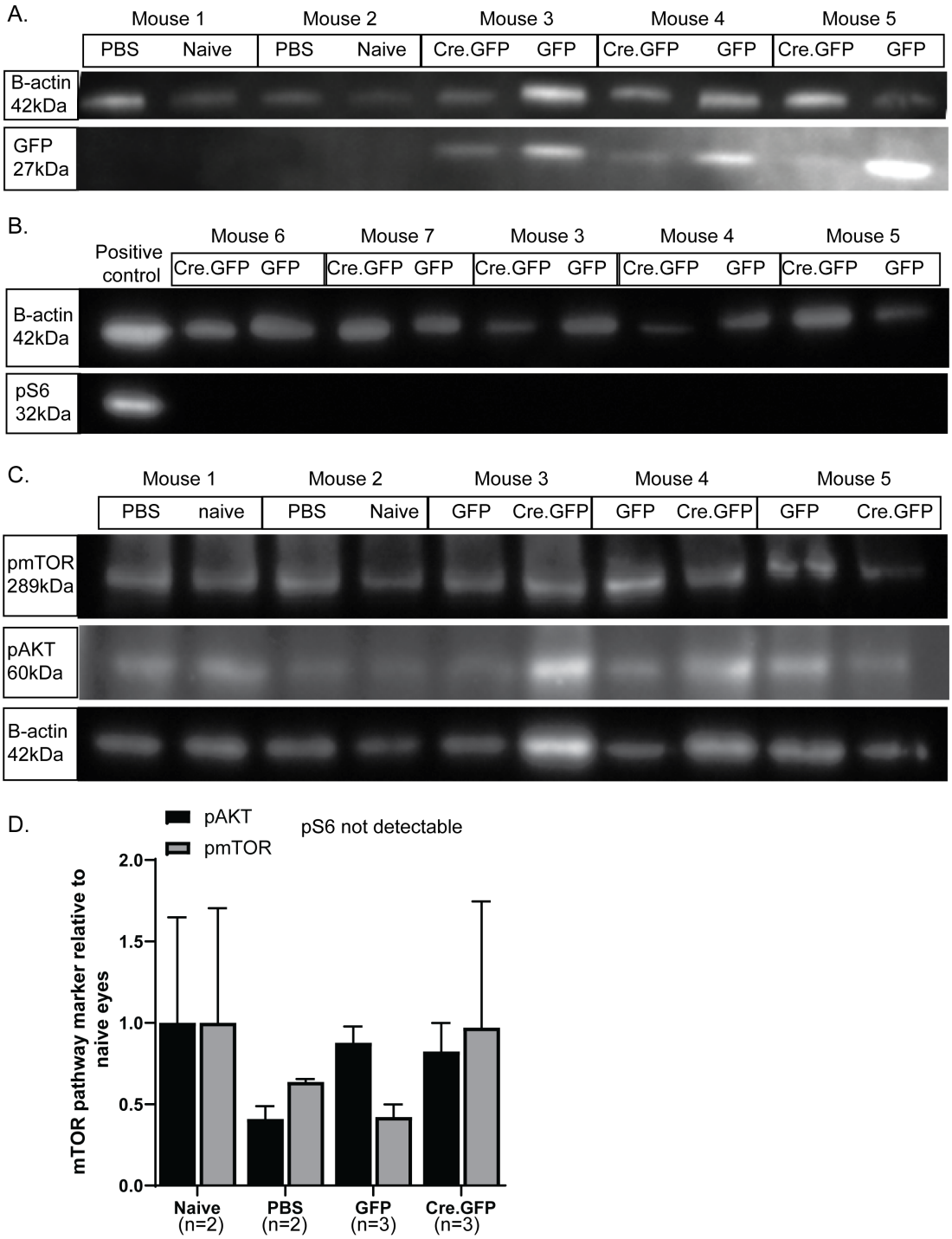

Fig. 3.14 **mTOR pathway activation could not be verified in western blots of whole retinal lysate *in vivo***. GFP signal from the viral tag was observed in AAV2.Cre.GFP- and AAV2.GFP-treated whole retinal lysate, as shown in panel A. The western blots in panels B and C and the graph in panel D, show that a clear pattern in pAKT or mTOR signal could not be detected, and pS6 could not be detected at all. p values measured by one-way ANOVA with Tukey's post-hoc analysis, n = 2 to 3 as specified, error bars = SD.

showed 42.3%±2.2 pS6-GFP-labelled cells, which increased to 64.5%±6.8 in AAV2.Cre.GFP-injected eyes (one-tailed T-test, p=0.0004). The average fold change in pS6 was 1.52±0.10.

The raw percentage of pS6-GFP-labelled cells in AAV2.Cre.GFP-treated eyes was significantly greater in p110α^{H1047R} mice compared to p110δ mice (two-tailed T-test, p=0.0116). However, no significant difference was found between the two mouse lines when looking at the fold change in pAKT and pS6 signal.

Therefore, activation of PI3K and the downstream activation of the PI3K/AKT/mTOR pathway was confirmed to result from Cre-mediated recombination in the conditional knock-in mice.

3.5 Discussion

Using viral Cre-mediated recombination in conditional knock-in PI3K mouse lines, PI3K was upregulated through activation of hyperactive p110α (p110α^{H1047R}) and p110δ. Both were shown to significantly promote RGC survival and axon regeneration in young adult mice following ONC injury, with no difference between the two isoforms. It should be noted that the p110α^{H1047R} and p110δ *in vivo* experiments were carried out at different times. However, the results obtained fit with the *in vitro* data, which showed no difference between the two isoforms in CNS neuron regeneration.

Both p110α^{H1047R} and p110δ were also shown to promote axon regeneration in aged mice, although to a lesser extent than in young mice. Aged C57BL/6J mice were shown to have lower regenerative potential than young C57BL/6J mice, which fits with the literature[34]. No difference between the two isoforms was seen.

Interestingly, only p110α^{H1047R} promoted RGC survival in aged mice. This could be due to the p110α^{H1047R} and p110δ data being collected at different times or the low n number for the aged p110α^{H1047R} data (n=4). From the *in vitro* data in DRG neurons, p110α was demonstrated to be essential for regeneration in both the soma and axons, whereas p110δ was only required in the axon. Perhaps this explains why the RGCs, in other words the soma, survived better under p110α^{H1047R} than under p110δ, while no difference was in the axon regeneration data.

The observed pro-regenerative effects were shown to be at least in part due to upregulation of the PI3K/AKT/mTOR pathway. Unfortunately, we were unable to isolate RGCs to assess mTOR pathway activation, so this was shown using IHC in whole retina, as in previous literature. To quantify this, pAKT and pS6 positive cells were counted. If this were to be examined more thoroughly, the fluorescence levels of pAKT and pS6 in RGCs could be compared between the treatment and control groups. Previous work looking at PTEN

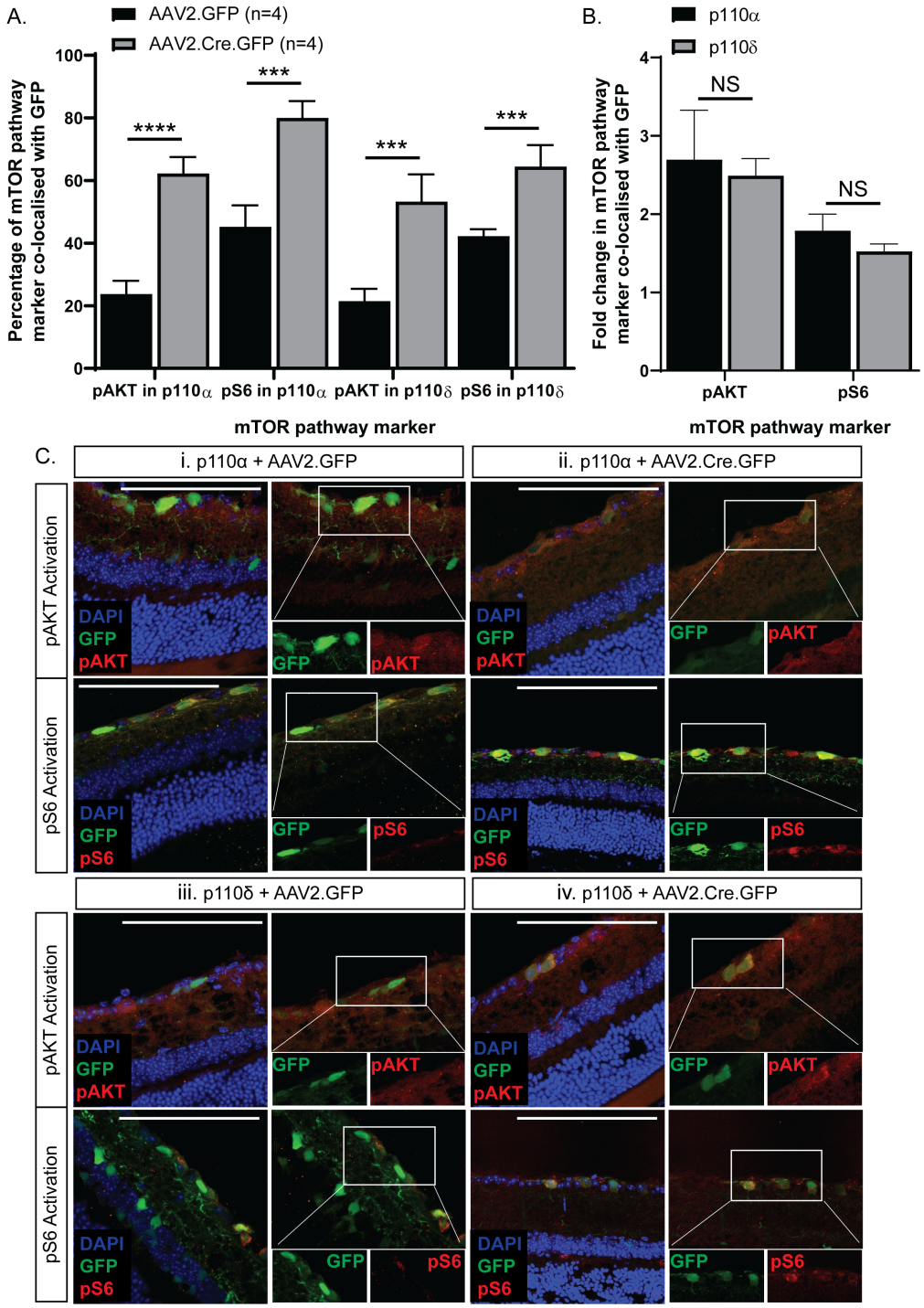

Fig. 3.15 **Transgenic PI3K upregulation via activation of p110α^{H1047R} or of p110δ resulted in increased mTOR pathway activity *in vivo*.** As shown in the graphs in panels A and B, pAKT and pS6 signal increased in AAV2.Cre.GFP-treated eyes compared to AAV2.GFP-treated eyes. Representative images are shown in panel C. Staining in the RGC layer was indicative of RGCs. p values measured by one-tailed T-test, n = 4, errors bars = SD. Scale bar = 100μm.

deletion had demonstrated the role of the mTOR pathway, both by using rapamycin, an mTOR pathway inhibitor, and by conditional knockout of a negative regulator of the mTOR pathway, tuberous sclerosis complex I (TSC1)[79]. The effect of rapamycin on regeneration in these conditional knock-in PI3K mice could be investigated to see to what extent this neutralised the effects seen.

Further work using the conditional knock-in PI3K mice could look at combining the p110α^{H1047R} and p110δ isoforms by crossing the two strains. Leading on from the transgenic work, a more translatable approach was developed using a viral vector for PI3K(p110δ). Unfortunately, as a commonly mutated cancer gene, the p110α^{H1047R} isoform was deemed too unsafe for viral work. In addition, the effect of targeting PI3K was compared to PTEN knockdown. These results are covered in **Chapter 4**.

Chapter 4

Viral Manipulation of the PI3K Pathway and its Effects on Axon Regeneration

4.1 Declaration

The work presented in **Chapters 3 and 4** of this thesis has been submitted to EMBO Molecular Medicine for publication. At the time of thesis submission, we are responding to reviewers' comments. This work is cited in the thesis as: *Barber, A.C., ****Evans, R.S.***, *Nieuwenhuis, B., Pearson, C.S., Fuchs, J., MacQueen, A.R., van Erp, S., Hänzi, B., Hulshof, L-A., Osborne, A., Conceição, R., Deshpande, S.S., Cave, J., ffrench-Constant, C., Smith, P.D., Okkenhaug, K., Eickholt, B.J., Martin, K.R., Fawcett, J.W., and Eva, R. (2020), PI3 kinase delta enhances axonal PIP3 to support axon regeneration in the adult CNS (not yet published). * = the authors contributed equally.

The phosphoinositide 3-kinase (PI3K) *in vitro* data from this paper is summarised in **Chapter 3.2**, and the transgenic PI3K *in vivo* data is presented in **Chapter 3.4**. Acknowledgments are covered in that chapter's declaration.

The viral phosphatase and tensin homolog (PTEN) knockdown and viral PI3K upregulation *in vivo* data from this paper is presented in the results section of this chapter. The data in this chapter was generated by me, under the supervision of A.C. Barber, with contributions from others declared below.

Viruses: The AAV2.shPTEN.GFP virus was kindly donated by Z. He. The AAV2.PI3K(p110δ) virus was generated by B. Hänzi, A. Osborne and L-A. Hulshof.

***In vitro* data (Fig 4.3A&C and Fig 4.4A&C):** R. Conceição quantified PTEN and PI3K levels in human embryonic kidney (HEK) 293 cells transfected with these viruses. While I was not involved in measuring the PTEN and PI3K levels *in vitro*, the data is presented in the

results section of this chapter alongside my *in vivo* data for completeness, with appropriate referencing in the text.

Regeneration data: The regeneration data was generated by me under the supervision of A.C. Barber. A.C. Barber counted axon regeneration alongside me and we compared values for accuracy and to check my counting technique. S.S. Deshpande created a program to speed up RGC survival analysis and did some manual counting to compare with data generated by the program. R. Conceição assisted by creating some retinal wholemounts during tissue collection.

Validation data: All validation data, including testing the viral vectors *in vitro* and *in vivo*, and quantifying PTEN knockdown, PI3K upregulation, and mTOR pathway activity *in vivo*, was generated by me.

R. Eva wrote the manuscript. R. Eva, J.W. Fawcett, B.J. Eickholt, K. Okkenhaug, B. Nieuwenhuis, S. van Erp, A.C. Barber and I edited the manuscript.

4.2 Introduction

4.2.1 PTEN Deletion Promotes RGC Survival and Axon Regeneration *In Vivo*

As described in detail in **Chapter 1.3.2**, Park et al. compared the effects on axon regeneration of several different cell growth control genes using a murine optic nerve crush (ONC) model. They found that transgenic knockout of phosphatase and tensin homolog (PTEN) significantly promoted both retinal ganglion cell (RGC) survival and axon regeneration in young adult mice[79]. These pro-regenerative results were also seen after spinal cord injury[58]. This effect was shown to be primarily due to mammalian target of rapamycin (mTOR) pathway activation. The group then investigated a more translatable approach, knocking down PTEN with viral short hairpin RNA (shRNA) targeted to PTEN, driven by a U6 promoter. The AAV2.shPTEN.GFP viral vector promoted regeneration after spinal cord injury[110]. In this chapter, we tested this viral vector in an ONC model, which had not been previously done before. Viral shRNA targeted to PTEN would give lower levels of PTEN knockdown than transgenic knockout. Therefore, less than 45% RGC survival and less axon regeneration than seen in Park et al. would be expected.

4.2.2 The p110α and p110δ Isoforms of PI3K Promote Axon Regeneration Both *In Vitro* and *In Vivo*

The phosphoinositide 3-kinase (PI3K) pathway is described in **Chapter 1.3**. As described in detail in **Chapter 3**, Barber et al. investigated the effects of the different PI3K isoforms on axon regeneration *in vitro* and found that hyperactive p110α (p110α^{H1047R}) and p110δ were involved in promoting axon regeneration. These two isoforms were then tested *in vivo*, using a conditional transgenic approach. Overall the work found that p110α^{H1047R} and p110δ promoted both RGC survival and axon regeneration in young adult mice, with no difference between the two isoforms. Moving forward with a more translatable approach, an AAV2.PI3K(p110δ) virus was generated, driven by a CAG promoter. The PI3K construct was too large to add a viral tag. Unfortunately, as a commonly mutated cancer gene, the p110α^{H1047R} isoform was deemed too unsafe for viral work.

All regeneration studies in this thesis follow the same experimental paradigm as in Park et al., allowing effective comparison. As mentioned, inserting a transgene at the Rosa26 locus results in moderate expression levels[72]. Therefore, viral PI3K(p110δ) would be expected to increase PI3K expression levels further than in the transgenic approach and to have greater regenerative effects. Viral AAV2.PI3K(p110δ) and AAV2.shPTEN.GFP were also compared. We hypothesised that PI3K upregulation would have greater regenerative effects than PTEN knockdown because PI3K directly increases phosphatidylinositol (3,4,5)-tris-phosphate (PIP3) levels, unlike PTEN which prevents the breakdown of already low PIP3 levels.

4.2.3 Aim

This work aimed to assess viral PTEN knockdown and viral PI3K(p110δ) upregulation using an ONC model. The same experimental paradigm was used throughout this thesis to allow comparison between the different groups. It was expected that viral PI3K(p110δ) would promote both survival and regeneration more than transgenic p110δ and viral PTEN knockdown.

4.3 Methods

Any references to **Chapter 2** are clearly stated in the text.

4.3.1 *In Vitro* Work

Before injecting the viruses *in vivo*, they were tested *in vitro*. Human embryonic kidney (HEK) 293 cells were transfected with AAV2.shPTEN.GFP (gifted by Z. He), AAV2.shScram.GFP (SignaGen Labs, cat no. SL100815), AAV2.shScram.GFP (Vigene Biosciences, cat no. P100042), AAV2.PI3K(p110δ) (produced for project), and AAV2.GFP (Vigene Biosciences, cat no. CV17169-AV2), as described in **Chapter 2.1**. Two AAV2.shScram.GFP viruses were trialled to see which gave the most GFP signal.

4.3.2 *In Vivo* Work

Viral Validation Work: Retinal Sections

For viral validation work *in vivo*, young adult (6 to 16 weeks old) C57BL/6J mice received a 2μL intravitreal injection of AAV2.shPTEN.GFP (gifted by Z. He) into the left eye and 2μL of AAV2.shScram.GFP (SignaGen Labs, cat no. SL100815) into the right eye, as described in **Chapter 2.3**. Another set of mice received a 2μL intravitreal injection of AAV2.PI3K(p110δ) (produced for project) into the left eye, and 2μL of AAV2.GFP (Vigene Biosciences, cat no. CV17169-AV2) into the right eye. All viruses were injected at a titre of 1.0 x 10^{13}GC/mL, a preoptimised titre for viral intravitreal injections. 2 weeks after injection, the mice were perfused, as described in **Chapter 2.5**.

Whole eyes were collected, post-fixed in 4% paraformaldehyde (PFA) at room temperature for 2 hours, and then transferred to 20% sucrose overnight at 4°C for cryoprotection, as described in **Chapter 2.6.2**. The eyes were then embedded in Tissue-Tek OCT compound and cryosectioned (12μm thick) using a Leica cryostat (Leica Biosystems, CM 3050S Research Cryostat).

Regeneration Studies

For the regeneration work, young adult (6 to 8 weeks old) C57BL/6J mice received a 2μL intravitreal injection of AAV2.shPTEN.GFP (gifted by Z. He), AAV2.shScram.GFP (SignaGen Labs, cat no. SL100815), AAV2.PI3K(p110δ) (produced for project), or AAV2.GFP (Vigene Biosciences, cat no. CV17169-AV2) into the left eye, as described in **Chapter 2.3**. 2 weeks after injection, the mice received an ONC injury behind the left eye, as described in **Chapter 2.4**. At 26 days post-ONC, the mice were intravitreally injected with cholera toxin subunit-β with an Alexa Fluor 555 conjugate (CTB-555) (Thermo Fisher Scientific, cat no. C22843), as described in **Chapter 2.3**. At 4 weeks post-ONC, mice were perfused, as described in **Chapter 2.5**.

The optic nerves were collected, post-fixed in 4% PFA at 4°C overnight, and transferred to 30% sucrose for at least 24 hours for cryoprotection, as described in **Chapter 2.6.1**. The nerves were then cryosectioned (14μm longitudinal sections) using a Leica cryostat (Leica Biosystems, CM 3050S Research Cryostat).

The retinas were collected, and four small incisions were made to form retinal whole-mounts (RWMs), as described in **Chapter 2.6.3**. RWMs were post-fixed in 4% PFA for 2 hours at room temperature, and then the solution was changed to phosphate-buffered saline (PBS), ready for immunohistochemistry (IHC).

4.3.3 Immunohistochemistry

IHC for HEK 293 Cells *In Vitro*

Having been fixed in 4% PFA, HEK 293 cells were counterstained with DAPI, and IHC against PI3K(p110δ) was performed for AAV2.PI3K(p110δ)- and AAV2.GFP- transfected cells, as described in **Chapter 2.7.1**.

Retinal Section Histology

Having been fixed in 4% PFA and sectioned, IHC was performed as described in **Chapter 2.7.2**. IHC against GFP and PI3K(p110δ) was used to identify the viral vectors. IHC against PTEN and PI3K(p110δ) was used to quantify PTEN knockdown and PI3K upregulation respectively. IHC against phospho-AKT (pAKT) and phospho-S6 ribosomal protein (pS6) was used to quantify PI3K/AKT/mTOR pathway activity.

Retinal Wholemount Histology

Having been fixed in 4% PFA, the RWMs were then stored in PBS at 4°C. IHC against Brn3A, an RGC marker, was performed on RWMs as described in **Chapter 2.7.3**.

4.3.4 Microscopy and Quantification

Viral Validation *In Vitro*

HEK 293 cells transfected with either AAV2.shPTEN.GFP, AAV2.shScram.GFP, or AAV2.GFP were counterstained with DAPI. HEK 293 cells transfected with either AAV2.PI3K(p110δ) or AAV2.GFP were immunostained for PI3K(p110δ) and counterstained with DAPI. These were imaged by confocal microscopy at x40 magnification. The images were used to confirm that the GFP viral tag or the PI3K(p110δ) signal was observed and that

this signal was not seen in untransfected (naive) cells. They also confirmed that PI3K(p110δ) signal was not seen in AAV2.GFP-transfected cells.

Viral Validation: Viral Tags

Successful viral transduction was confirmed in retinal sections injected with AAV2.shPTEN.GFP, AAV2.shScram.GFP and AAV2.GFP, immunostained for GFP and counterstained with DAPI. For AAV2.PI3K(p110δ), sections were immunostained for PI3K(p110δ) and counterstained with DAPI. GFP or PI3K(p110δ) signal was used to confirm the presence of the viral vectors, and eye cups were imaged using a Zeiss AxioScan Z1 at x20 magnification (0.22μm/pixel) by the team at the Histopathology/ISH core facility at the Cancer Research UK (CRUK) Cambridge. The RGC layer of retinal sections was imaged using confocal microscopy at x40 magnification.

PTEN Knockdown and PI3K Upregulation *In Vivo*

Some data from R. Conceição was included in the results section for completeness. HEK 293 cells transfected with each virus were analysed using western blots and immunoblotting for PTEN and PI3K(p110δ), as described in **Chapter 2.8**. The amount of PI3K(p110δ) and PTEN signal was quantified using Image J Fiji (Fiji-win64) and expressed relative to the β-actin signal for each sample. The average signal relative to β-actin for AAV2.GFP-transfected cells was calculated. All values were then expressed relative to this average for AAV2.GFP.

For the *in vivo* work, which I did, retinal sections transduced with either AAV2.shPTEN.GFP or AAV2.shScram.GFP were immunostained with PTEN antibody and imaged by confocal microscopy at x95 magnification, using consistent settings. Retinal sections transduced with either AAV2.PI3K(p110δ) or AAV2.GFP were immunostained with PI3K(p110δ) antibody and imaged by confocal microscopy at x40 magnification, using consistent settings.

Several RGCs were then analysed by drawing around each RGC and using Image J Fiji (Fiji-win64) to quantify the fluorescence value of each RGC. The average fluorescence value of the RGCs was found and compared to that seen from the respective control virus.

RGC Survival

Percentage RGC survival was calculated as described in **Chapter 2.9.4**. In brief, Brn3A-stained RWMs were imaged at x20 magnification using fluorescence microscopy. For each

image, the number of RGCs was quantified using a counting program in Image J Fiji (Fiji-win64). The number of surviving RGCs in the ONC (left) eye was expressed as a percentage relative to the number of RGCs in the uninjured contralateral control (right) eye.

Axon Regeneration

Axon regeneration was calculated as described in **Chapter 2.9.5**. In brief, the CTB-555-labelled axons were visualised using fluorescence microscopy at x40 magnification, counting the number of axons at 0.5mm increments from the crush site. Modelling the nerve as a cylinder, the number of regenerating axons per nerve was calculated at each increment using a previously developed formula. Four sections were counted per nerve and used to average the total number of regenerating axons per nerve.

Axonal sections were imaged using a Zeiss AxioScan Z1 at x40 magnification (0.11μm/pixel) by the Histopathology/ISH core facility at the CRUK Cambridge Institute.

Viral Validation: PI3K/AKT/mTOR Pathway Activation

Retinal sections injected with the viral vectors and immunostained with either pAKT or pS6 were examined at x40 magnification by fluorescence microscopy, as described in **Chapter 2.9.3**. In brief, for AAV2.shPTEN.GFP and AAV2.shScram.GFP, 100 GFP-positive RGCs, identified using DAPI and GFP signal from the viral vector, were counted and identified as either positive or negative for pAKT. This method was repeated for retinal sections immunostained with pS6. Four mice were counted for each group (100 RGCs per mouse), and the average was expressed as a percentage of GFP-positive cells co-localised with pAKT or pS6.

AAV2.PI3K(p110δ) lacked a clear viral tag, so the total number of pS6-positive RGCs was counted across the retina from 12 retinal sections, sampled sequentially throughout the whole eye, using βIII tubulin (Tuj1) as a marker of RGC neurons. This method was repeated for AAV2.GFP-transduced retinal sections for comparison. The pAKT signal was not clear enough to count in this way.

Representative images were taken at x80 magnification by confocal microscopy.

4.4 Results

4.4.1 Viral Validation

AAV2.shPTEN.GFP, AAV2.shScram.GFP, AAV2.PI3K(p110δ), and AAV2.GFP successfully transfected HEK 293 cells *in vitro*

Before using the AAV2.shPTEN.GFP, AAV2.shScram.GFP, AAV2.PI3K(p110δ), and AAV2.GFP viruses *in vivo*, successful viral transfection was confirmed *in vitro* using HEK 293 cells, as shown in **Fig. 4.1**. Signal from the viral tag, GFP, was detected from all viruses, except AAV2.PI3K(p110δ). AAV2.shScram.GFP (SignaGen Labs, cat no. SL100815) gave noticeably stronger GFP signal than AAV2.shScram.GFP (Vigene Biosciences, cat no. P100042) so this virus was used *in vivo*. PI3K(p110δ) signal was seen for the AAV2.PI3K(p110δ) virus but was absent in the AAV2.GFP virus, confirming antibody specificity, as seen in **Fig. 4.4 panel C**.

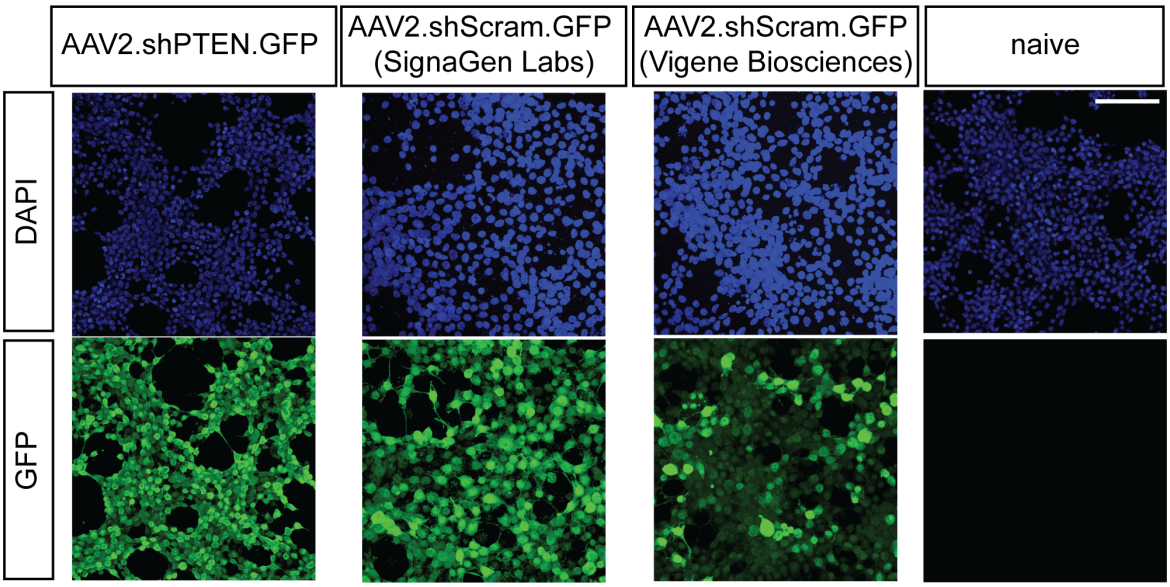

Fig. 4.1 **AAV2.shPTEN.GFP and AAV2.shScram.GFP were tested *in vitro*.** One AAV2.shPTEN.GFP and two AAV2.shScram.GFP viruses were tested in HEK 293 cells prior to *in vivo* work. The presence of GFP signal indicates successful transfection. AAV2.shScram.GFP from SignaGen Labs gave a stronger signal than AAV2.shScram.GFP from Vigene Biosciences. Scale bar = 100μm.

AAV2.shPTEN.GFP, AAV2.shScram.GFP, AAV2.PI3K(p110δ), and AAV2.GFP successfully transduced RGCs *in vivo*

Viral transduction of RGCs was tested *in vivo*. Young adult (6 to 16 weeks old) C57BL/6J mice were injected intravitreally with 2μL of either AAV2.shPTEN.GFP or AAV2.PI3K(p110δ) in the left eye and 2μL of either AAV2.shScram.GFP or AAV2.GFP respectively in the right eye. The eyes were collected 2 weeks later and 12μm retinal sections were produced.

Successful viral transduction of AAV2.shPTEN.GFP, AAV2.shScram.GFP, and AAV2.GFP *in vivo* was confirmed by signal from the viral tag, GFP, in the RGC layer. The presence of PI3K(p110δ) was confirmed for the AAV2.PI3K(p110δ) virus. Eye cup images showed signal throughout the retina, and closer inspection of the retinal sections confirmed that this signal was in the RGC layer, as shown in **Fig. 4.2**, where staining was indicative of RGCs.

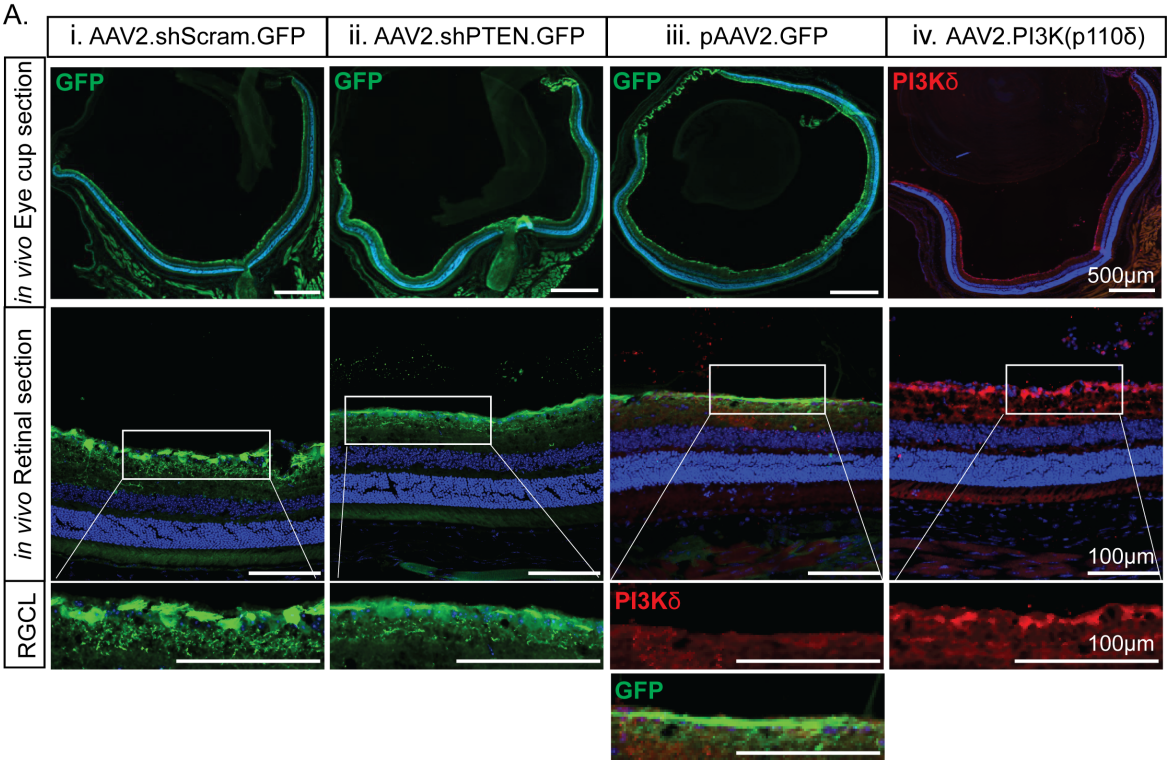

Fig. 4.2 **Successful viral transduction of AAV2.shPTEN.GFP, AAV2.shScram.GFP, AAV2.PI3K(p110δ) and AAV2.GFP was confirmed *in vivo*.** In panel A, eye cups and zoomed in images of the RGC layer showed GFP signal in RGCs throughout the retina for AAV2.shScram.GFP (i), AAV2.shPTEN.GFP (ii) and AAV2.GFP (iii), and PI3K(p110δ) signal in RGCs throughout the retina for AAV2.PI3K(p110δ) (iv). Staining was indicative of RGCs. Scale bar = 500μm for eye cups, 100μm for retinal sections.

Successful PTEN Knockdown and PI3K Upregulation were confirmed both *in vitro* and *in vivo*

To confirm that the AAV2.shPTEN.GFP virus resulted in PTEN knockdown, an antibody against PTEN was used in HEK 293 cells *in vitro* and in retinal sections *in vivo*, as shown in **Fig. 4.3**. Western blots of transfected HEK 293 cells performed by R. Conceição (included here for comparison with my *in vivo* work) showed 1.28±0.15 signal (n=3 wells) in AAV2.shScram.GFP-treated cells (fold change in PTEN relative to AAV2.GFP-treated cells), which decreased to 0.10±0.03 (n=3 wells) in AAV2.shPTEN.GFP-treated cells (one-tailed T-test, $p<0.0001$). There was 12.8-fold more PTEN signal in the control group than the PTEN knockdown group *in vitro*. In retinal sections, staining in the RGC layer was indicative of RGCs and a fluorescence value per RGC of 22.5±11.4 (n=20 RGCs) was observed in AAV2.shScram.GFP-treated eyes, which significantly decreased to 4.1±2.0 (n=19 RGCs) in AAV2.shPTEN.GFP-treated eyes (one-tailed T-test, $p<0.0001$). There was 5.5-fold more PTEN signal in the control group than the PTEN knockdown group *in vivo*.

To confirm that the AAV2.PI3K(p110δ) virus resulted in PI3K upregulation, an antibody against PI3K(p110δ) was used in HEK 293 cells *in vitro* and in retinal sections *in vivo*. Western blots of transfected HEK 293 cells performed by R. Conceição (included here for comparison with my *in vivo* work) showed 1.00±0.76 signal (n=3 wells) in AAV2.GFP-treated cells (fold change in PI3K(p110δ) relative to AAV2.GFP-treated cells), which increased to 46.08±8.79 (n=3 wells) in AAV2.PI3K(p110δ)-treated cells (one-tailed T-test, $p=0.0005$), as shown in **Fig. 4.4**. There was 46.1-fold more PI3K(p110δ) signal in the AAV2.PI3K(p110δ) group compared to control *in vitro*. In retinal sections, a fluorescence value per RGC of 5.7±2.5 (n=41 RGCs) was observed in AAV2.GFP-treated eyes, which significantly increased to 7.6±3.9 (n=31 RGCs) in AAV2.PI3K(p110δ)-treated eyes (one-tailed T-test, $p=0.0080$). There was 1.3-fold more PI3K(p110δ) signal in the AAV2.PI3K(p110δ) group compared to control *in vivo*.

4.4.2 RGC Survival and Axon Regeneration

Adult (6 to 8 weeks old) C57BL/6J mice received a 2μL intravitreal injection of either AAV2.shPTEN.GFP, AAV2.shScram.GFP, AAV2.PI3K(p110δ), or AAV2.GFP into the left eye. 2 weeks later, ONC surgery was performed. At 26 days post-ONC, 2μL of cholera toxin subunit-β with an Alexa Fluor 555 conjugate (CTB-555) was intravitreally injected into the left eye. At 4 weeks post-ONC, the eyes and optic nerves were collected, as summarised in **Fig. 4.5**.

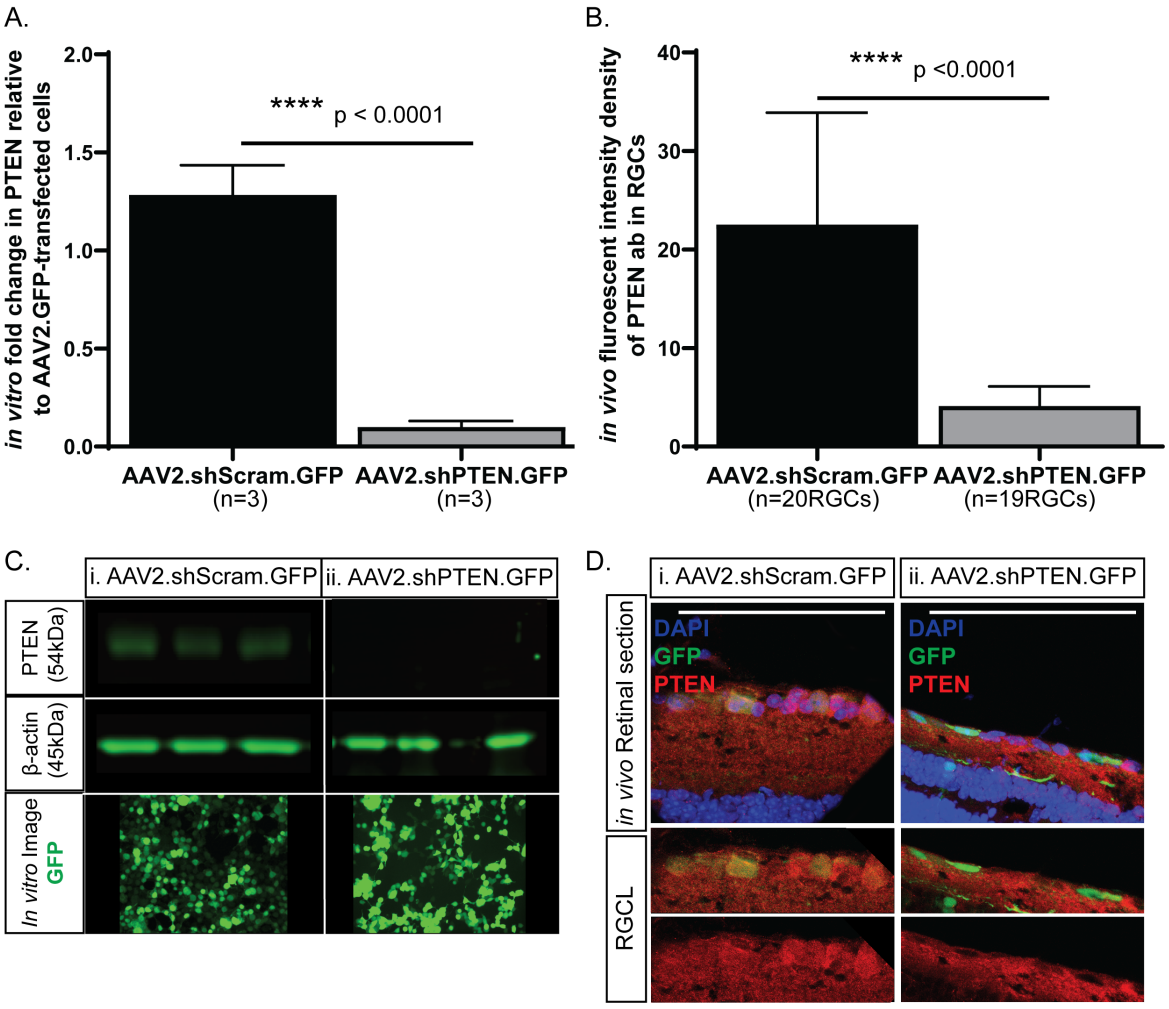

Fig. 4.3 **AAV2.shPTEN.GFP successfully knocked down PTEN levels both *in vitro* and *in vivo*** In panel A and C, a 12.8-fold knockdown of PTEN was shown *in vitro*. In panel B and D, a 5.5-fold knockdown was shown *in vivo*. Staining in the RGC layer of retinal sections was indicative of RGCs. p values measured by one-tailed T-test, n = 3 for *in vitro* and 19 to 20 for *in vivo* as specified, error bars = SD. Scale bar = 100μm. *in vitro* data provided by R. Conceição

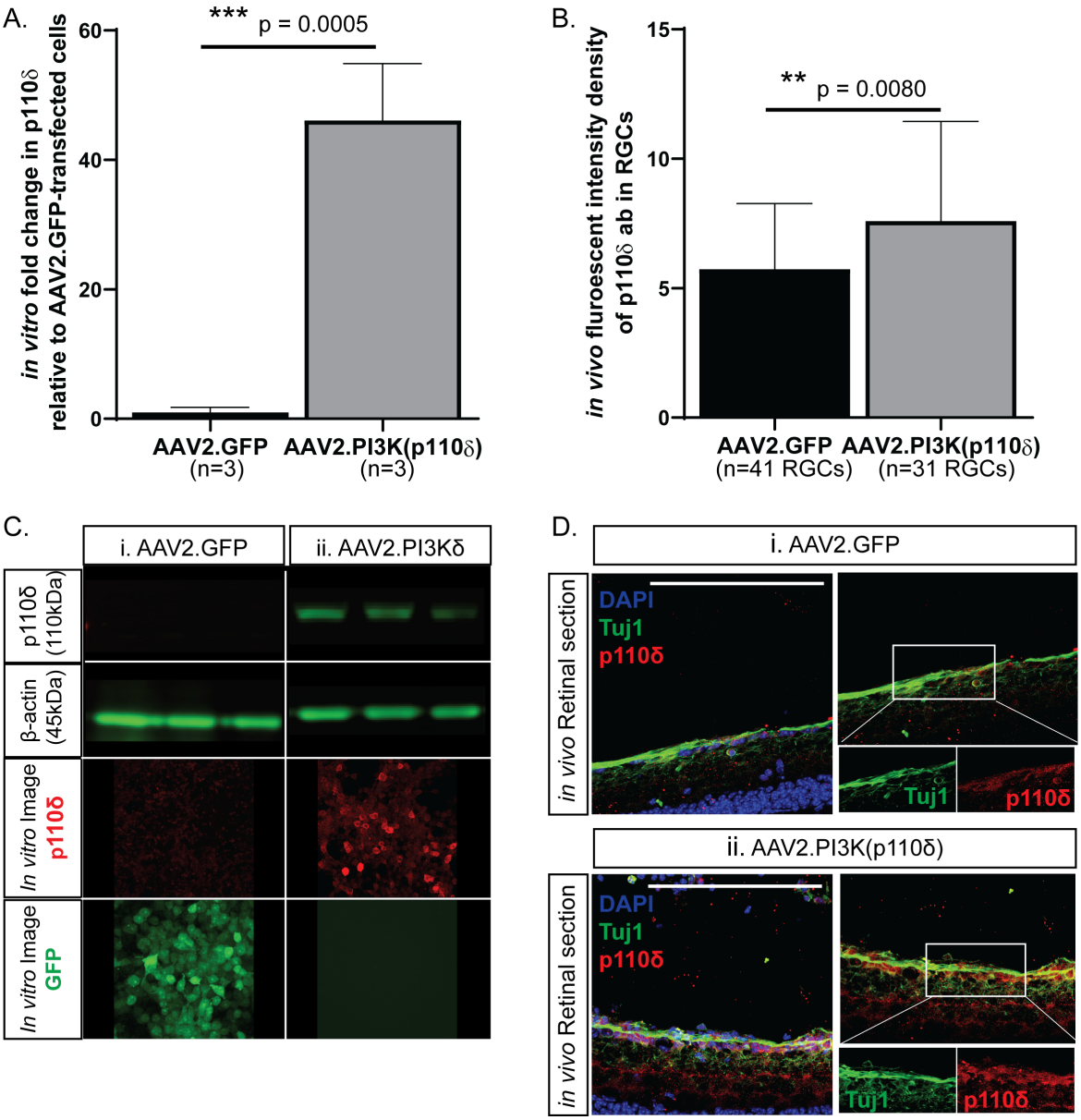

Fig. 4.4 **AAV2.PI3K(p110δ) successfully upregulated PI3K(p110δ) levels both *in vitro* and *in vivo***. In panel A and C, a 46.1-fold increase of p110δ was shown *in vitro*. In panel B and D, a 1.3-fold increase of PI3K(p110δ) was shown *in vivo*. p values measured by one-tailed T-test, n = 3 for *in vitro* and n = 31 to 41 for *in vivo* as specified, error bars = SD. Scale bar = 100μm. *in vitro* data provided by R. Conceição.

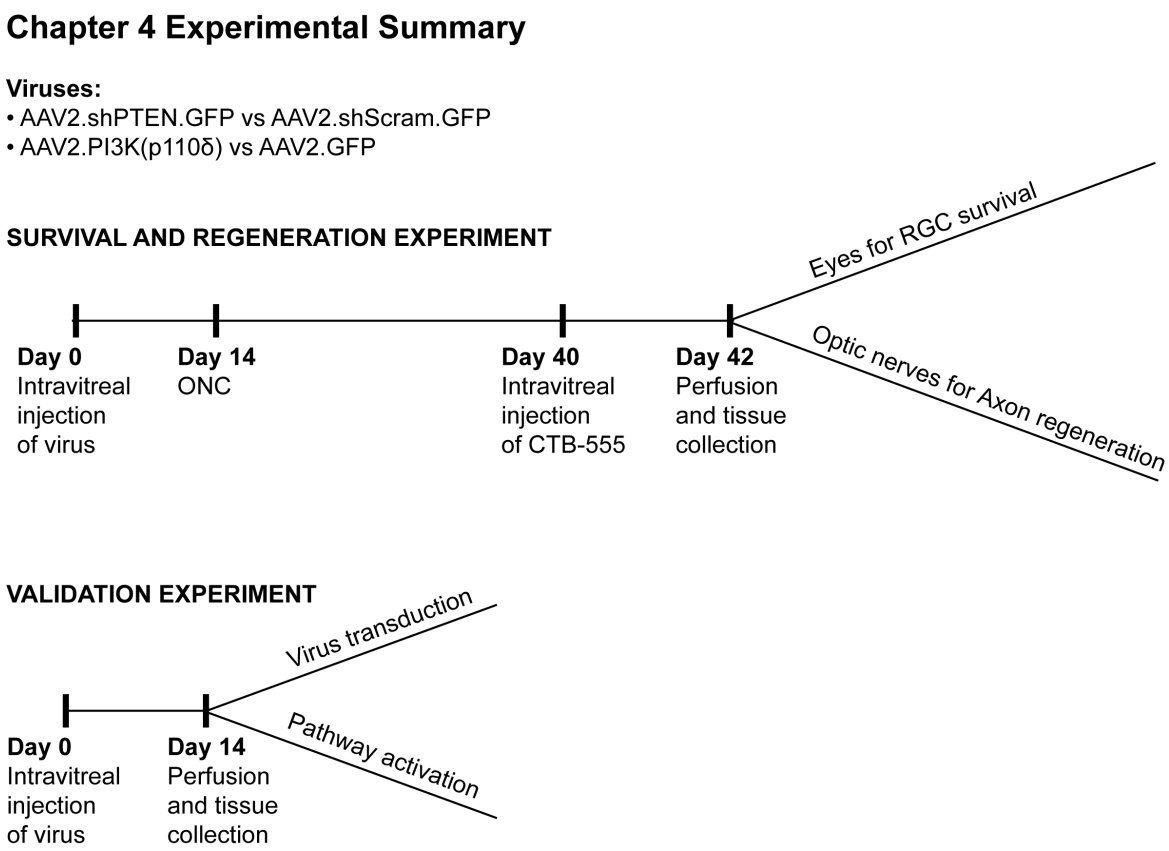

Fig. 4.5 **Chapter 4 Experimental Summary**.

PTEN knockdown promoted RGC Survival, but PI3K upregulation had no significant effect

The retinas were collected at 4 weeks post-ONC and IHC against Brn3A, an RGC marker, was used to quantify RGCs. The number of surviving RGCs in the ONC (left) eye was expressed as a percentage relative to the uninjured contralateral control (right) eye.

Young adult (6 to 8 weeks old) mice treated with AAV2.shPTEN.GFP showed 14.7%±7.6 (n=6 retinas) RGC survival at 4 weeks post-ONC, which was a significant increase from the 5.0%±3.9 (n=8 retinas) RGC survival seen in the AAV2.shScram.GFP-treated mice (see **Fig. 4.6**, one-tailed T-test, p=0.0044). Therefore, viral PTEN knockdown promotes RGC survival at 4 weeks post-ONC.

Young adult (6 to 8 weeks old) mice treated with AAV2.PI3K(p110δ) showed 11.3%±11.8 (n=7 retinas) RGC survival at 4 weeks post-ONC, compared to 4.7%±1.7 (n=4 retinas) RGC survival seen in the AAV2.GFP-treated mice (see **Fig. 4.7**). The increase in survival was not statistically significant. Therefore, viral PI3K upregulation had no significant effect on RGC survival at 4 weeks post-ONC in this experiment.

Comparison of viral PI3K upregulation with transgenic PI3K upregulation, which showed 11.4%±5.8 RGC survival in **Chapter 3.4.4**, and with viral PTEN knockdown, showed no statistical difference between the groups, as shown in **Fig. 4.8**.

PTEN knockdown and PI3K upregulation promoted axon regeneration

2 days before tissue collection, the left eyes were intravitreally injected with 2μL of CTB-555. At 4 weeks post-ONC, the optic nerves were dissected, and 14μm thick sections were produced. Axons were counted using the CTB-555 fluorescence at 0.5mm increments.

Young adult (6 to 8 weeks old) mice treated with AAV2.shPTEN.GFP showed 117±93 regenerating axons (n=5 nerves) at 0.5mm from the crush site, which was a significant increase compared to 16±11 axons (n=4 nerves) in the AAV2.shScram.GFP-treated mice (see **Fig. 4.9**, two-way ANOVA with Tukey's post-hoc analysis, p = 0.0090). Regenerating axons were seen up to 1.5mm from the crush site. Therefore, viral PTEN knockdown promotes axon regeneration at 4 weeks post-ONC.

Young adult (6 to 8 weeks old) mice treated with AAV2.PI3K(p110δ) showed 180±96 regenerating axons (n=6 nerves) at 0.5mm from the crush site, significantly more than the 31±20 axons (n=5 nerves) in the AAV2.GFP-treated mice (see **Fig. 4.10**, two-way ANOVA with Tukey's post-hoc analysis, p < 0.0001). At 1.0mm from the crush site, the AAV2.PI3K(p110δ) mice showed 104±80 regenerating axons, compared to 7±6 axons in the control (two-way ANOVA with Tukey's post-hoc analysis, p = 0.0072). Regenerating axons

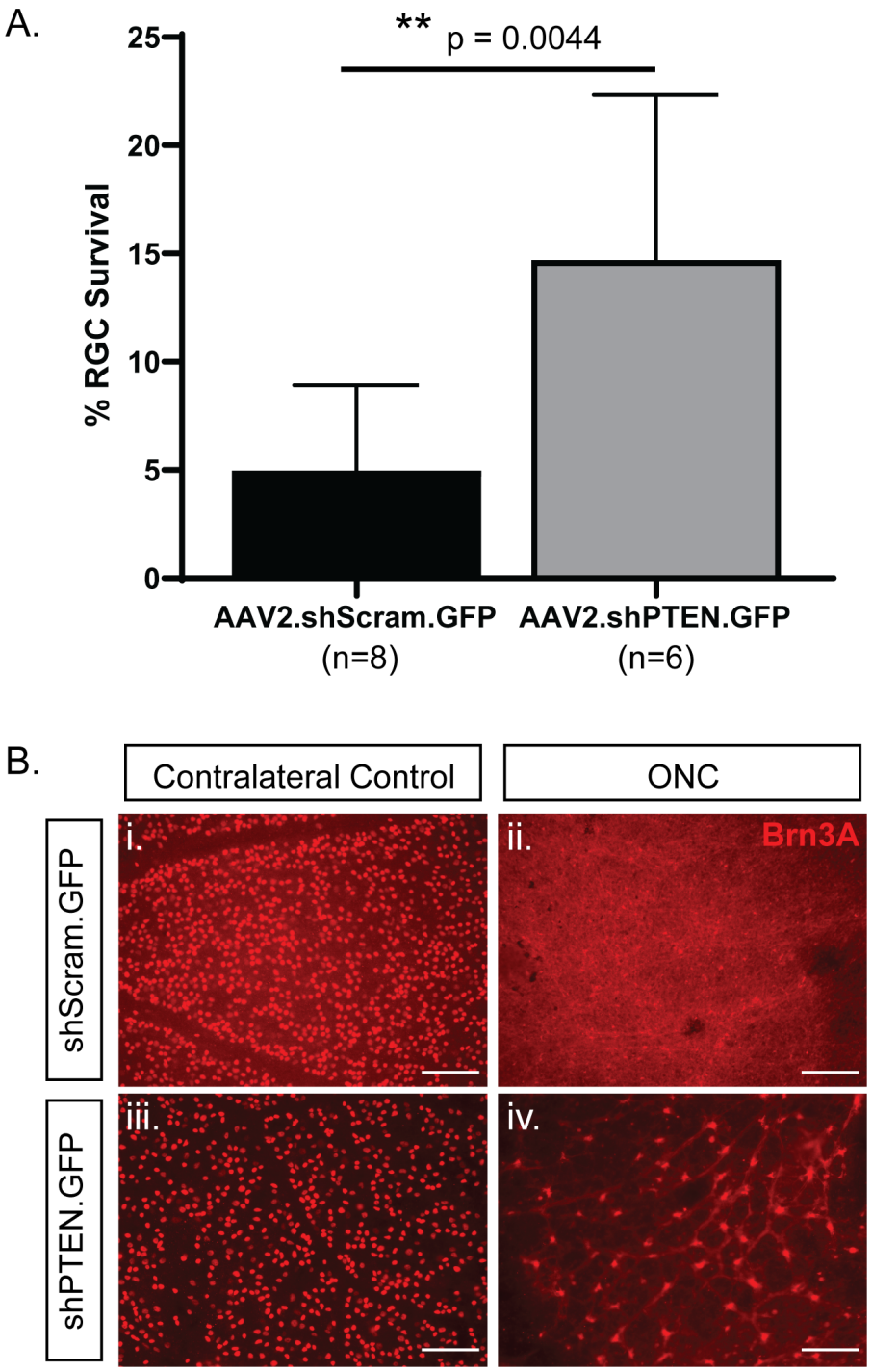

Fig. 4.6 **Viral PTEN knockdown promoted RGC Survival.** As seen in panel A, AAV2.shPTEN.GFP promotes RGC survival 4 weeks post-ONC injury. RWMs were stained with Brn3A (red), which was used to quantify RGCs. The number of RGCs in the ONC (left) eye (panels Bii and Biv) was expressed as a percentage survival relative to the uninjured contralateral control (right) eye (Bi and Biii). p values measured by one-tailed T-test, n = 6 to 8 as specified, error bars = SD. Scale bar = 100μm.

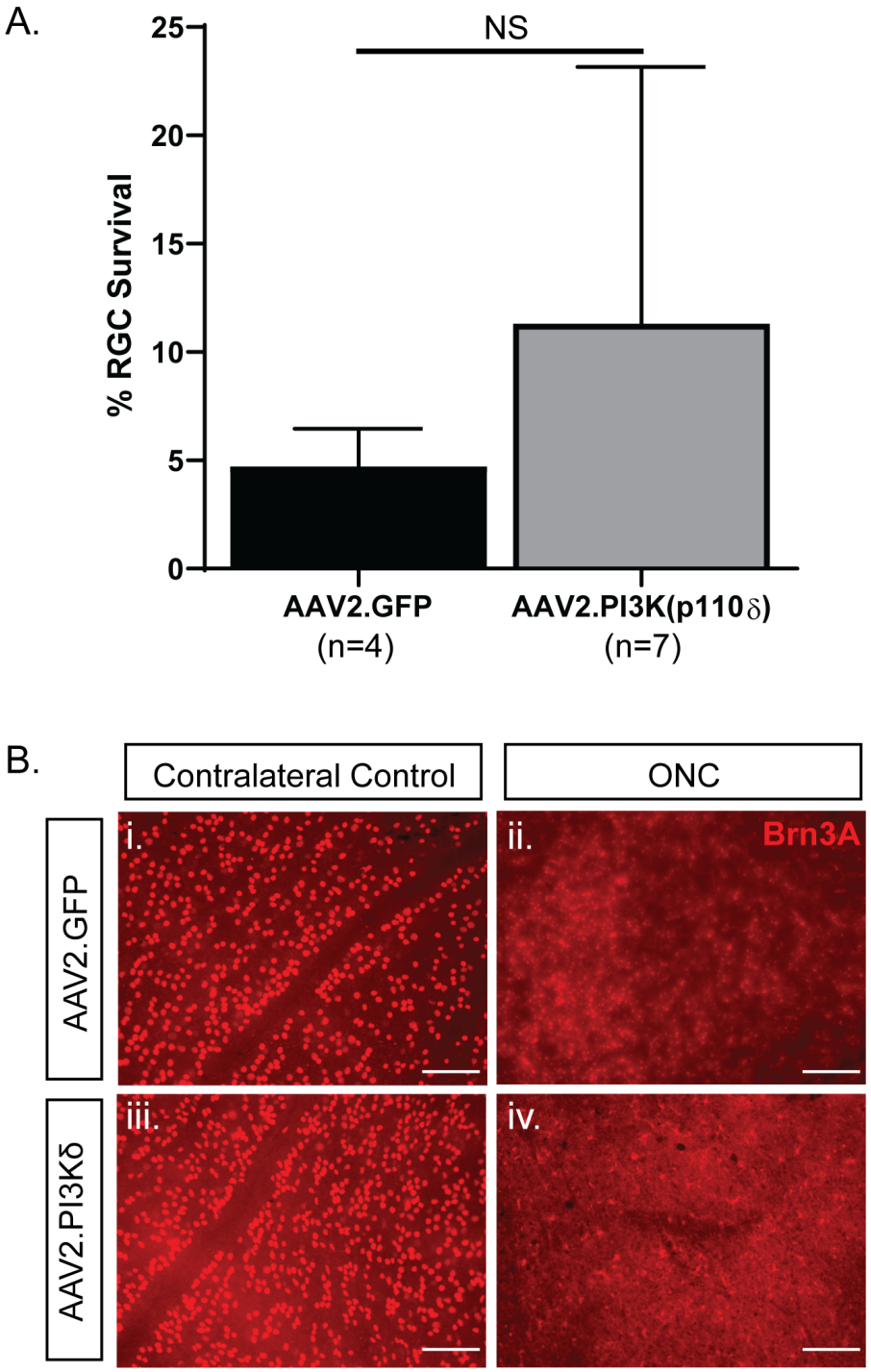

Fig. 4.7 **Viral PI3K upregulation had no significant effect on RGC survival.** As seen in panel A, viral PI3K(p110δ) had no significant effect on RGC survival 4 weeks post-ONC injury. RWMs were stained with Brn3A (red), which was used to quantify RGCs. The number of RGCs in the ONC (left) eye (panels Bii and Biv) was expressed as a percentage survival relative to the uninjured contralateral control (right) eye (Bi and Biii). p values measured by one-tailed T-test, n = 4 to 7 as specified, error bars = SD. Scale bar = 100μm.

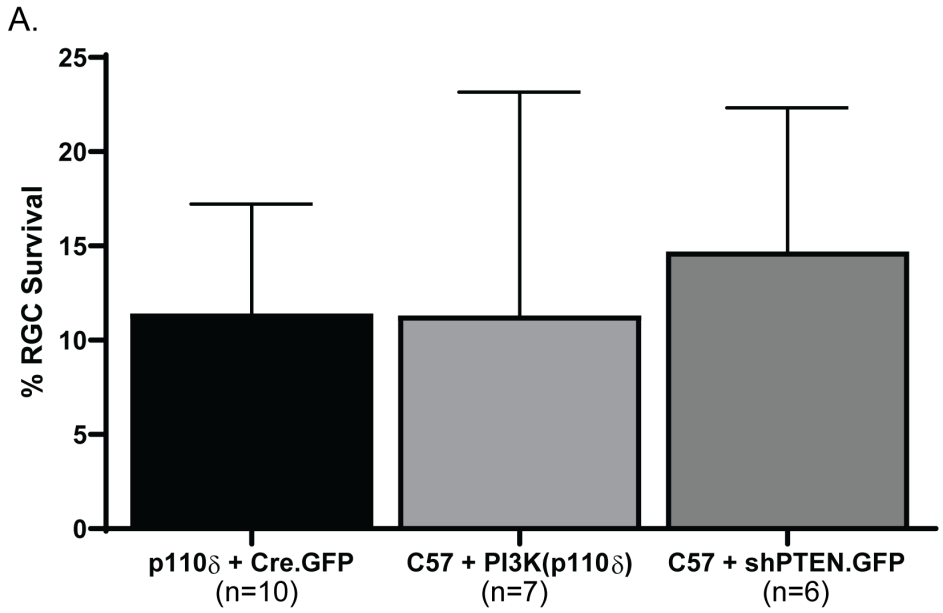

Fig. 4.8 **Comparison of viral PI3K upregulation with transgenic PI3K upregulation and viral PTEN knockdown showed no difference between groups.** RGC survival data from PI3K upregulation, both viral and transgenic, PTEN knockdown were all compared. p values measured by one-way ANOVA with Tukey's post-hoc analysis, n = 6 to 10 as specified, error bars = SD.

were seen up to 3.0mm from the crush site. Therefore, viral PI3K upregulation promotes axon regeneration at 4 weeks post-ONC.

The viral and transgenic PI3K upregulation strategies were compared in **Fig. 4.11**. 180±96 regenerating axons were observed at 0.5mm from the crush site in the viral strategy, which was significantly more than 61±36 axons in the transgenic strategy (two-way ANOVA with Tukey's post-hoc analysis, p = 0.0495). No statistical significance was found between AAV2.shPTEN.GFP-treated mice compared to AAV2.PI3K(p110δ)-treated mice or AAV2.Cre.GFP-treated p110δ mice. Therefore, viral PI3K upregulation promotes axon regeneration more than the transgenic strategy, but not significantly more than viral PTEN knockdown at 4 weeks post-ONC.

4.4.3 mTOR Pathway Activation

IHC against mTOR pathway markers (pAKT and pS6) was performed on the retinal sections used for viral validation.

In the PTEN knockdown mice, the percentage of GFP-labelled cells in the RGC layer co-localised with either pAKT or pS6 was quantified and compared to control injection, as shown in **Fig. 4.12**. Staining was indicative of RGCs. Eyes injected with AAV2.shScram.GFP

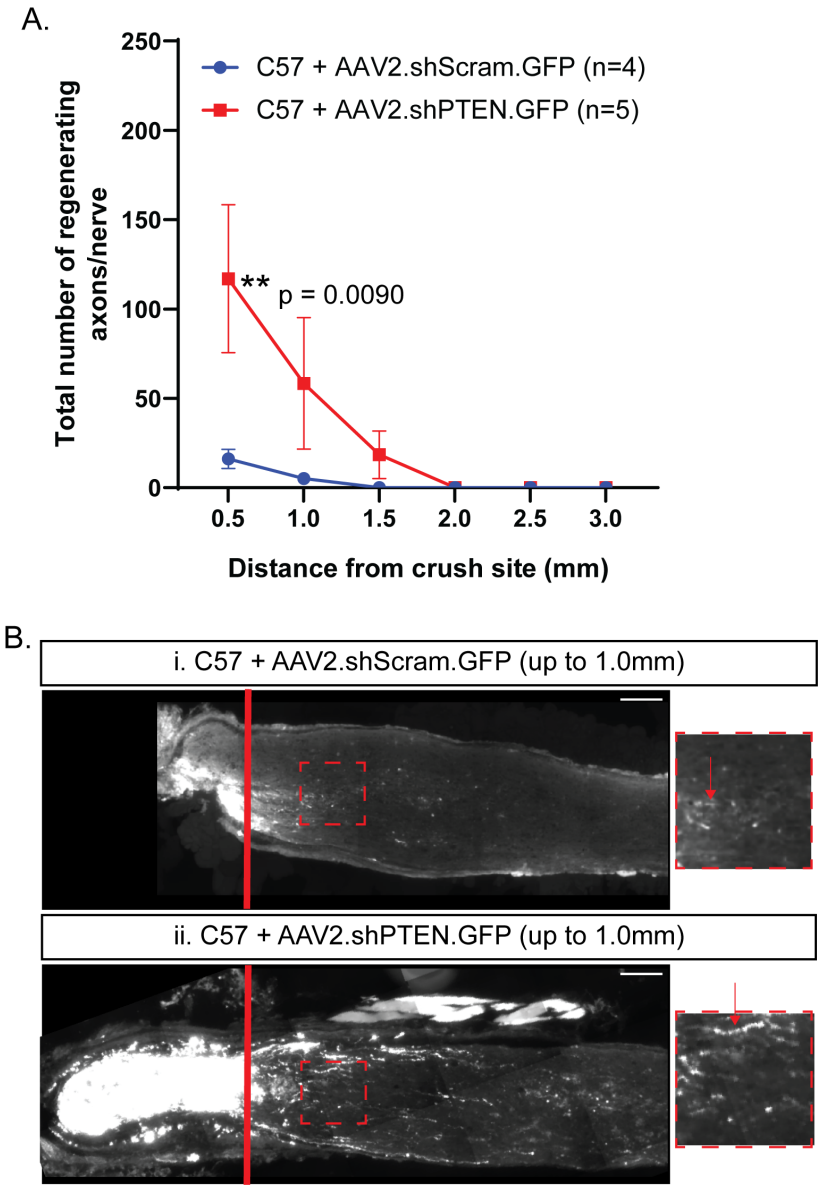

Fig. 4.9 **Viral PTEN knockdown promoted axon regeneration.** As shown in panel A, AAV2.shPTEN.GFP promoted axon regeneration following ONC injury. Images of crushed nerves are shown in panel B for AAV2.shScram.GFP (Bi) and for AAV2.shPTEN.GFP (Bii). p values measured by two-way ANOVA with Tukey's post hoc analysis, n = 4 to 5 as specified, error bars = SEM. Scale bar = 100μm.

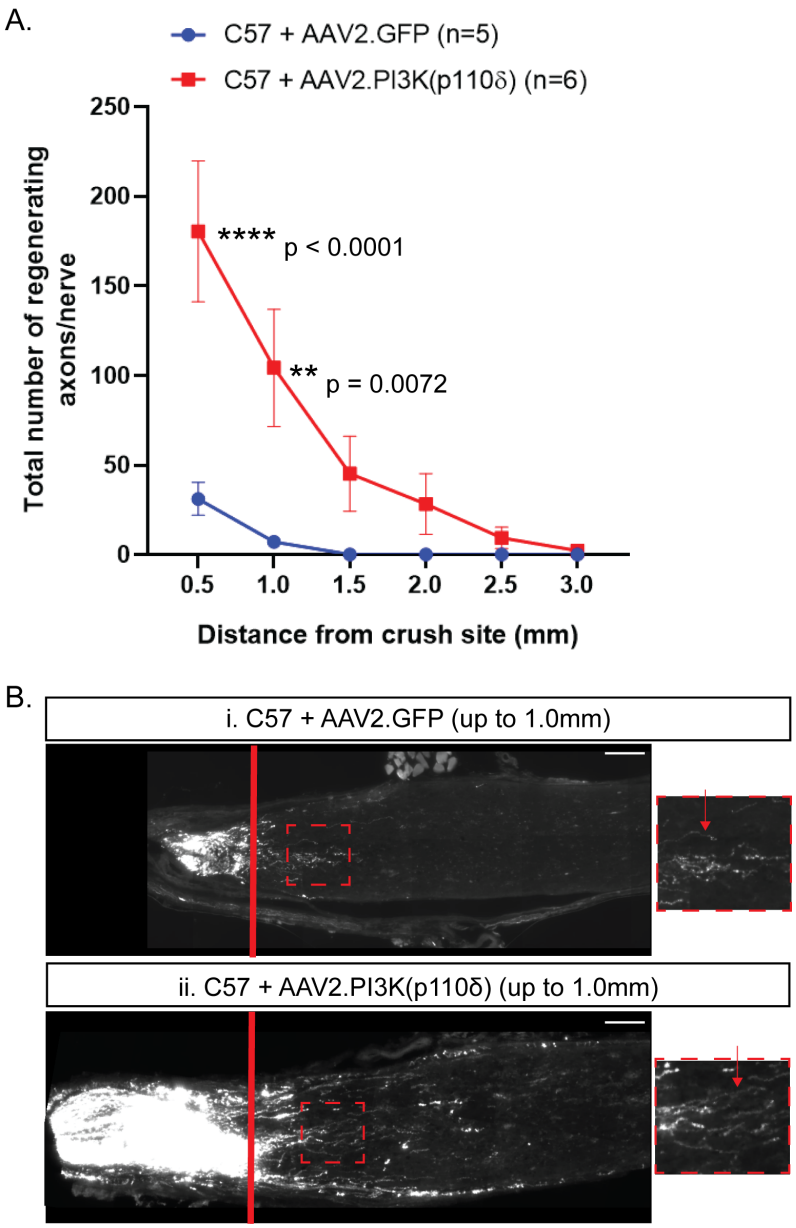

Fig. 4.10 **Viral PI3K upregulation promoted axon regeneration.** As shown in panel A, AAV2.PI3K(p110δ promoted axon regeneration following ONC injury. Images of crushed nerves are shown in panel B for AAV2.GFP (Bi) and for AAV2.PI3K(p110δ) (Bii). p values measured by two-way ANOVA with Tukey's post hoc analysis, n = 5 to 6 as specified, error bars = SEM. Scale bar = 100μm.

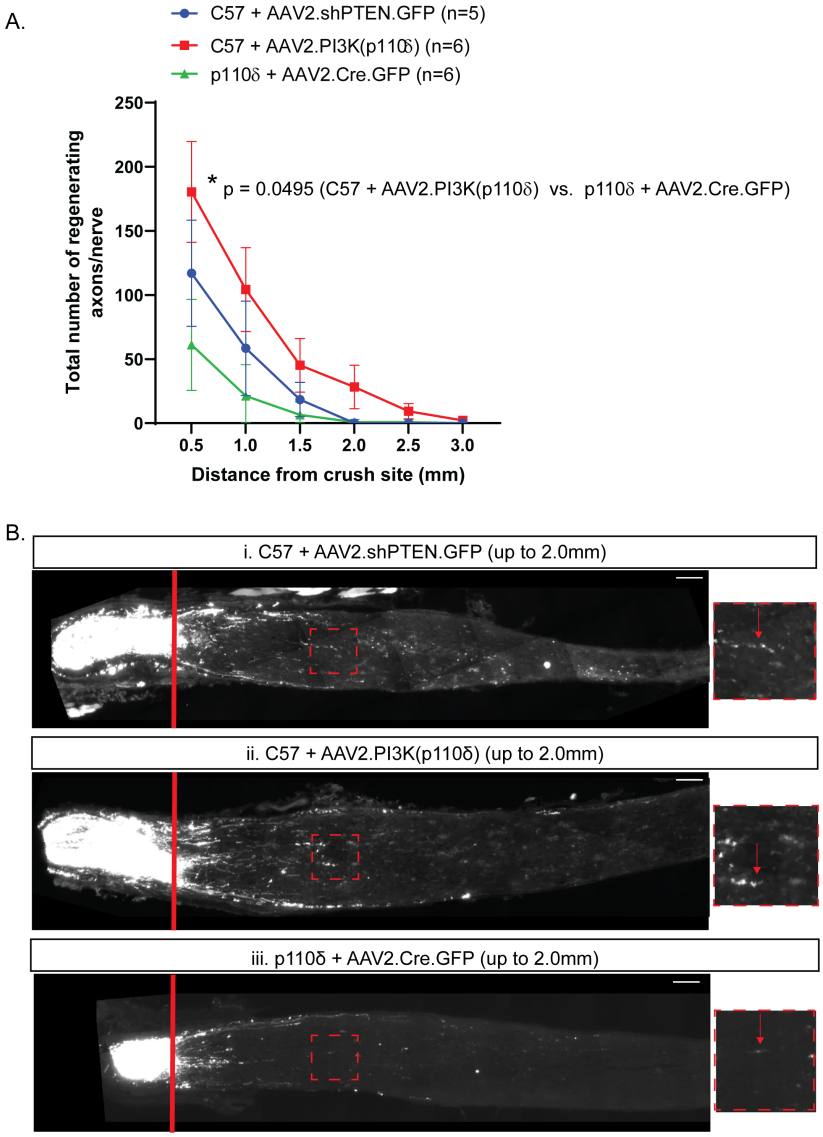

Fig. 4.11 **Viral PI3K upregulation promoted axon regeneration more than the transgenic approach, but not significantly more than viral PTEN knockdown.** As shown in panel A, viral PI3K upregulation promoted axon regeneration following ONC injury significantly more than the transgenic approach. However, no significant difference was seen when comparing viral PI3K upregulation with viral PTEN knockdown. Images of crushed nerves are shown in panel B for AAV2.shPTEN.GFP in C57BL/6J (Bi), AAV2.PI3KDelta in C57BL/6J (Bii) and AAV2.Cre.GFP in the p110δ transgenic (Biii). p values measured by two-way ANOVA with Tukey's post hoc analysis, n = 5 to 6 as specified, error bars = SEM. Scale bar = 100μm.

showed 27.0%±5.0 pAKT-GFP-labelled cells, which increased 48.8%±7.0 in the AAV2.shPTEN.GFP-injected eyes (one-tailed T-test, p=0.0012). The average fold change in pAKT was 1.91±0.34. Eyes injected with AAV2.shScram.GFP showed 51.8%±4.6 pS6-GFP-labelled cells, which increased to 72.0%±6.3 in the AAV2.shPTEN.GFP-injected eyes (one-tailed T-test, p=0.0010). The average fold change in pS6 was 1.41±0.23.

In the PI3K upregulation mice, the AAV2.PI3K(p110δ) virus lacked a clear viral tag, so Tuj1 was used to label RGCs. The total number of pS6-labelled RGCs was counted across 12 retinal sections, as shown in **Fig. 4.13**. Eyes injected with AAV2.GFP showed 650±64 pS6-positive RGCs, which increased to 1140±85 in the AAV2.PI3K(p110δ) eyes (one-tailed T-test, p<0.0001). The average fold change in pS6 was 1.77±0.25.

No significant differences were found in the fold-change of pS6 signal when comparing viral PI3K upregulation with the transgenic strategy and with viral PTEN knockdown.

4.5 Discussion

Both viral PTEN knockdown and viral PI3K upregulation promoted axon regeneration, with no significant difference between the two. Viral PTEN knockdown also promoted RGC survival, but surprisingly viral PI3K upregulation had no significant effect in this experiment. There was a high level of variation in the viral PI3K upregulation data, and repeating this experiment to increase the n size would likely result in significant survival, especially as transgenic PI3K upregulation did promote RGC survival.

Next, viral and transgenic PI3K upregulation were compared. No significant difference in RGC survival was found between these experiments, but viral PI3K(p110δ) showed significantly greater axon regeneration as expected. Unfortunately, the PI3K(p110δ) antibody gave high levels of background signal *in vivo*, so it was not easily possible to quantify PI3K(p110δ) levels for comparison of the two approaches.

mTOR pathway activation was quantified and compared across the different groups. It was particularly difficult to assess pS6 and pAKT levels in eyes treated with the AAV2.PI3K(p110δ) virus because the virus lacked a viral tag, so this was quantified differently from the other groups. Although fold change was compared, this was not very accurate due to the different counting methods used. As mentioned in **Chapter 3**, if a method for isolating RGCs were optimised, this would allow more accurate quantification of mTOR pathway markers.

Treatment with rapamycin, an mTOR inhibitor, neutralised most of the pro-regenerative effects of transgenic PTEN knockdown in Park et al.[79]. It would be interesting to investigate what pathways other than the PI3K/AKT/mTOR pathway are involved in promoting

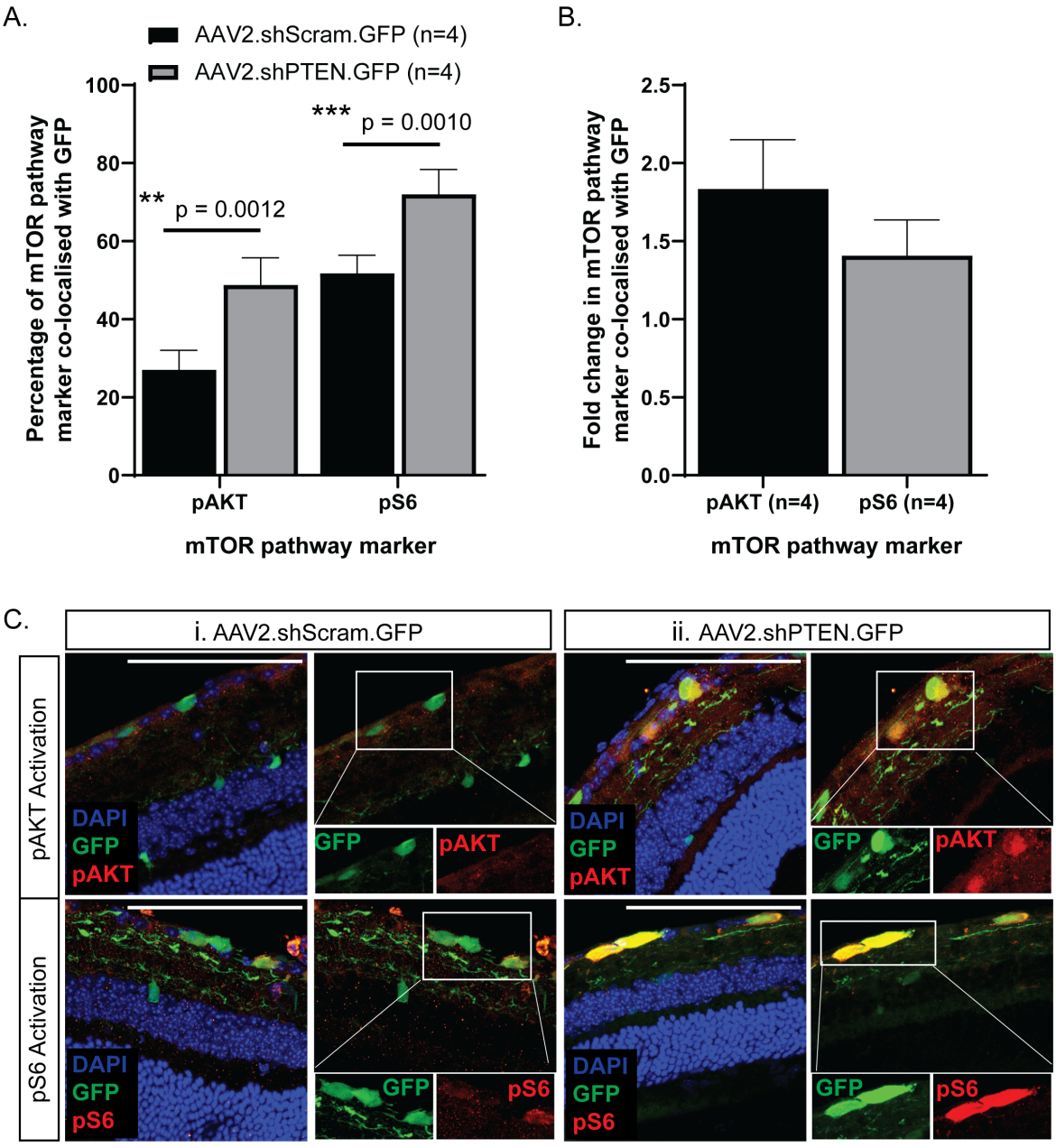

Fig. 4.12 **Viral PTEN knockdown resulted in increased mTOR pathway activity *in vivo*.** As shown in the graphs in panels A and B, pAKT and pS6 signal increased in AAV2.shPTEN.GFP-treated eyes compared to AAV2.shScram.GFP-treated eyes. Representative images are shown in panel C. Staining in the RGC layer was indicative of RGCs. p values measured by one-tailed T-test, n = 4, error bars = SD. Scale bar = 100μm.

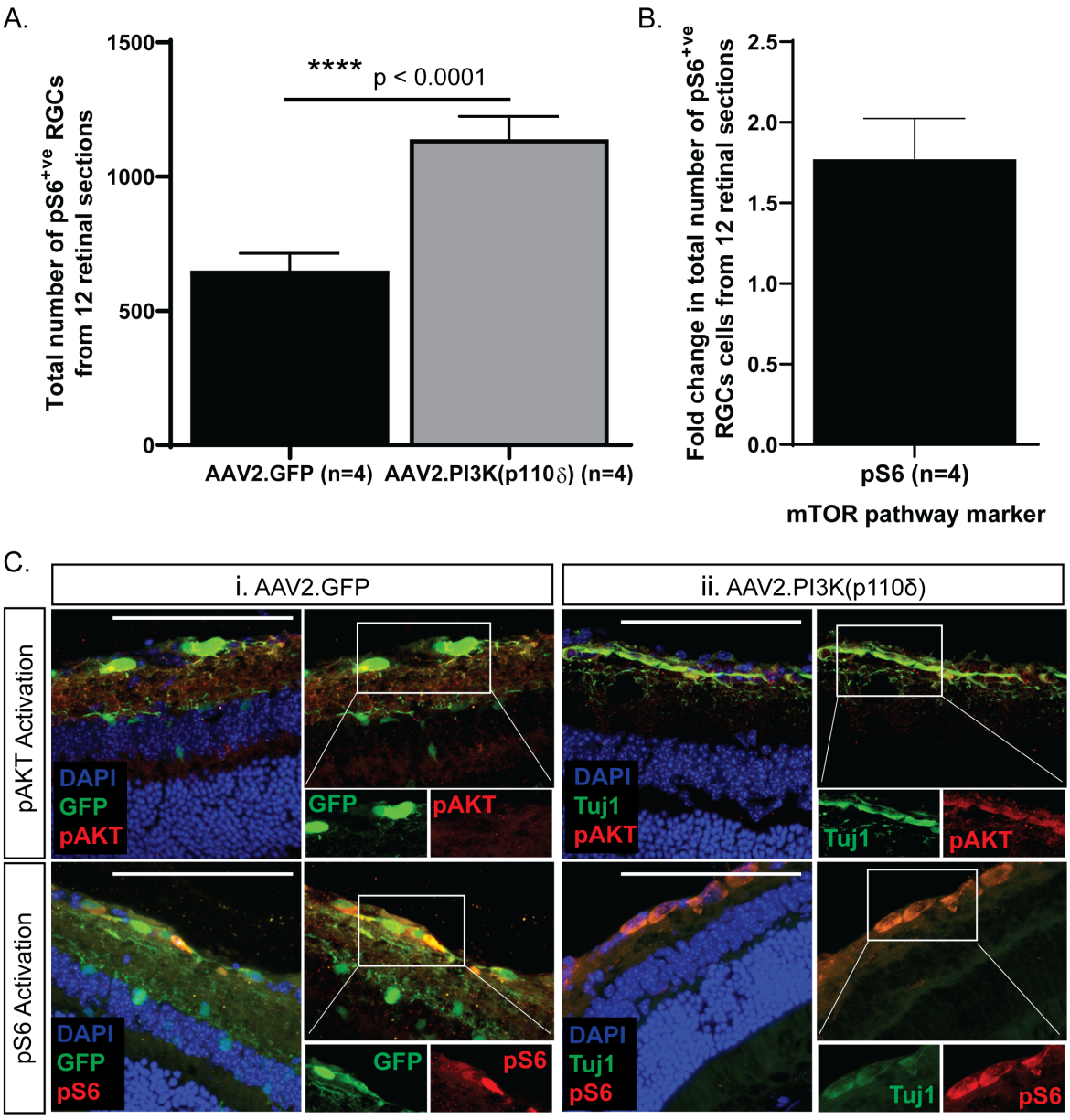

Fig. 4.13 **Viral PI3K upregulation resulted in increased mTOR pathway activity *in vivo*.** As shown in the graphs in panels A and B, pS6 signal increased in AAV2.PI3K(p110δ)-treated eyes compared to AAV2.GFP-treated eyes. Representative images are shown in panel C. p values measured by one-tailed T-test, n = 4, error bars = SD. Scale bar = 100μm.

regeneration. It would also be interesting to see to what extent mTOR inhibition neutralised the effects of PI3K upregulation.

Further work could investigate these viruses in aged mice to see whether these pro-regenerative effects are conserved with aging, like with transgenic PI3K upregulation. Additional work combining PI3K upregulation with other approaches was investigated in **Chapter 5**.

Chapter 5

Combining PI3K Upregulation with Other Strategies

5.1 Declaration

Some of the work presented in this thesis chapter is being prepared for publication, along with some insulin data not shown in this thesis, which was generated by S.S. Desphande. At the time of thesis submission, the manuscript has not yet been submitted. This work will be cited as: **Evans, R.S.**, Deshpande, S.S., Conceição, R., Hänzi, B., Hulshof, L-A., Osborne, A., Fawcett, J.W., Martin, K.R., Eva, R., Barber, A.C.. (2019) Translatable methods to stimulate mTOR mediated axon regeneration. (Manuscript in preparation).

The work presented in this thesis chapter was all generated by me, under the supervision of A.C. Barber, with contributions from others declared below.

Viruses: The AAV2.shPTEN.GFP virus was gifted by Z. He. The AAV2.PI3K(p110δ), AAV2.Integrin.V5 and AAV2.Kindlin.GFP viruses were generated by B. Hänzi, A. Osborne and L-A. Hulshof.

***In vitro* data (Fig 5.2)**: R. Conceição quantified PTEN and PI3K levels in human embryonic kidney (HEK) 293 cells transfected with the AAV2.PI3K(p110δ), AAV2.shPTEN.GFP and AAV2.shScram.GFP viruses. While I was not involved in measuring the PTEN and PI3K levels *in vitro*, the data is presented in the results section of this chapter for completeness with my *in vivo* data, with appropriate referencing in the text.

Regeneration data: All regeneration data was generated by me under the supervision of A.C. Barber.

Validation data: All validation data, including testing the viral vectors *in vitro* and *in vivo*, and quantifying mTOR pathway activity, was generated by me.

5.2 Introduction

5.2.1 Combination of Strategies for Robust Axon Regeneration

As described more fully in **Chapter 1.4**, it is becoming increasingly clear that combining clinical interventions is required for robust axon regeneration beyond the optic chiasm and into the brain. Having assessed phosphoinositide 3-kinase (PI3K) upregulation individually in **Chapters 3 and 4**, the next step was to try combining this with other approaches, like phosphatase and tensin homolog (PTEN) knockdown and integrin activation.

It was demonstrated that PI3K upregulation increased phosphatidylinositol (3,4,5)-tris-phosphate (PIP3) levels generated, resulting in pro-regenerative effects. By simultaneously knocking down PTEN, PIP3 levels would be expected to increase further by reducing the conversion from PIP3 to phosphatidylinositol(3,4)-bis-phosphate (PIP2) and could potentially have greater pro-regenerative effects than PI3K upregulation alone.

As described in **Chapter 1.3**, integrin activation upregulates the mammalian target of rapamycin (mTOR) pathway downstream of PIP3, and upregulates other pathways, including the focal adhesion kinase (FAK) pathway. Integrin activation has been shown to have pro-regenerative effects both *in vitro* and *in vivo*. Combination of integrin-α9 and kindlin-1 has been shown to lead to more robust axonal regeneration in spinal cord injury[12]. Therefore, in this experiment we introduced integrin-α9 and kindlin-1 in combination with PI3K upregulation, expecting to further enhance the regenerative effects seen from PI3K upregulation alone.

5.2.2 Aim

I investigated the effects on retinal ganglion cell (RGC) survival and axon regeneration of combining PI3K upregulation with either PTEN knockdown or with integrin activation, using the same experimental paradigm as in Chapters 3 and 4. We hypothesised that the combination treatments would increase both RGC survival and axon regeneration compared to PI3K upregulation alone.

5.3 Methods

Any references to **Chapter 2** are clearly stated in the text.

5.3.1 *In Vitro* Work

Before injecting the viruses *in vivo*, they were tested *in vitro*. Human embryonic kidney (HEK) 293 cells were transfected with AAV2.Integrin.V5 (produced for project, using integrin α9) and AAV2.Kindlin.GFP (produced for project, using kindlin-1), as described in **Chapter 2.1**. AAV2.PI3K(p110δ) (produced for project) and AAV2.GFP (Vigene Biosciences, cat no. CV17169-AV2) were validated in **Chapter 4.4.1**.

5.3.2 *In Vivo* Work

Viral Validation Work: Retinal Sections

For viral validation work *in vivo* in **Part 1**, young adult (6 to 16 weeks old) C57BL/6J mice were intravitreally injected with 2μL of AAV2.PI3K(p110δ) (produced for project) plus 2μL of AAV2.shPTEN.GFP (gifted by Z. He) into the left eye and as a control, 2μL of AAV2.PI3K(p110δ) (produced for project) plus 2μL of AAV2.shScram.GFP (SignaGen Labs, cat no. SL100815) into the right eye, as described in **Chapter 2.3**. The two injections were performed 4 days apart. All viruses were injected at a titre of 1.0 x 10^{13}GC/mL, a preoptimised titre for viral intravitreal injections.

For viral validation work *in vivo* in **Part 2**, young adult (6 to 16 weeks old) C57BL/6J mice were injected intravitreally with 2μL of AAV2.PI3K(p110δ), then 2μL of either AAV2.Integrin.V5 or AAV2.GFP, then 2μL of AAV2.Kindlin.GFP or AAV2.GFP. Another group of mice was intravitreally injected with 2μL of AAV2.Integrin.V5 and 2μL AAV2.Kindlin.GFP, without the AAV2.PI3K(p110δ), as a control. Each injection was performed 4 days apart.

2 weeks after the final injection, the mice were perfused, as described in **Chapter 2.5**. Whole eyes were collected, post-fixed in 4% paraformaldehyde (PFA) at room temperature for 2 hours, and then transferred to 20% sucrose overnight at 4°C for cryoprotection, as described in **Chapter 2.6.2**. The eyes were then embedded in Tissue-Tek OCT compound and cryosectioned (12μm thick) using a Leica cryostat (Leica Biosystems, CM 3050S Research Cryostat).

Regeneration Studies

For the regeneration work in **Part 1**, young adult (6 to 8 weeks old) C57BL/6J mice were intravitreally injected in the left eye with 2μL of AAV2.PI3K(p110δ) (produced for project) plus 2μL of AAV2.shPTEN.GFP (gifted by Z. He), or 2μL of AAV2.PI3K(p110δ) (produced

for project) plus 2μL of AAV2.shScram.GFP (SignaGen Labs, cat no. SL100815), as described in **Chapter 2.3**.

For the regeneration work in **Part 2**, young adult (6 to 8 weeks old) C57BL/6J mice were intravitreally injected with 2μL of AAV2.PI3K(p110δ), then 2μL of either AAV2.Integrin.V5 or AAV2.GFP, then 2μL of AAV2.Kindlin.GFP or AAV2.GFP. Another group of mice was intravitreally injected with 2μL of AAV2.Integrin.V5 and 2μL AAV2.Kindlin.GFP, without the AAV2.PI3K(p110δ), as a control. Each injection was performed 4 days apart.

In the second round of **Part 2**, the number of injections was reduced from 3 to 2. Young adult (6 to 8 weeks old) C57BL/6J mice were intravitreally injected with 2μL total of AAV2.PI3K(p110δ) plus AAV2.Kindlin.GFP or 2μL total of PI3K(p110δ) plus AAV2.GFP. One week later, all mice were injected with 2μL of AAV2.Integrin.V5.

2 weeks after the final injection, the mice received an optic nerve crush (ONC) injury behind the left eye, as described in **Chapter 2.4**. At 26 days post-ONC, the mice were intravitreally injected with cholera toxin subunit-β with an Alexa Fluor 555 conjugate (CTB-555) (Thermo Fisher Scientific, cat no. C22843), as described in **Chapter 2.3**. At 4 weeks post-ONC, mice were perfused, as described in **Chapter 2.5**.

The optic nerves were collected, post-fixed in 4% PFA at 4°C overnight, and transferred to 30% sucrose for at least 24 hours for cryoprotection, as described in **Chapter 2.6.1**. The nerves were then cryosectioned (14μm longitudinal sections) using a Leica cryostat (Leica Biosystems, CM 3050S Research Cryostat).

The retinas were collected, and four small incisions were made to form retinal whole-mounts (RWMs), as described in **Chapter 2.6.3**. RWMs were post-fixed in 4% PFA for 2 hours at room temperature, and then the solution was changed to phosphate-buffered saline (PBS), ready for immunohistochemistry (IHC).

5.3.3 Immunohistochemistry

IHC for HEK 293 Cells *In Vitro*

Having been fixed in 4% PFA, HEK 293 cells were counterstained with DAPI. IHC against V5 was performed on AAV2.Integrin.V5- and AAV2.GFP- transfected cells, as described in **Chapter 2.7.1**.

Retinal Section Histology

Having been fixed in 4% PFA and sectioned, IHC was performed as described in **Chapter 2.7.2**. IHC against PI3K(p110δ), GFP and V5 was used to identify the viral vectors. IHC

against phospho-AKT (pAKT) and phospho-S6 ribosomal protein (pS6) was used to quantify PI3K/AKT/mTOR pathway activity.

Retinal Wholemount Histology

Having been fixed in 4% PFA, the RWMs were then stored in PBS at 4°C. IHC against Brn3A, an RGC marker, was performed on RWMs as described in **Chapter 2.7.3**.

5.3.4 Microscopy and Quantification

Viral Validation *In Vitro*

HEK 293 cells transfected with either AAV2.Integrin.V5 or AAV2.GFP were immunostained for V5 and counterstained with DAPI. HEK 293 cells transfected with AAV2.Kindlin.GFP were counterstained with DAPI. These were imaged by confocal microscopy at x40 magnification. The images were used to confirm that the V5 or GFP viral tag signal was observed and that this signal was not seen in untransfected (naive) cells. They also confirmed that V5 signal was not seen in AAV2.GFP-transfected cells.

Viral Validation: Viral Tags

Successful viral transduction was confirmed in retinal sections injected with AAV2.Integrin.V5, immunostained for V5, and counterstained with DAPI. For AAV2.Kindlin.GFP and AAV2.GFP, slides were immunostained for GFP and counterstained with DAPI. For AAV2.PI3K(p110δ), sections were immunostained for PI3K(p110δ) and counterstained with DAPI. V5, GFP or PI3K(p110δ) signal was used to confirm the presence of the viral vectors, and eye cups were imaged using a Zeiss AxioScan Z1 at x20 magnification (0.22μm/pixel) by the team at the Histopathology/ISH core facility at the Cancer Research UK (CRUK) Cambridge. The RGC layer of retinal sections was imaged using confocal microscopy at x40 magnification.

Combination of PI3K Upregulation and PTEN Knockdown *in vitro*

Some data from R. Conceição was included in the results section for completeness. HEK 293 cells transfected with a combination of PI3K(p110δ) plus either AAV2.shPTEN.GFP or AAV2.shScram.GFP were analysed using western blots and immunoblotting for PTEN and PI3K(p110δ), as described in **Chapter 2.8**. The amount of PI3K(p110δ) and PTEN signal was quantified using Image J Fiji (Fiji-win64) and expressed relative to the β-actin signal

for each sample. The average signal relative to β-actin for AAV2.GFP-transfected cells was calculated. All values were then expressed relative to this average for AAV2.GFP.

RGC Survival

Percentage RGC survival was calculated as described in **Chapter 2.9.4**. In brief, Brn3A-stained RWMs were imaged at x20 magnification using fluorescence microscopy. For each image, the number of RGCs was quantified using a counting program in Image J Fiji (Fiji-win64). The number of surviving RGCs in the ONC (left) eye was expressed as a percentage relative to the number of RGCs in the uninjured contralateral control (right) eye.

Axon Regeneration

Axon regeneration was calculated as described in **Chapter 2.9.5**. In brief, the CTB-555-labelled axons were visualised using fluorescence microscopy at x40 magnification, counting the number of axons at 0.5mm increments from the crush site. Modelling the nerve as a cylinder, the number of regenerating axons per nerve was calculated at each increment using a previously developed formula. Four sections were counted per nerve and used to average the total number of regenerating axons per nerve.

Axonal sections were imaged using a Zeiss AxioScan Z1 at x40 magnification (0.11μm/pixel) by the Histopathology/ISH core facility at the CRUK Cambridge Institute.

Viral Validation: PI3K/AKT/mTOR Pathway Activation

Retinal sections injected with the viral vectors and immunostained with either pAKT or pS6 were examined at x40 magnification by fluorescence microscopy, as described in **Chapter 2.9.3**. In brief, 100 GFP-positive RGCs, identified using DAPI and GFP signal from the viral vector, were counted and identified as either positive or negative for pAKT. This method was repeated for retinal sections immunostained with pS6. Four mice were counted for each group (100 RGCs per mouse), and the average was expressed as a percentage of GFP-positive cells co-localised with pAKT or pS6. Representative images were taken at x80 magnification by confocal microscopy.

5.4 Results Part 1: Combination of PI3K Upregulation and PTEN Knockdown

This chapter investigates PI3K upregulation combined with either PTEN knockdown (**Part 1**) or integrin activation (**Part 2**), as summarised in **Fig. 5.1**.

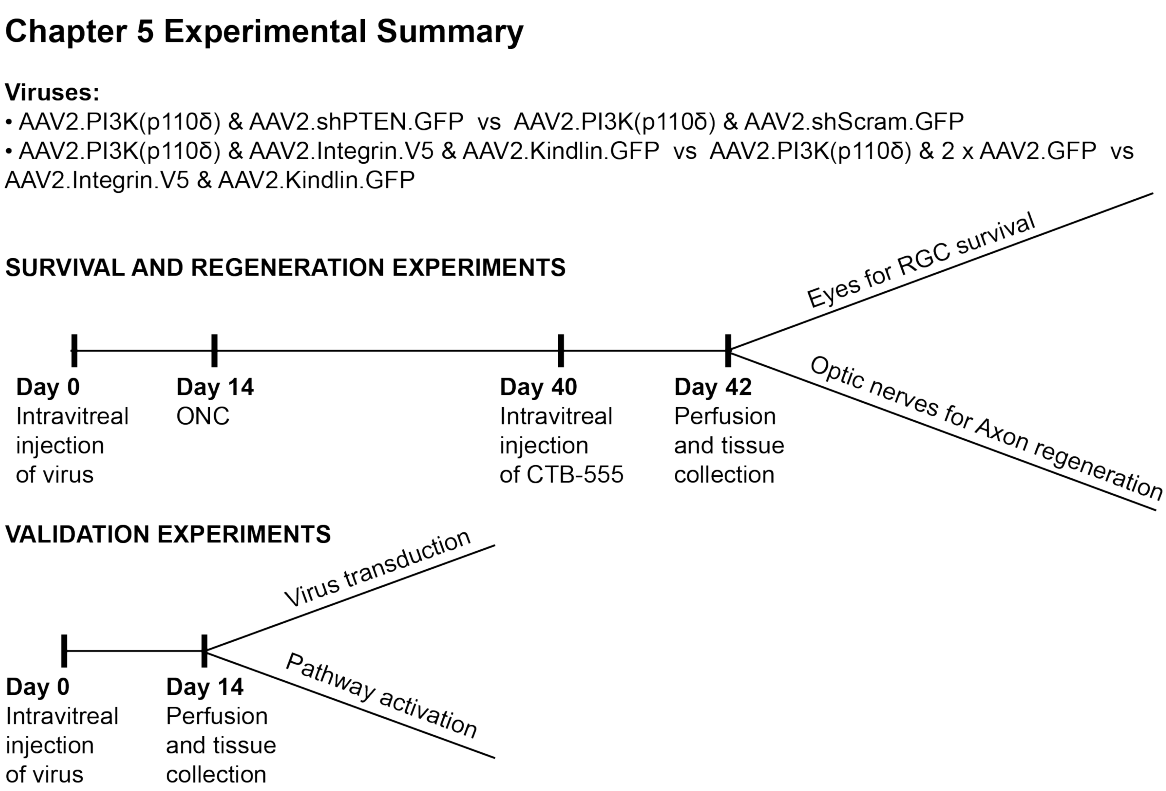

Fig. 5.1 **Chapter 5: Experimental summary.**

5.4.1 Viral Validation

Before performing regeneration experiments, AAV2.PI3K(p110δ) (produced for project), AAV2.shPTEN.GFP (gifted by Z. He), and AAV2.shScram.GFP (SignaGen Labs, cat no. SL100815) were validated *in vitro* and *in vivo* in **Chapter 4.4.1**.

Successful PTEN knockdown and PI3K upregulation was confirmed *in vitro*

R. Conceição transfected HEK 293 cells with AAV2.shScram.GFP, AAV2.shPTEN.GFP, AAV2.GFP, AAV2.PI3K(p110δ), AAV2.PI3K(p110δ) plus AAV2.shScram.GFP, and AAV2.PI3K(p110δ) plus AAV2.shPTEN.GFP. These were immunoblotted for PTEN and

PI3K(p110δ) using the western blot technique (included here for completeness with my *in vivo* work).

HEK 293 cells treated with AAV2.PI3K(p110δ) plus AAV2.shScram.GFP showed 1.48±0.18 PTEN signal (n=3 wells) (fold change in PTEN relative to AAV2.GFP-treated cells), which decreased to 0.14±0.09 in HEK 293 cells treated with AAV2.PI3K(p110δ) plus AAV2.shPTEN.GFP (one-way ANOVA with Tukey's post-hoc analysis, $p<0.0001$), as shown in **Fig. 5.2**. There was 10.3-fold more PTEN signal in the control group than the PTEN knockdown group.

HEK 293 cells treated with AAV2.PI3K(p110δ) plus AAV2.shScram.GFP showed 27.45±14.89 PI3K(p110δ) signal (n=3 wells) (fold change in PI3K(p110δ) relative to AAV2.GFP-treated cells) and HEK 293 cells treated with AAV2.PI3K(p110δ) plus AAV2.shPTEN.GFP showed 31.40±7.76 signal (n=3 wells). As expected, there were no significant differences in PI3K(p110δ) signal between the two groups.

As expected, the results showed no significant differences in PTEN signal or PI3K(p110δ) signal between individually transfecting with AAV2.shPTEN.GFP or AAV2.PI3K(p110δ) versus in combination, as shown in **Fig. 5.2**.

A combination of AAV2.PI3K(p110δ) plus either AAV2.shPTEN.GFP or AAV2.shScram.GFP successfully transduced RGCs *in vivo*.

Viral transduction of RGCs was tested *in vivo*. Young adult (6 to 16 weeks old) C57BL/6J mice were intravitreally injected with 2μL of AAV2.PI3K(p110δ) plus 2μL of AAV2.shPTEN.GFP in the left eye and as a control, 2μL of AAV2.PI3K(p110δ) plus 2μL of AAV2.shScram.GFP in the right eye. The two injections were performed 4 days apart. The eyes were collected 2 weeks after the second injection, and 12μm retinal sections were produced.

Successful viral transduction *in vivo* was confirmed by signal from the viral tag, GFP, in the RGC layer from the AAV2.shPTEN.GFP and AAV2.shScram.GFP viruses. The presence of PI3K(p110δ) was confirmed for the AAV2.PI3K(p110δ) virus. Eye cup images showed signal throughout the retina, and closer inspection of the retinal sections confirmed that this signal was in the RGC layer, as shown in **Fig. 5.3**, where staining was indicative of RGCs.

5.4.2 RGC Survival and Axon Regeneration

Young adult (6 to 8 weeks old) C57BL/6J mice were intravitreally injected in the left eye with 2μL of AAV2.PI3K(p110δ) plus 2μL of either AAV2.shPTEN.GFP or AAV2.shScram.GFP. The two injections were performed 4 days apart. 2 weeks after the final injection, ONC injury

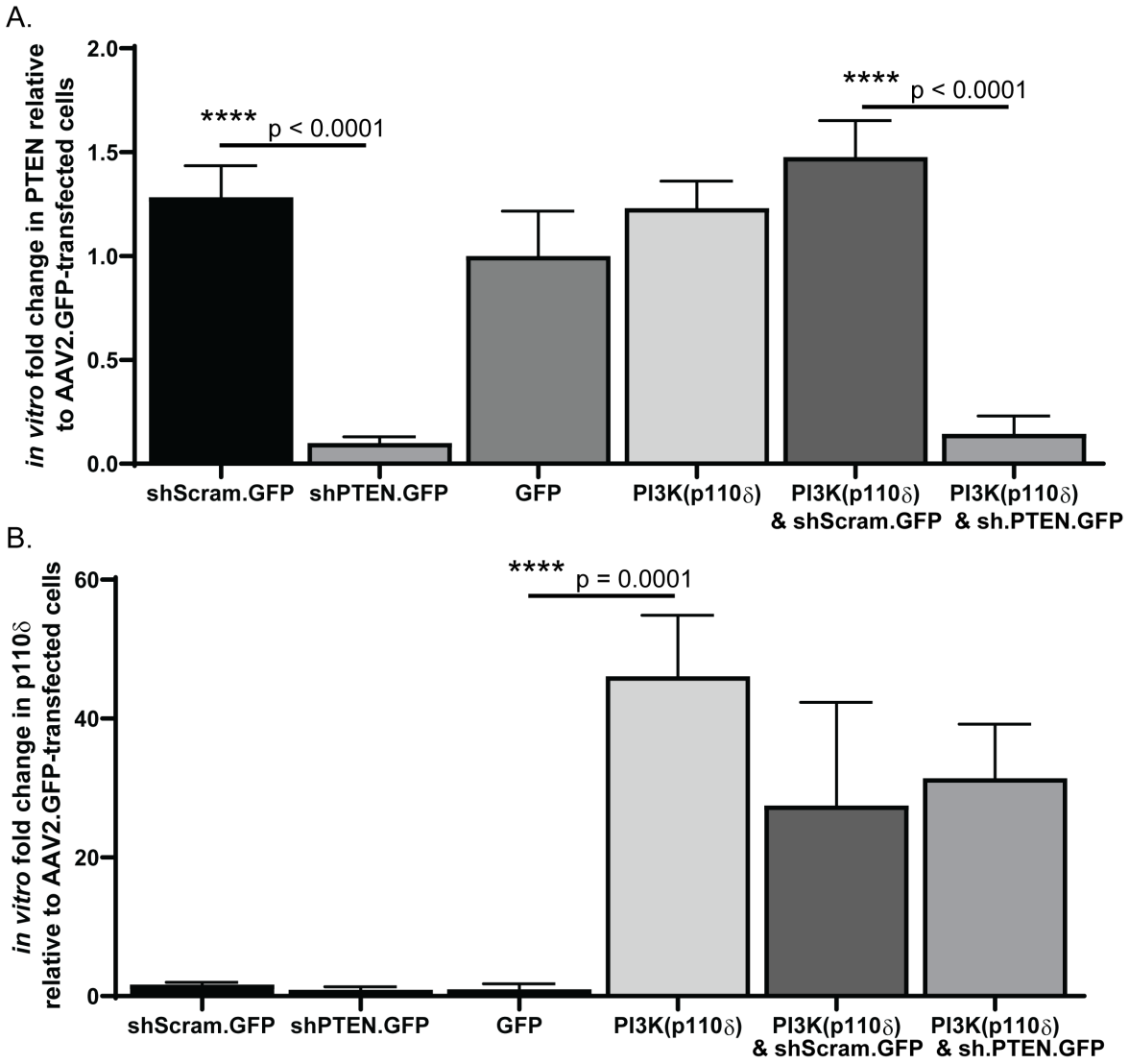

Fig. 5.2 **Combination of PI3K upregulation and PTEN knockdown *in vitro*.** HEK 293 cells were transfected with AAV2.shScram.GFP, AAV2.shPTEN.GFP, AAV2.GFP, AAV2.PI3K(p110δ), AAV2.PI3K(p110δ) plus AAV2.shScram.GFP, or AAV2.PI3K(p110δ) plus AAV2.shPTEN.GFP. In panel A, the fold change in PTEN signal is shown for all groups. In panel B, the fold change in PI3K(p110δ) signal is shown for all groups. p values measured by one-way ANOVA with Tukey's post-hoc analysis, n = 3, error bars = SD. Data provided by R. Conceição.

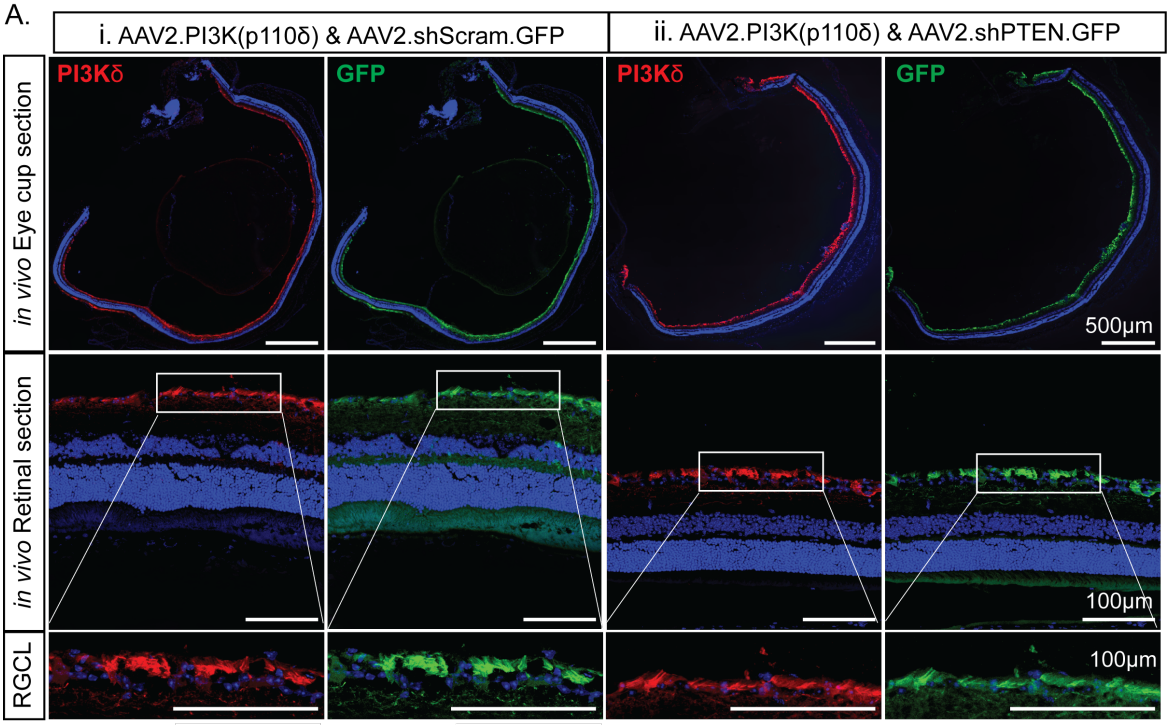

Fig. 5.3 **Successful viral transduction of AAV2.PI3K(p110δ) plus AAV2.shPTEN.GFP or AAV2.shScram.GFP was confirmed *in vivo*.** Eye cups and zoomed in images of the RGC layer showed GFP signal in RGCs throughout the retina for AAV2.shScram.GFP (Ai) and AAV2.shPTEN.GFP (Aii). PI3K(p110δ) signal was seen in RGCs throughout the retina for AAV2.PI3K(p110δ) (Ai and Aii). Staining was indicative of RGCs. Scale bar = 500μm for eye cups, 100μm for retinal sections.

was performed behind the left eye. At 26 days post-ONC, 2μL of cholera toxin subunit-β with an Alexa Fluor 555 conjugate (CTB-555) was intravitreally injected into the left eye. At 4 weeks post-ONC, the eyes and optic nerves were collected.

Combining PI3K upregulation with PTEN knockdown promoted RGC survival compared to the control but was not significantly greater than AAV2.PI3K(p110δ) or AAV2.shPTEN.GFP delivered individually.

The retinas were collected at 4 weeks post-ONC and IHC against Brn3A, an RGC marker, was used to quantify RGCs. The number of surviving RGCs in the ONC (left) eye was expressed as a percentage relative to the uninjured contralateral control (right) eye.

Young adult (6 to 8 weeks old) mice treated with AAV2.PI3K(p110δ) plus AAV2.shPTEN.GFP showed 17.6%±7.6 (n=10 retinas) RGC survival, which was a significant increase from the 7.8%±3.1 (n=9 retinas) RGC survival seen in mice treated with AAV2.PI3K(p110δ) plus AAV2.shScram.GFP (one-way ANOVA with Tukey's post-hoc analysis, p=0.0378), as shown in **Fig. 5.4**. Interestingly, mice treated with AAV2.PI3K(p110δ) plus AAV2.shScram.GFP showed a slightly decreased RGC survival (7.8%) compared to AAV2.PI3K(p110δ) alone (11.3%), but this was not statistically significant. Therefore, a combination of viral PI3K upregulation and PTEN knockdown promoted RGC survival at 4 weeks post-ONC relative to control.

Comparing the combination of PI3K upregulation and PTEN knockdown with AAV2.PI3K(p110δ) and AAV2.shPTEN.GFP delivered separately, no significant differences were seen. Therefore, this approach did not yield significantly greater results than individually targeting either PI3K upregulation or PTEN knockdown.

Combination of PI3K upregulation with PTEN knockdown promoted axon regeneration compared to control, but less so than AAV2.PI3K(p110δ) delivered individually.

2 days before tissue collection, the left eyes were intravitreally injected with 2μL of CTB-555. At 4 weeks post-ONC, the optic nerves were dissected, and 14μm thick sections were produced. Axons were counted using the CTB-555 fluorescence at 0.5mm increments.

Young adult (6 to 8 weeks old) mice treated with AAV2.PI3K(p110δ) plus AAV2.shPTEN.GFP showed 77±26 regenerating axons (n=6 nerves) at 0.5mm from the crush site, significantly higher than the 32±17 axons (n=8 nerves) in the control group (two-way ANOVA with Tukey's post-hoc analysis, p=0.0009). The treatment group also showed 33±23 regenerating axons at 1.0mm from the crush site, significantly higher than the 15±10 axons in the control group (two-way ANOVA with Tukey's post-hoc analysis, p=0.0335), as shown

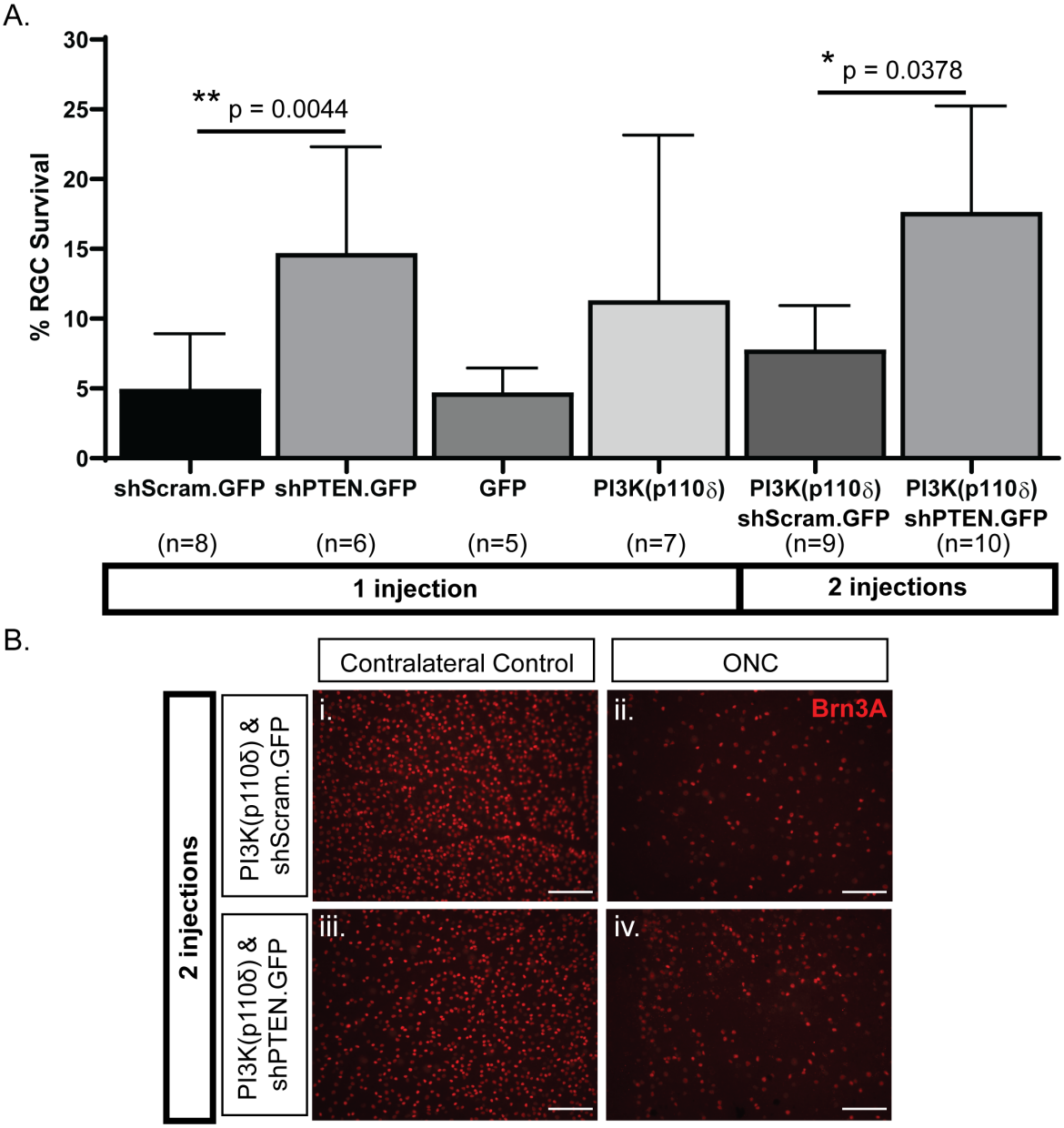

Fig. 5.4 **Combination of PI3K upregulation with PTEN knockdown promoted RGC survival compared to control**. As seen in panel A, AAV2.PI3K(p110δ) plus AAV2.shPTEN.GFP promoted RGC survival 4 weeks post-ONC injury compared to control, but not significantly more than AAV2.PI3K(p110δ) or AAV2.shPTEN.GFP delivered individually. RWMs were stained with Brn3A (red), which was used to quantify RGCs. The number of RGCs in the ONC (left) eye (panels Bii and Biv) was expressed as a percentage survival relative to the uninjured contralateral control (right) eye (Bi and Biii). p values measured by one-way ANOVA with Tukey's post-hoc analysis, n = 5 to 10 as specified, error bars = SD. Scale bar = 100μm.

in **Fig. 5.5**. Regenerating axons were seen up to 3.0mm from the crush site. Therefore, the combination of PI3K upregulation and PTEN knockdown increased axon regeneration compared to the control.

Comparing these results with AAV2.PI3K(p110δ) delivered individually, the AAV2.PI3K(p110δ)-treated mice (180 axons) showed significantly greater axon regeneration than both AAV2.PI3K(p110δ) plus AAV2.shPTEN.GFP (77 axons) (two-way ANOVA with Tukey's post-hoc analysis, p=0.0128) and AAV2.PI3K(p110δ) plus AAV2.shScram.GFP (32 axons) (two-way ANOVA with Tukey's post-hoc analysis, p=0.0003) at 0.5mm from the crush site. AAV2.PI3K(p110δ)-treated mice (104 axons) also showed significantly greater axon regeneration than AAV2.PI3K(p110δ) plus AAV2.shPTEN.GFP (33 axons) (two-way ANOVA with Tukey's post-hoc analysis, p=0.0391) and AAV2.PI3K(p110δ) plus AAV2.shScram.GFP (15 axons) (two-way ANOVA with Tukey's post-hoc analysis, p=0.0056) at 1.0mm from the crush site.

Comparing these results with AAV2.shPTEN.GFP delivered individually, AAV2.shPTEN.GFP-treated mice (117 axons) showed significantly greater axon regeneration than AAV2.PI3K(p110δ) plus AAV2.shScram.GFP (32 axons) (two-way ANOVA with Tukey's post-hoc analysis, p=0.2200) at 0.5mm from the crush site.

Therefore, this combination approach did not yield significantly greater results than individually targeting PI3K upregulation or PTEN knockdown. In fact, PI3K upregulation individually gave significantly greater results than in combination with PTEN knockdown.

5.4.3 mTOR Pathway Activation

Viral PI3K upregulation combined with viral PTEN knockdown increases the mTOR pathway activity.

IHC against mTOR pathway markers (pAKT and pS6) was performed on the retinal sections used for viral validation. The percentage of GFP-labelled cells in the RGC layer co-localised with either pAKT or pS6 was quantified and compared to control injection, as shown in **Fig. 5.6**. Staining was indicative of RGCs.

Eyes injected with AAV2.PI3K(p110δ) plus AAV2.shScram.GFP (control) showed 49.3%±7.5 pAKT-GFP-labelled cells, which increased in AAV2.PI3K(p110δ) plus AAV2.shPTEN.GFP-injected eyes (treatment) to 73.5%±5.1 (one-tailed T-test, p=0.0009). The average fold change in pAKT was 1.5±0.2. The control-injected eyes showed 65.6%±6.4 pS6-GFP-labelled cells, which increased in treatment-injected eyes to 80.5%±6.4 (one-tailed T-test, p=0.0092). The average fold change in pS6 was 1.2±0.1.

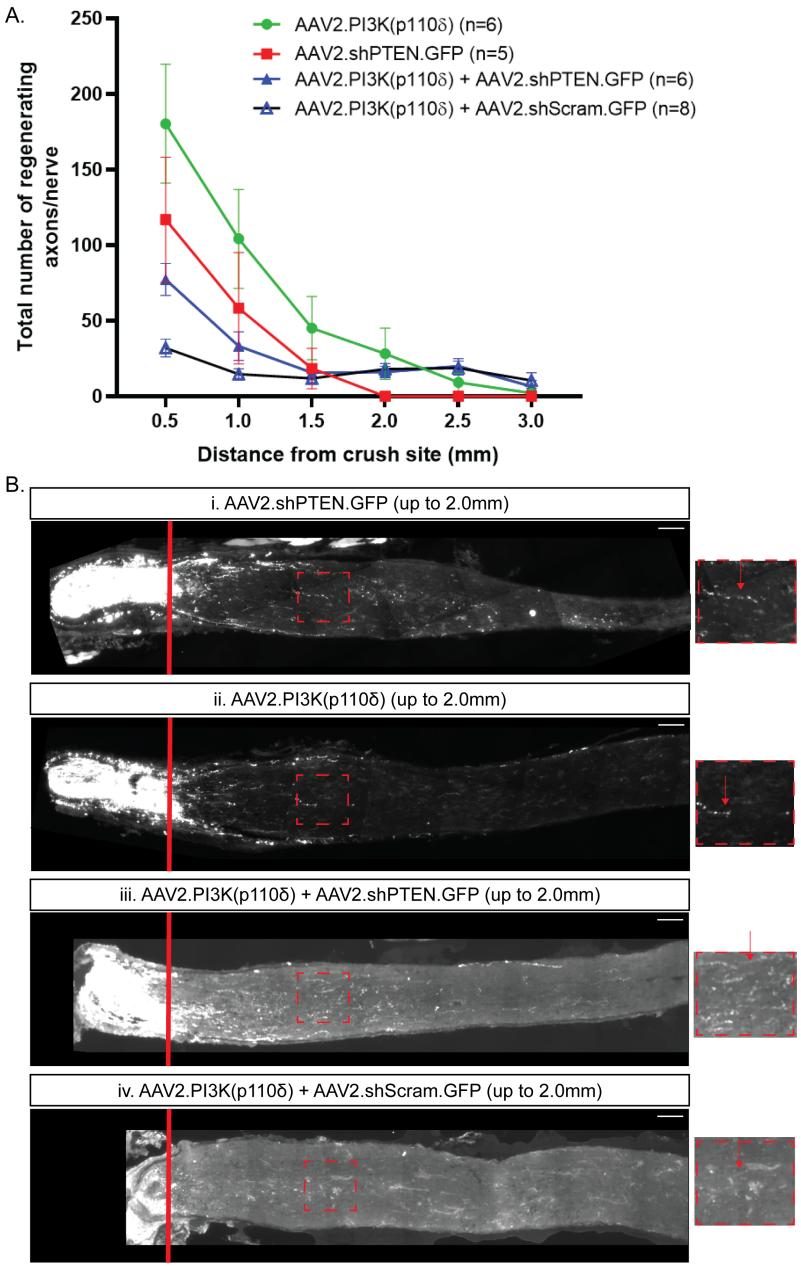

Fig. 5.5 **Combination of PI3K upregulation with PTEN knockdown promoted axon regeneration compared to control.** As shown in panel A, AAV2.PI3K(p110δ) plus AAV2.shPTEN.GFP promoted axon regeneration following ONC injury compared to control. Images of crushed nerves are shown in panel B for AAV2.shPTEN.GFP (Bi), AAV2.PI3K(p110δ) (Bii), AAV2.PI3K(p110δ) plus AAV2.shPTEN.GFP (Biii), and for AAV2.PI3K(p110δ) plus AAV2.shScram.GFP (Biv) p values measured by two-way ANOVA with Tukey's post-hoc analysis but not marked on graph, n = 5 to 8 as specified, error bars = SEM. Scale bar = 100μm.

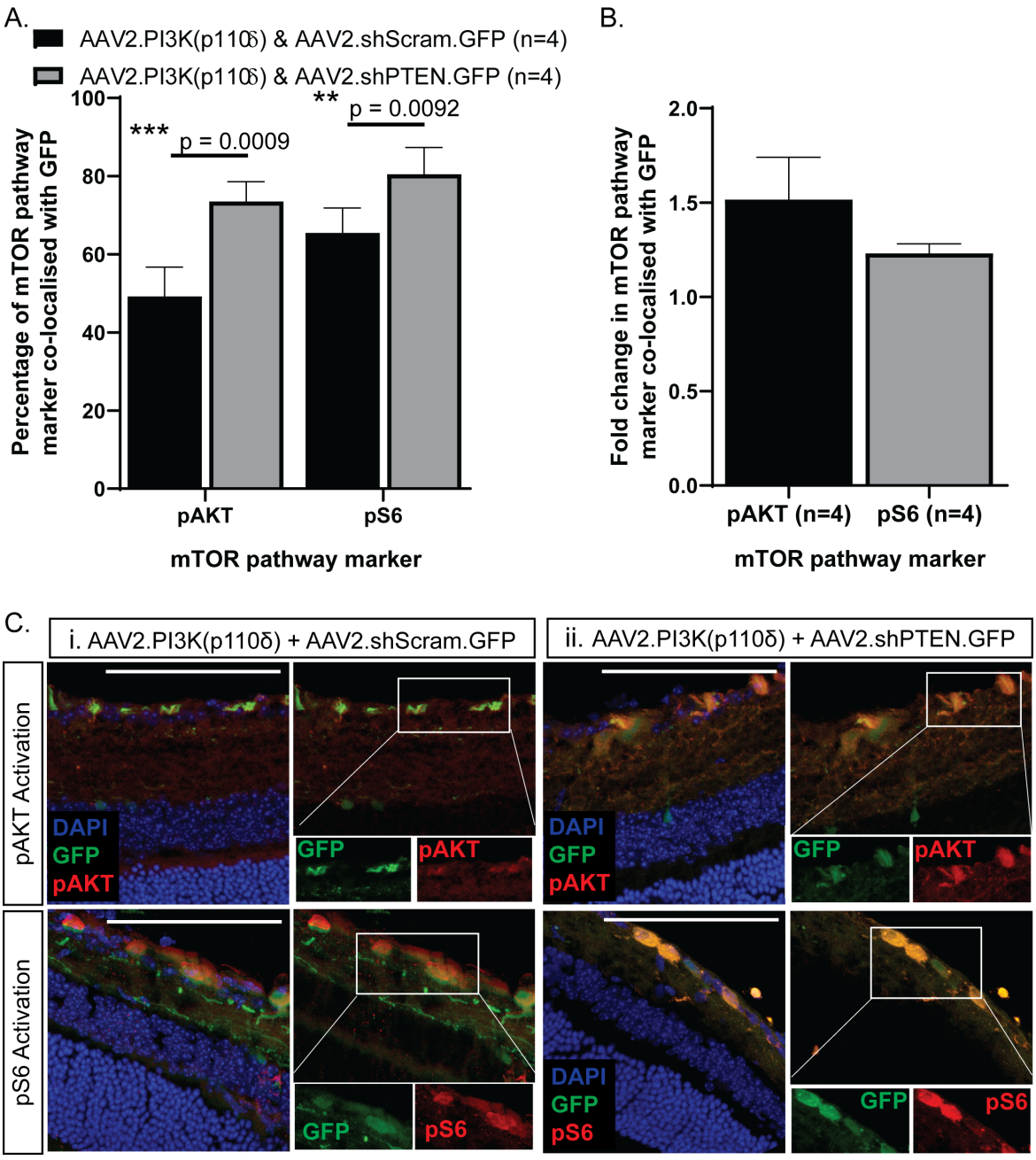

Fig. 5.6 **Combination of viral PI3K upregulation with viral PTEN knockdown resulted in increased mTOR pathway activity *in vivo*.** As shown in the graphs in panels A and B, pAKT and pS6 signal increased in retinal sections from C57BL/6J mice injected with AAV2.PI3K(p110δ) plus AAV2.shPTEN.GFP compared to AAV2.PI3K(p110δ) plus AAV2.shScram.GFP. Representative images are shown in panel C. Staining in the RGC layer was indicative of RGCs. p values measured by one-tailed T-test, n = 4, error bars = SD. Scale bar = 100μm.

Transgenic PI3K upregulation combined with viral PTEN knockdown increases mTOR pathway activity

For comparison, mTOR pathway activation was investigated using transgenic PI3K upregulation with viral PTEN knockdown. Young adult (6 to 16 weeks old) hyperactive p110α (p110α^{H1047R}) mice and p110δ mice were intravitreally injected with 2μL of AAV2.Cre.GFP plus 2μL of AAV2.shPTEN.GFP in the left eye and as a control, 2μL of AAV2.Cre.GFP plus 2μL of AAV2.shScram.GFP in the right eye. The two injections were performed 4 days apart. The eyes were collected 2 weeks after the second injection, and 12μm retinal sections were produced.

IHC against mTOR pathway markers (pAKT and pS6) was performed on retinal sections. The percentage of GFP-labelled cells in the RGC layer co-localised with either pAKT or pS6 was quantified and compared to control injection, as shown in **Fig. 5.7**. Staining was indicative of RGCs.

In the p110α^{H1047R} mice, the AAV2.Cre.GFP plus AAV2.shScram.GFP-injected eyes (control) showed 60.3%±7.4 pAKT-GFP-labelled cells, which increased to 82.8%±5.3 in AAV2.Cre.GFP plus AAV2.shPTEN.GFP-injected eyes (treatment) (one-tailed T-test, p=0.0013). The average fold change in pAKT was 1.4±0.1. The control-injected eyes showed 80.0%±5.4 pS6-GFP-labelled cells, which increased to 90.0%±1.6 in treatment-injected eyes (one-tailed T-test, p=0.0059). The average fold change in pS6 was 1.1±0.1.

In the p110δ mice, the control-injected eyes showed 48.8%±12.0 pAKT-GFP-labelled cells, which increased to 77.8%±5.4 in treatment-injected eyes (one-tailed T-test, p=0.0023). The average fold change in pAKT was 1.7±0.5. The control-injected eyes showed 64.5%±10.4 pS6-GFP-labelled cells, which increased to 87.5%±1.3 in treatment-injected eyes (one-tailed T-test, p=0.0023). The average fold change in pS6 was 1.4±0.2.

On comparison of mTOR pathway activation in the viral versus the transgenic PI3K(p110δ) approach, there were no significant differences in pAKT and pS6 levels. Interestingly, the PI3K(p110δ) viral approach showed significantly less pAKT and pS6 signal than in the transgenic p110α^{H1047R} mice (two-tailed T-test, p=0.0453 for pAKT and p=0.0358 for pS6). However, when fold-change was assessed, no significant differences were seen.

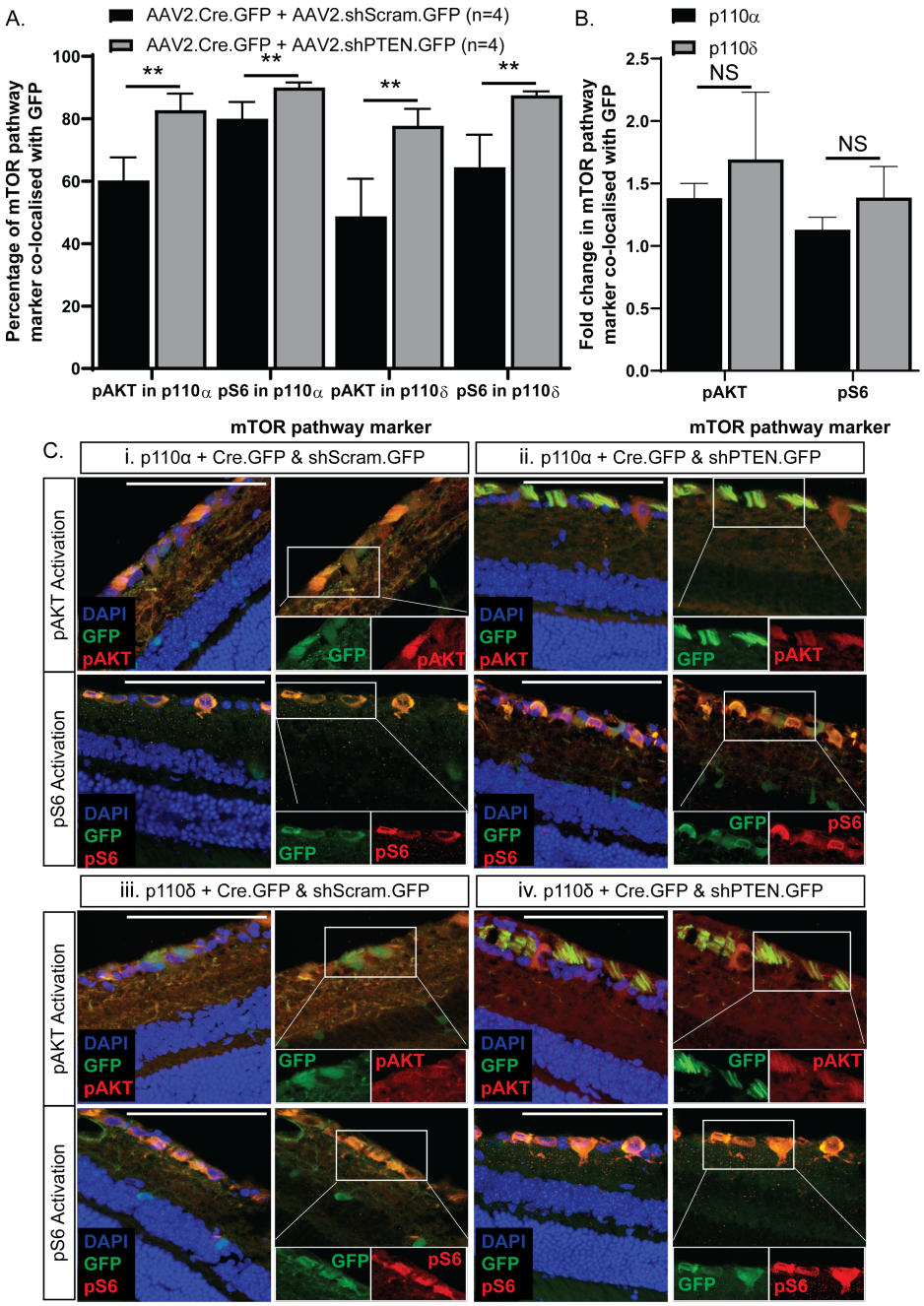

Fig. 5.7 **Combination of transgenic PI3K upregulation with viral PTEN knockdown resulted in increased mTOR pathway activity *in vivo*.** As shown in the graphs in panels A and B, pAKT and pS6 signal increased in retinal sections from p110δ mice and p110 hyperactive alpha mice injected with AAV2.Cre.GFP plus AAV2.shPTEN.GFP compared to AAV2.Cre.GFP plus AAV2.shScram.GFP. Representative images are shown in panel C. Staining in the RGC layer was indicative of RGCs. p values measured by one-tailed T-test, n = 4, error bars = SD. Scale bar = 100μm.

5.5 Results Part 2: Combination of PI3K Upregulation and Integrin Activation

5.5.1 Viral Validation

Prior to performing regeneration experiments, AAV2.PI3K(p110δ) (produced for project) and AAV2.GFP (Vigene Biosciences, cat no. CV17169-AV2) were validated *in vitro* and *in vivo* in **Chapter 4.4.1**.

AAV2.Integrin.V5 and AAV2.Kindlin.GFP successfully transfected HEK 293 cells *in vitro*

Before using the AAV2.Integrin.V5 and AAV2.Kindlin.GFP viruses *in vivo*, successful viral transfection was confirmed *in vitro* using HEK 293 cells, as shown in **Fig. 5.8**. Signal from the viral tags, V5 and GFP, was detected from the viruses, confirming successful transfection. V5 signal was seen for the AAV2.Integrin.V5 virus but was absent in the AAV2.GFP virus, confirming antibody specificity.

AAV2.PI3K(p110δ), AAV2.Integrin.V5, AAV2.Kindlin.GFP and AAV2.GFP successfully transduced RGCs *in vivo*

Viral transduction of RGCs was tested *in vivo*. Young adult (6 to 16 weeks old) C57BL/6J mice were injected intravitreally with 2μL of AAV2.PI3K(p110δ), then 2μL of either AAV2.Integrin.V5 or AAV2.GFP, then 2μL of AAV2.Kindlin.GFP or AAV2.GFP. Another group of mice was intravitreally injected with 2μL of AAV2.Integrin.V5 and 2μL AAV2.Kindlin.GFP, without the AAV2.PI3K(p110δ), as a control. Each injection was performed 4 days apart. The eyes were collected 2 weeks after the final injection, and 12μm retinal sections were produced.

Successful viral transduction of AAV2.Integrin.V5, AAV2.Kindlin.GFP, and AAV2.GFP *in vivo* was confirmed by signal from the viral tag, V5 or GFP, in the RGC layer. The presence of PI3K(p110δ) was confirmed for the AAV2.PI3K(p110δ) virus. Eye cup images showed signal throughout the retina, and closer inspection of the retinal sections confirmed that this signal was in the RGC layer, as shown in **Fig. 5.9**, where staining was indicative of RGCs.

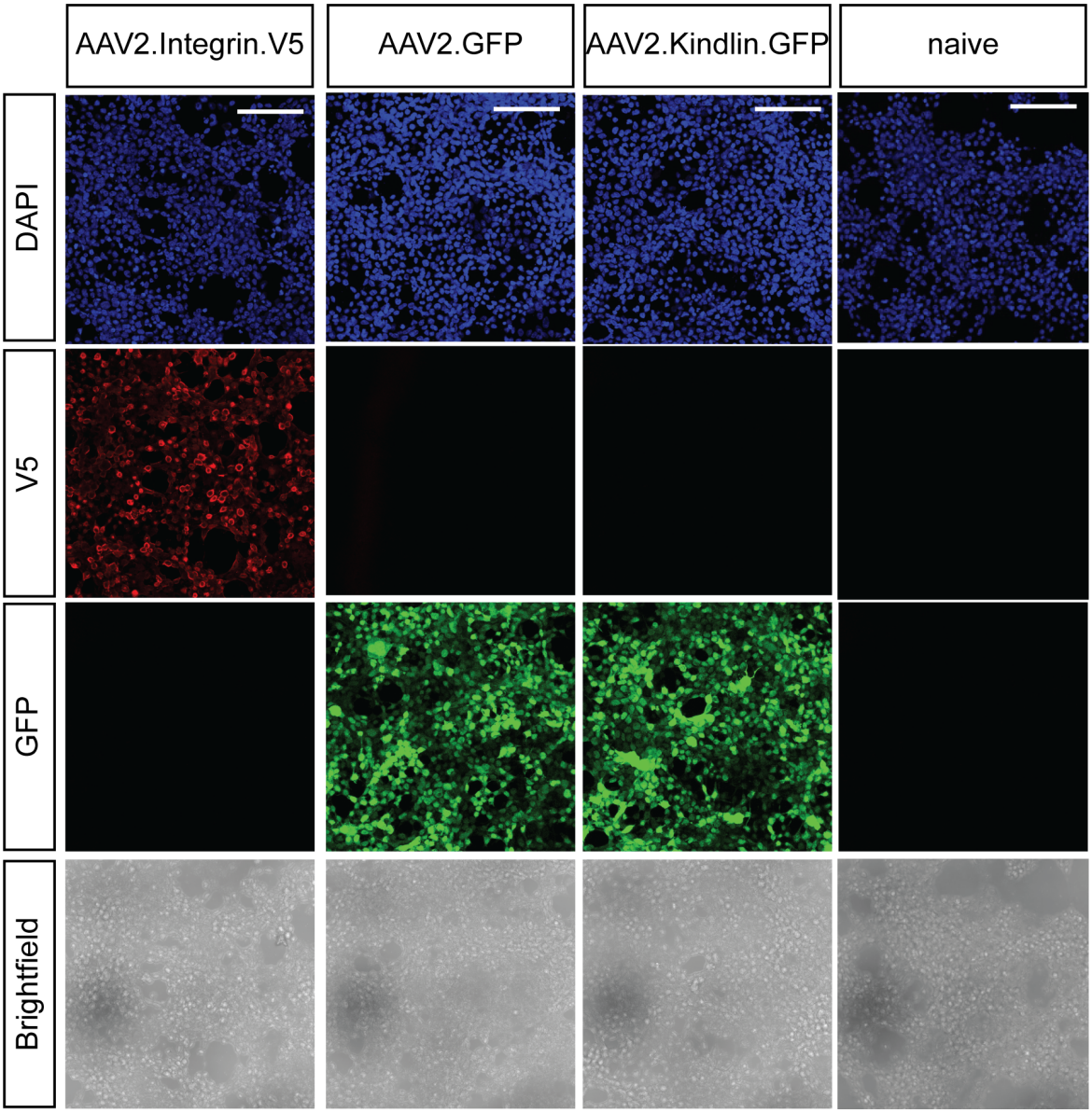

Fig. 5.8 **AAV2.Integrin.V5 and AAV2.Kindlin.GFP were tested *in vitro*.** AAV2.Integrin.V5 and AAV2.Kindlin.GFP were tested in HEK 293 cells prior to *in vivo* work. The presence of GFP signal in AAV2.Kindlin.GFP indicated successful transfection. V5 signal was seen from AAV2.Integrin.V5 but not in AAV2.GFP, confirming antibody specificity.

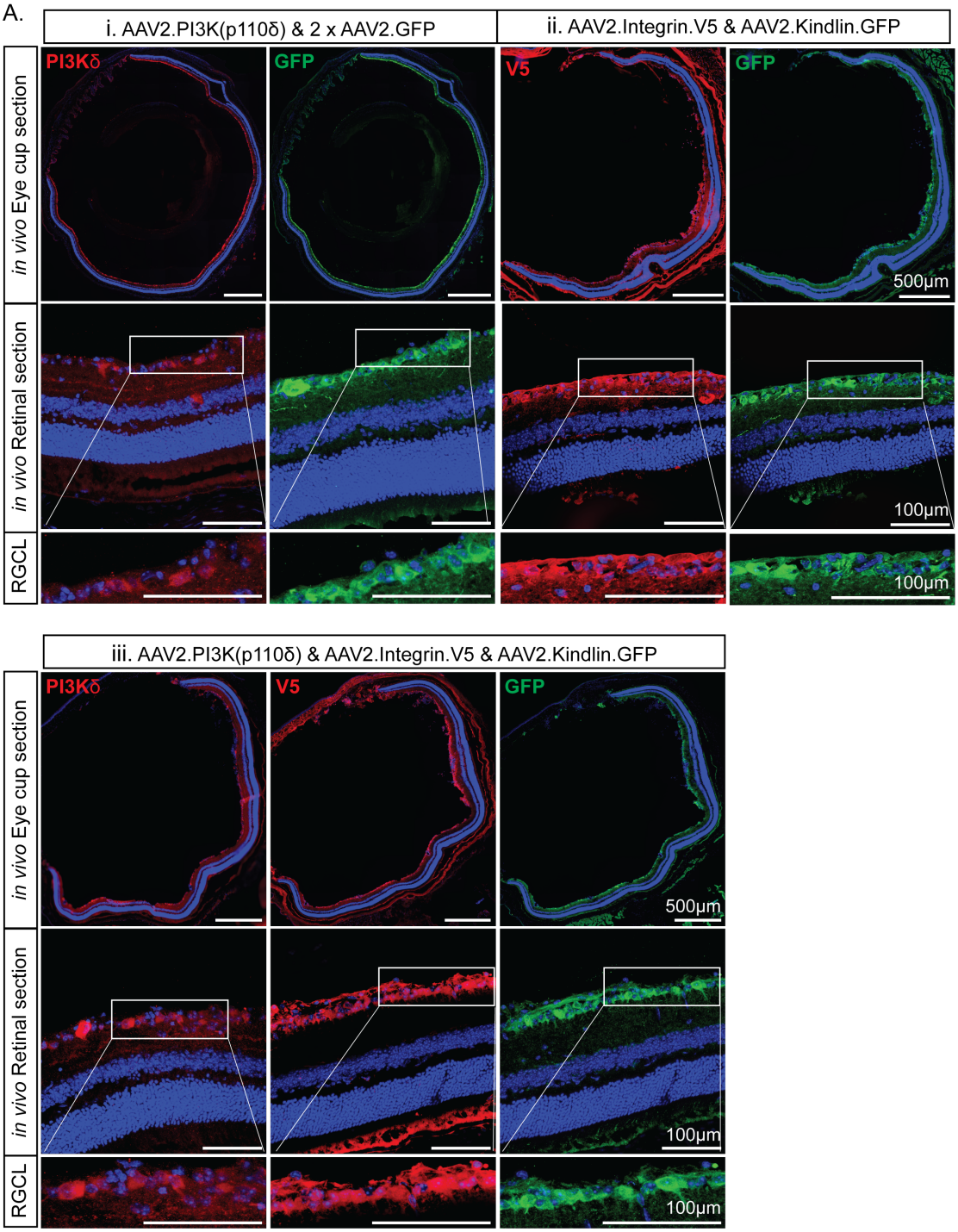

Fig. 5.9 **Viruses for PI3K upregulation and integrin activation were successfully transduced *in vivo*.** Eye cups and zoomed in images of the RGC layer showed p110δ signal in RGCs throughout the retina from AAV2.PI3K(p110δ) (Ai and Aiii), V5 signal in RGCs throughout the retina from AAV2.Integrin.V5 (Aii and Aiii), and GFP signal in RGCs throughout the retina for AAV2.GFP (Ai) and for AAV2.Kindlin.GFP (Aii and Aiii). Staining was indicative of RGCs. Scale bar = 500μm for eye cups, 100μm for retinal sections.

5.5.2 RGC Survival and Axon Regeneration

Young adult (6 to 8 weeks old) C57BL/6J mice were injected intravitreally with 2μL of AAV2.PI3K(p110δ), then 2μL of either AAV2.Integrin.V5 or AAV2.GFP, then 2μL of AAV2.Kindlin.GFP or AAV2.GFP. Another group of mice was intravitreally injected with 2μL of AAV2.Integrin.V5 and 2μL AAV2.Kindlin.GFP, without the AAV2.PI3K(p110δ), as a control. Each injection was performed 4 days apart.

As this experiment was unsuccessful, a second round of the experiment was performed, reducing the number of injections from three to two. Young adult (6 to 8 weeks old) C57BL/6J mice were intravitreally injected with 2μL total of AAV2.PI3K(p110δ) plus AAV2.Kindlin.GFP or 2μL total of PI3K(p110δ) plus AAV2.GFP. 1 week later, the mice were intravitreally injected with either 2μL of AAV2.Integrin.V5 or 2μL AAV2.GFP.

2 weeks after the final injection, ONC surgery was performed. At 26 days post-ONC, 2μL of cholera toxin subunit-β with an Alexa Fluor 555 conjugate (CTB-555) was intravitreally injected into the left eye. At 4 weeks post-ONC, the eyes and optic nerves were collected,

Combination of PI3K upregulation with integrin activation promoted RGC Survival compared to control with two injections, but not with three injections

The retinas were collected at 4 weeks post-ONC and IHC against Brn3A, an RGC marker, was used to quantify RGCs. The number of surviving RGCs in the ONC (left) eye was expressed as a percentage relative to the uninjured contralateral control (right) eye.

Mice treated with AAV2.PI3K(p110δ) plus AAV2.Integrin.V5 and AAV2.Kindlin.GFP spread over three injections showed 9.8%±7.5 (n=5 retinas) RGC survival compared to mice treated with AAV2.PI3K(p110δ) plus two doses of AAV2.GFP spread over 3 injections, which showed 5.7%±2.0 (n=8 retinas) survival (see **Fig. 5.10**). No significant difference was found between the groups.

Mice treated with AAV2.PI3K(p110δ) plus AAV2.Integrin.V5 and AAV2.Kindlin.GFP spread over two injections showed 9.0%±2.8 (n=7 retinas) RGC survival, which was significantly higher than the 7.0%±1.4 (n=8 retinas) RGC survival in AAV2.PI3K(p110δ) plus two doses of AAV2.GFP (one-tailed T-test, p=0.0496), as seen in **Fig. 5.11**. Mice treated with AAV2.PI3K(p110δ) plus AAV2.Integrin.V5 and AAV2.Kindlin.GFP also showed significantly higher RGC survival than the control with AAV2.Integrin.V5 and AAV2.Kindlin.GFP alone, which showed 2.0%±0.9 (n=7 retinas) RGC survival one-tailed T-test, p<0.0001). On comparison with AAV2.PI3K(p110δ) delivered individually, no significant differences were found in RGC survival.

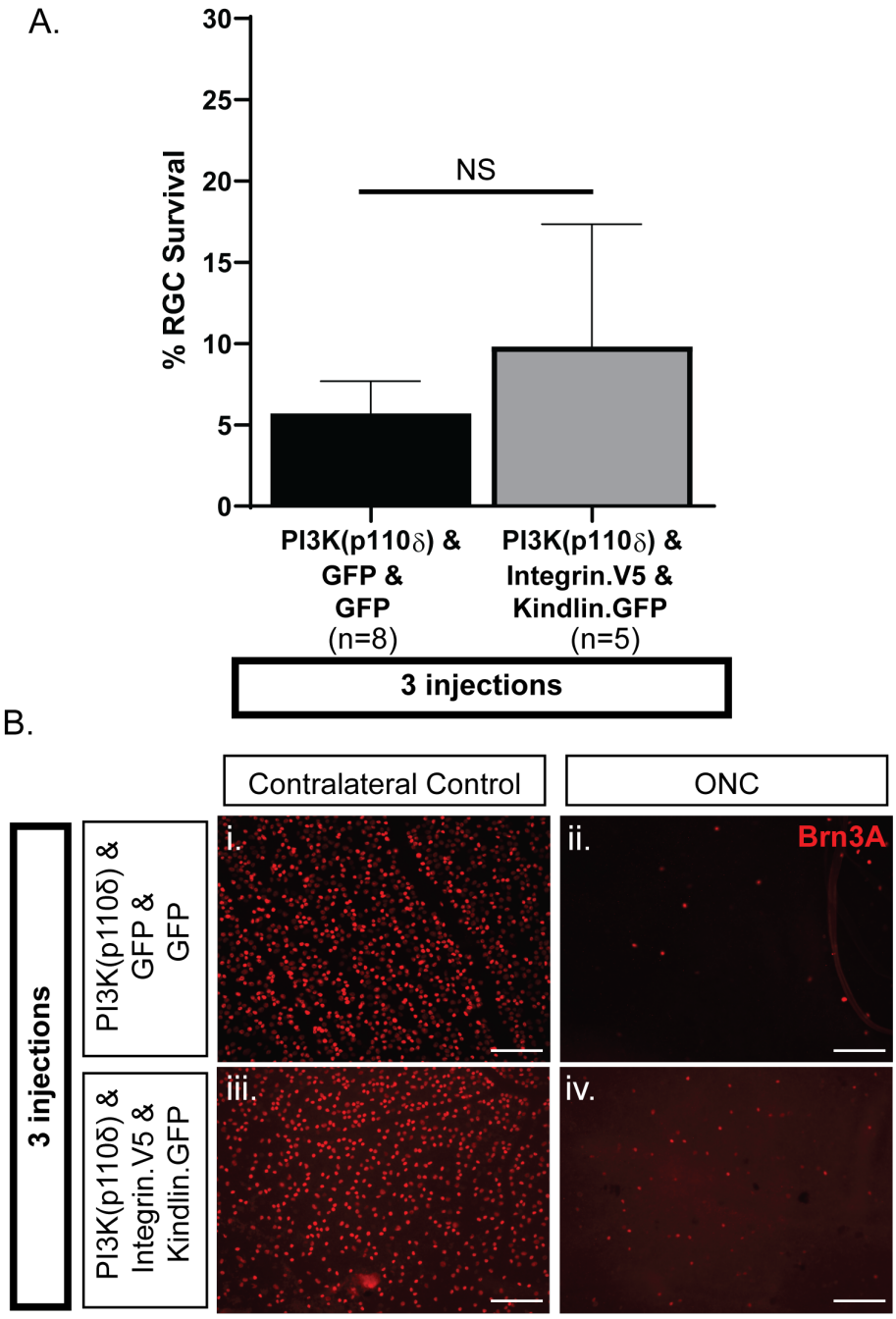

Fig. 5.10 **3 Injections: Combination of PI3K upregulation with integrin activation had no significant effect on RGC survival compared to control**. As seen in panel A, AAV2.PI3K(p110δ) plus AAV2.Integrin.V5 and AAV2.Kindlin.GFP had no significant effect on RGC survival 4 weeks post-ONC injury. RWMs were stained with Brn3A (red), which was used to quantify RGCs. The number of RGCs in the ONC (left) eye (Bii and Biv) was expressed as a percentage survival relative to the uninjured contralateral control (right) eye (Bi and Biii). p values measured by one-tailed T-test, n = 5 to 8 as specified, error bars = SD. Scale bar = 100μm.

Therefore, the combination of PI3K upregulation with integrin activation resulted in a very slight increase in RGC survival compared to control but was not significantly different from PI3K upregulation alone.

Combination of PI3K upregulation with integrin activation had no significant effect on axon regeneration in this experiment

2 days before tissue collection, the left eyes were intravitreally injected with 2μL of CTB-555. At 4 weeks post-ONC, the optic nerves were dissected, and 14μm thick sections were produced. Axons were counted using the CTB-555 fluorescence at 0.5mm increments.

Mice treated with AAV2.PI3K(p110δ) plus AAV2.Integrin.V5 and AAV2.Kindlin.GFP spread over two injections showed 61±37 regenerating axons at 0.5mm from the crush site, which was significantly more than the 23±14 axons in the AAV2.Integrin.V5 and AAV2.Kindlin.GFP (two-way ANOVA with Tukey's post-hoc analysis, p=0.0217), as seen in **Fig. 5.12**. However, no significant difference was seen when comparing AAV2.PI3K(p110δ) plus AAV2.Integrin.V5 and AAV2.Kindlin.GFP with AAV2.PI3K(p110δ) plus two doses of AAV2.GFP. Therefore, PI3K upregulation combined with integrin activation had no significant effect on axon regeneration in this experiment.

The AAV2.PI3K(p110δ)-treated mice (180 axons) showed significantly greater axon regeneration than both AAV2.PI3K(p110δ) plus AAV2.Integrin.V5 and AAV2.Kindlin.GFP (61 axons) (two-way ANOVA with Tukey's post-hoc analysis, p=0.0142) and AAV2.PI3K(p110δ) plus AAV2.GFP (68 axons) (two-way ANOVA with Tukey's post-hoc analysis, p=0.0124) at 0.5mm from the crush site. Again at 1.0mm from the crush site, AAV2.PI3K(p110δ)-treated mice (104 axons) showed significantly greater axon regeneration than both AAV2.PI3K(p110δ) plus AAV2.Integrin.V5 and AAV2.Kindlin.GFP (13 axons) (two-way ANOVA with Tukey's post-hoc analysis, p=0.0160) and AAV2.PI3K(p110δ) plus AAV2.GFP (25 axons) (two-way ANOVA with Tukey's post-hoc analysis, p=0.0222).

5.5.3 FAK Pathway Activation

I tried to optimise phospho-FAK IHC to measure FAK pathway activation, but it was difficult to find a good antibody for retinal sections. D'Onofio et al. were able to detect pFAK *in vivo* in western blots of whole retinal lysate, which would be interesting to try[21]. However, this would require collecting new animal tissue and was not pursued because pro-regenerative effects were not seen.

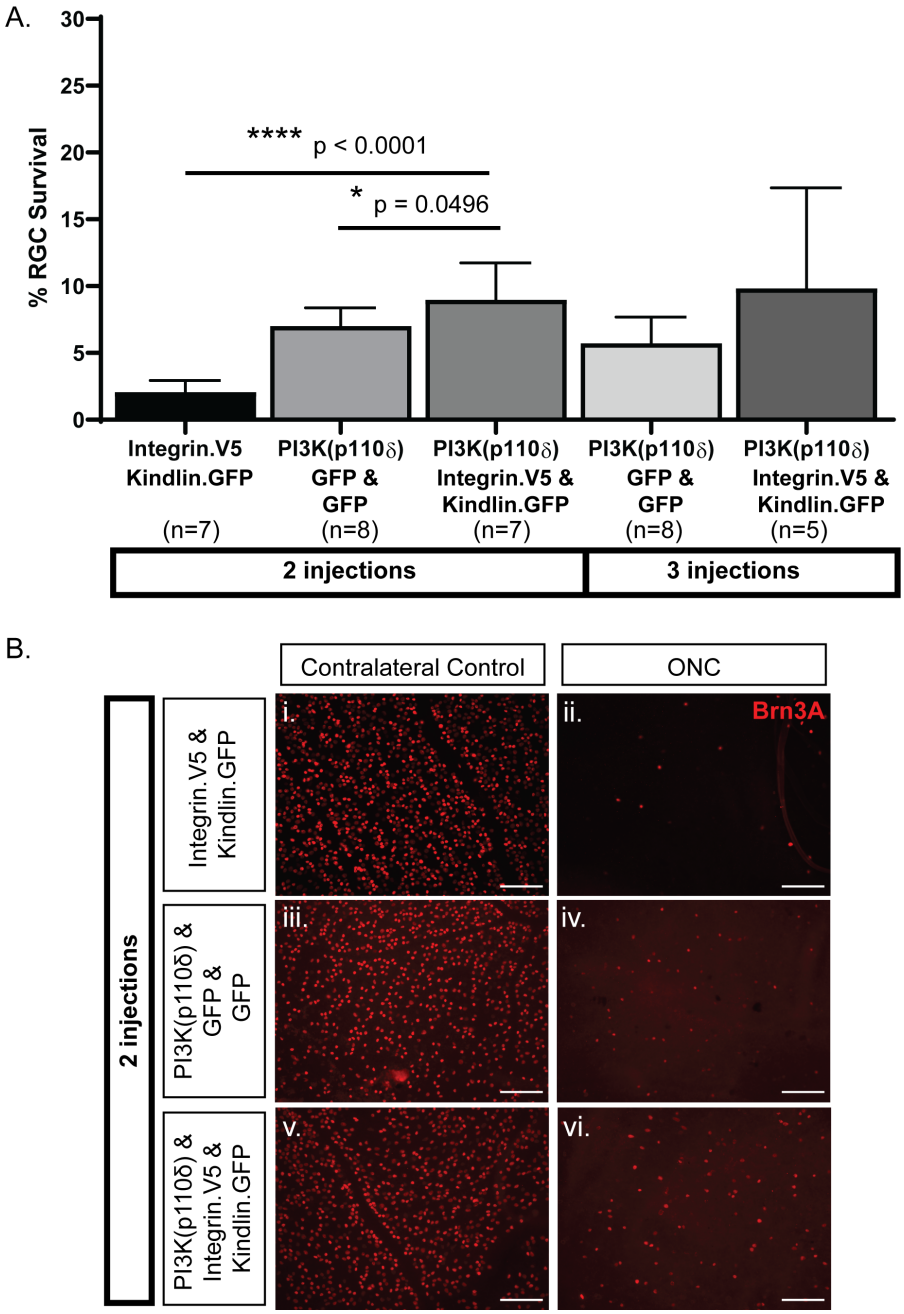

Fig. 5.11 **2 Injections: Combination of PI3K upregulation with integrin activation promoted RGC survival compared to control. Integrin activation alone had no significant effect.**. As seen in panel A, AAV2.PI3K(p110δ) plus AAV2.Integrin.V5 and AAV2.Kindlin.GFP promoted RGC survival 4 weeks post-ONC injury, but AAV2.Integrin.V5 and AAV2.Kindlin.GFP had no significant effect. RWMs were stained with Brn3A (red), which was used to quantify RGCs. The number of RGCs in the ONC (left) eye (panels Bii, Biv, and Bvi) was expressed as a percentage survival relative to the uninjured contralateral control (right) eye (Bi, Biii, and Bvi). p values measured one-way ANOVA, n = 5 to 8 as specified, error bars = SD. Scale bar = 100μm.

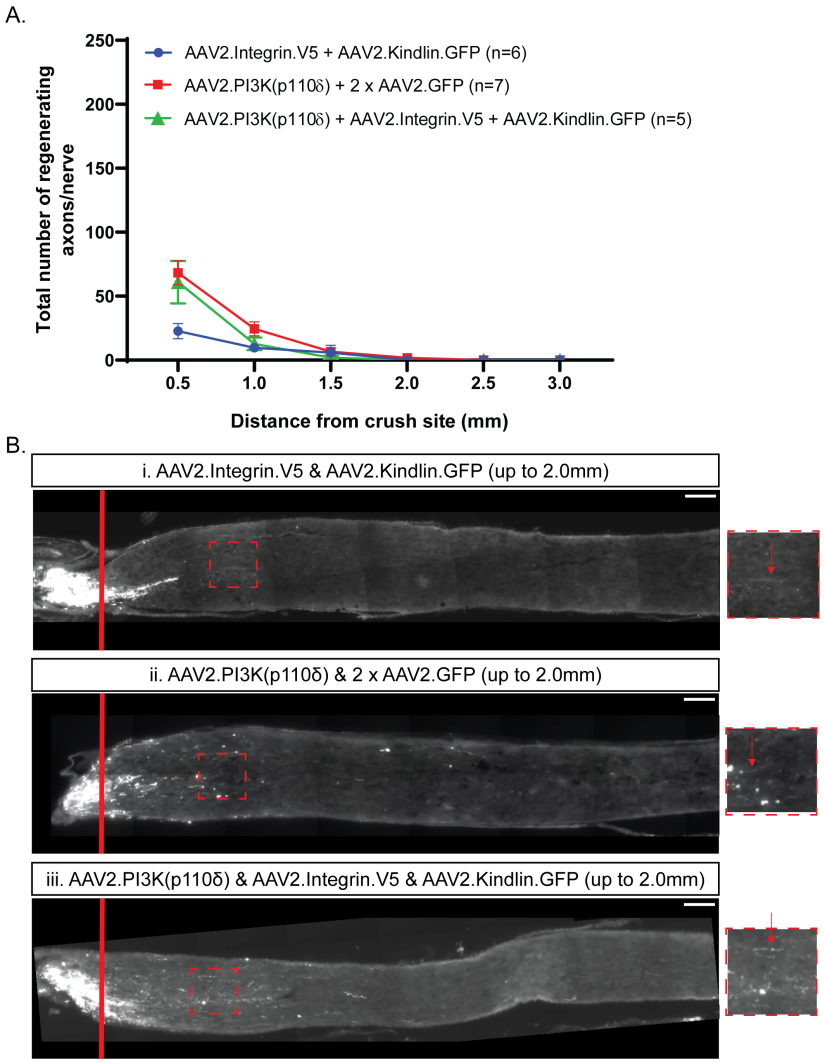

Fig. 5.12 **Combination of PI3K upregulation with integrin activation had no significant effect on axon regeneration compared to control.** As shown in panel A, AAV2.PI3K(p110δ) plus AAV2.Integrin.V5 plus AAV2.Kindlin.GFP had no significant effect on axon regeneration following ONC injury compared to control. Images of crushed nerves are shown in panel B for AAV2.Integrin.V5 plus AAV2.Kindlin.GFP (Bi), AAV2.PI3K(p110δ) plus two doses of AAV2.GFP (Bi) and AAV2.PI3K(p110δ) plus AAV2.Integrin.V5 and AAV2.Kindlin.GFP (Biii). p values measured by two-way ANOVA with Tukey's post-hoc analysis, n = 5 to 7 as specified, error bars = SEM. Scale bar = 100μm.

5.5.4 Summary of Strategies Tested in this Thesis

The viral treatment strategies investigated in this thesis were: PTEN knockdown, PI3K upregulation, PI3K upregulation combined with PTEN knockdown, and PI3K upregulation combined with integrin activation.

On comparison of the data, shown in **Fig. 5.13**, no significant differences were found between the groups. The combination of PI3K upregulation and PTEN knockdown showed the greatest percentage RGC survival, while AAV2.PI3K(p110δ) showed the greatest axon regeneration.

5.6 Discussion

In my experiments, delivery of more than one viral vector appeared to lessen the pro-regenerative effects seen from the viruses individually. It would be expected that the controls, AAV2.PI3K(p110δ) plus AAV2.shScram.GFP (2 vectors, 7.8% survival) and AAV2.PI3K(p110δ) plus two doses of AAV2.GFP (3 vectors, 7.0% survival), would have the same RGC survival as AAV2.PI3K(p110δ) alone (11.3% survival). However, a slight decrease was seen, although this was not statistically significant. This dulling effect was even more apparent in axon regeneration, with significantly less regeneration from multiple viruses compared to AAV2.PI3K(p110δ) alone.

Combining AAV2.PI3K(p110δ) plus AAV2.shPTEN.GFP significantly promoted RGC survival and axon regeneration compared to control. This was demonstrated to be due to mTOR pathway activation. However, this approach was not significantly greater than AAV2.PI3K(p110δ) alone and showed significantly less axon regeneration. As mentioned above, this is likely due to a negative effect of using multiple viruses.

Combining AAV2.PI3K(p110δ) plus AAV2.Integrin.V5 and AAV2.Kindlin.GFP had no significant effect on axon regeneration and only marginally increased RGC survival compared to control when two injections were given. Taken together with the fact that the AAV2.Integrin.V5 and AAV2.Kindlin.GFP control showed no significant effect on RGC survival or axon regeneration, it is likely these viruses were not functioning as expected, and this should be investigated further. For example, pFAK IHC could be optimised to see if the pathway was being activated as expected.

Future work could combine PI3K upregulation with other strategies. From this study, it was shown that combining multiple viruses reduces effectiveness, so non-viral strategies like insulin eye drops (unpublished work) or recombinant Oncomodulin[51] should be tested.

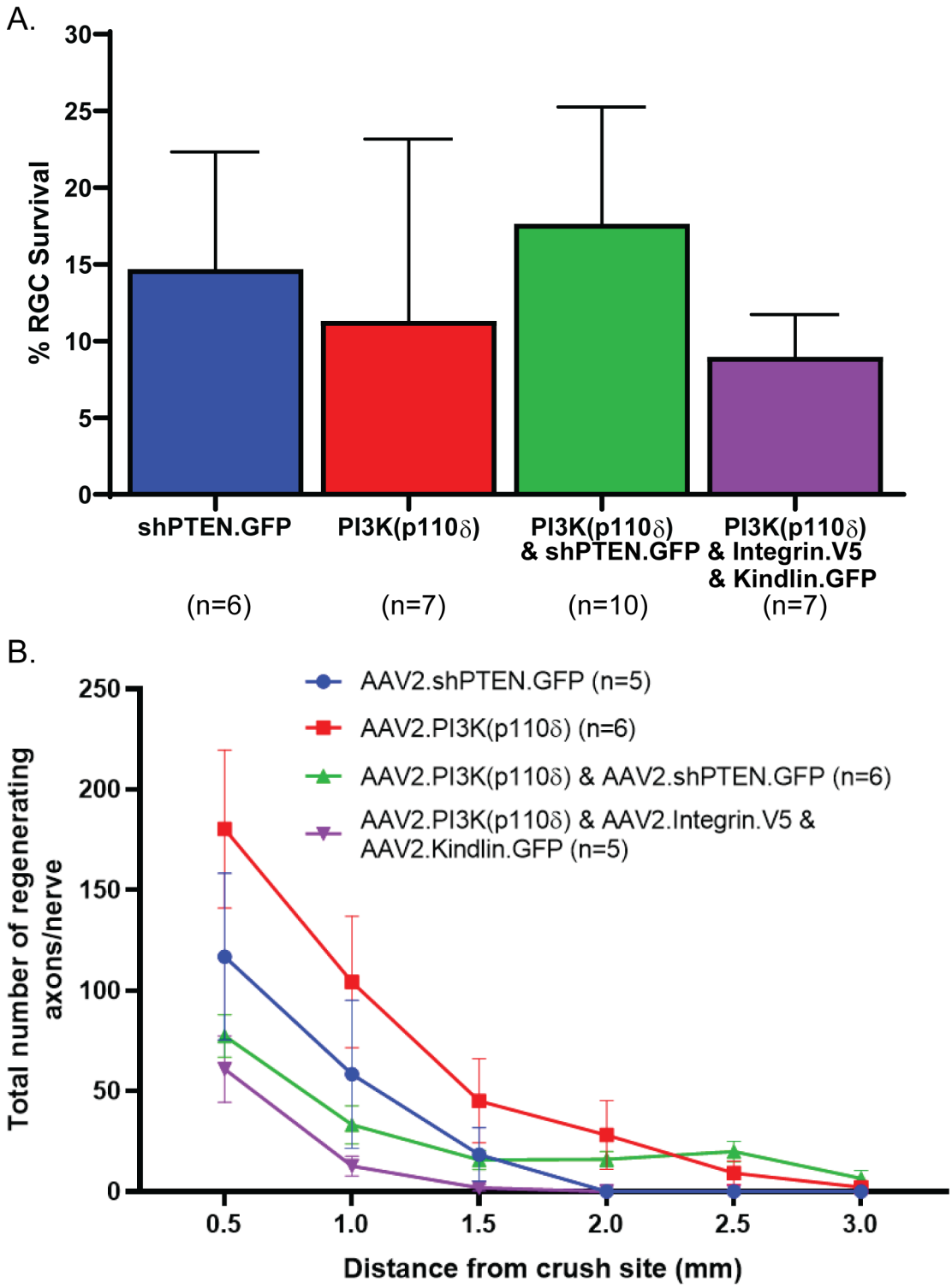

Fig. 5.13 **Comparison of RGC Survival and Axon Regeneration in the Different Treatment Strategies.** p values measured by one-way ANOVA (graph A) or two-way ANOVA (graph B) with Tukey's post-hoc analysis, n = 5 to 10 as specified, error bars = SD (graph A) and SEM (graph B).

Chapter 6

Discussions and Conclusions

Optic nerve disorders, including glaucoma, are highly prevalent and on the rise in an aging population. In such disorders, retinal ganglion cells (RGCs) and their axons are damaged and lost, ultimately resulting in vision loss. RGC axons, as with other central nervous system (CNS) axons, have limited regenerative potential, so there are currently no treatments to restore visual function. In this thesis, several therapeutic strategies were investigated using an optic nerve crush (ONC) model to assess RGC survival and axon regeneration.

In **Chapter 3**, three conditional knock-in phosphoinositide 3-kinase (PI3K) mouse lines were established and maintained: hyperactive p110α (p110α^{H1047R}), p110δ and isolated p110δ mice. Using viral Cre-mediated recombination, either the p110α^{H1047R} or the p110δ isoform was expressed. Both isoforms significantly promoted RGC survival and axon regeneration in young adult (6 to 8 weeks old) mice 4 weeks post-ONC injury, with no difference between the two.

It is well-known that neurodegenerative diseases, like glaucoma and Alzheimer's disease, primarily impact the aging population and more work needs to be done to elucidate the effect of aging on CNS axon regeneration. Both PI3K isoforms also promoted axon regeneration in aged adult (9 to 12 months) mice, although to a lesser degree than in young mice. Aged p110α^{H1047R} mice showed significant RGC survival, while p110δ mice showed no significant effect. In Geoffroy et al., little, if any, axon regeneration was seen in a corticospinal tract (CST) model using PTEN knockout to promote regeneration in aged mice[34]. The fact that regeneration was recorded here is promising, although comparison with PTEN knockout in an ONC model would be more meaningful than the CST model.

While transgenic work is informative, this is not translatable. In **Chapter 4**, viral PI3K upregulation was investigated using AAV2.PI3K(p110δ). Unfortunately, the p110α^{H1047R} isoform was not made into a virus due to safety concerns. Viral phosphatase tensin homolog (PTEN) knockdown using shRNA targeted against PTEN was also investigated for compari-

son. Viral PTEN knockdown promoted RGC survival in young adult (6 to 8 weeks old) mice at 4 weeks post-ONC injury, while viral PI3K upregulation had no significant effect in this experiment. As the PI3K transgenic approach showed significant RGC survival, it is likely that with a larger sample size, the PI3K viral approach would also promote RGC survival. Both viral PTEN knockdown and PI3K upregulation promoted axon regeneration, with no significant difference between the two. Viral PI3K upregulation showed significantly more axon regeneration than the PI3K transgenic approach, as expected. However, no significant difference was seen in terms of RGC survival. It would be interesting to test these viruses in aged mice, as in **Chapter 3**. It would be expected that PTEN knockdown would result in little, if any, regeneration like in the CST study [34]. Given the transgenic PI3K approach did promote regeneration, I would expect this would be seen to a greater extent from viral PI3K(p110δ), which could be a potential advantage of this strategy over PTEN knockdown.

It is worth considering how these results compare to existing data in the literature. At 4 weeks post-ONC, approximately 40% RGC survival was observed from transgenic PTEN deletion and from transgenic SOCS3 deletion, whereas co-deletion resulted in over 60% RGC survival[95]. In contrast, viral PTEN knockdown in this thesis only resulted in 14.7% RGC survival and viral PI3K upregulation resulted in 11.3% survival. RNA interference methods only partially suppress the expression of target genes, as opposed to complete suppression by genetic deletion, so a lower value is to be expected from viral PTEN knockdown. In this thesis, RGCs were quantified by Brn3A staining, whereas Sun et al. used Tuj1 staining, which may account for a small level of discrepancy in RGC survival.

At 4 weeks post-ONC, transgenic PTEN deletion resulted in around 1750 regenerating axons at 0.5mm from the crush site and around 1000 axons at 1.0mm from the crush site[79]. SOCS3 deletion yielded similar results, whereas co-deletion of PTEN and SOCS3 resulted in around 6000 regenerating axons at 0.5mm from the crush site[95]. In contrast, viral PTEN knockdown in this thesis only resulted in 117 regenerating axons at 0.5mm from the crush site and viral PI3K upregulation resulted in 180 regenerating axons at 0.5mm. These values are only a small fraction of those obtained from the He group. Again, viral PTEN knockdown would be expected to be less effective than transgenic deletion.

At 2 weeks post-ONC, the He group found that transgenic PTEN deletion resulted in just under 1500 regenerating axons at 0.5mm from the crush site and around 1000 axons at 1.0mm [79, 95]. In Kurimoto et al., the Benowitz group repeated this transgenic PTEN deletion experiment and found only 400 regenerating axons at 0.5mm and 200 axons at 1.0mm at 2 weeks post-ONC[51]. They also showed that zymosan resulted in about 150 regenerating axons at 0.5mm from the crush site and around 100 axons at 1.0mm. Zymosan combined with cAMP showed 325 regenerating axons at 0.5mm and 175 axons at 1.0mm[51].

In Duan et al., the Sanes group found that at 2 weeks post-ONC, intravitreal injection of viral vectors carrying either IGF1 or OPN resulted in around 63 regenerating axons at 0.5mm from the crush site and little, if any, at 1.0mm[23]. However, a combination of IGF1 and OPN yielded around 500 regenerating axons at 0.5mm and 125 axons at 1.0mm. All papers use the same method to quantify axon regeneration, yet the values from both these studies are significantly less than those found by Park et al.. Whilst still higher than the values obtained in this thesis, these axon regeneration results are closer in range to our data.

Despite being lower than data in the literature, the data presented in this thesis is still valid as each treatment was compared to an appropriate control carried out and analysed in parallel. Comparison of viral PTEN knockdown and viral PI3K upregulation was also carried out and analysed in parallel so this is more accurate to compare than with data from other groups. While this data is not record-breaking in terms of survival and regeneration, it is still informative and provides another strategy for promoting regeneration that can be combined with other targets.

It has become increasingly clear in the field that combining multiple strategies is required for robust regeneration along the optic nerve and into the brain. In **Chapter 5**, viral PI3K upregulation was combined with either PTEN knockdown or with integrin activation. While the combination of PI3K upregulation with PTEN knockdown promoted RGC survival and axon regeneration compared to control, the RGC survival was not significantly greater than viral PI3K alone, and the axon regeneration seen was significantly less. Integrin activation had no significant effects, except a very minor increase in RGC survival when combined with PI3K(p110δ). The viruses used need to be validated further. It became clear from both studies that combining multiple viruses reduces their effectiveness. Therefore, combining a viral approach, like AAV2.PI3K(p110δ) with alternative approaches like insulin eye drops (unpublished work) or recombinant Oncomodulin[51] may be a better strategy to adopt.

The role of the mammalian target of rapamycin (mTOR) pathway in the regenerative effects seen was demonstrated with phospho-AKT (pAKT) and phospho-S6 ribosomal protein (pS6) signal in retinal sections. As mentioned in the chapters, this could be investigated more thoroughly using RGC isolation and rapamycin. The contributions from other pathways, like the focal adhesion kinase (FAK) pathway, could also be assessed in future work.

While testing the pro-regenerative effects of these viruses in murine tissue is informative, the next step would be to test in human tissue. During the first 2 years of my Ph.D., R. Conceição and S.S. Deshpande, under the supervision of A.C. Barber, made several attempts to optimise retinal explant cultures, both in mice and human tissue. However, they faced many challenges, including difficulties obtaining fresh human tissue and issues with culturing

RGCs *ex vivo*. In the final year of my Ph.D., I hoped to carry on this work and test the viruses under the supervision of Professor Christopher Leung at the University of Hong Kong.

The C. Leung lab has developed a highly specialized and robust *ex vivo* human retinal modelling system. In brief, human retinas are dissected out and processed using an RGC isolation kit that targets thy-1 positive RGCs. These RGCs are then grown as single cells in culture, with the number of axons peaking at 3 weeks and cultures viable for over 2 months. My work planned to transfect these single cell cultures with the viruses used in this thesis, both individually and in combination. 2 weeks after transfection, axon number, length, and branching were to be measured using microfluidic chambers, where Tau staining could be used to identify axons. I was awarded a small grant to pursue this part of the project but unfortunately, was unable to complete the work due to logistical issues. However, it would be interesting for future work. As mentioned in Chapter 3, the p110δ construct was then tested by S. van Erpp in human neurons maturing *in vitro* (human embryonic stem cells).

The ultimate aim of such regenerative research is to re-establish the visual pathway circuitry in the brain and restore visual function. Connection to central targets in the brain is still not robust and pathfinding errors are common so further work investigating guidance cues in the adult optic chiasm may help to address these issues. While this thesis focused on assessing regeneration, the next step would be to measure functional recovery, using visual field tests and electroretinography.

Overall, the data presented in this thesis demonstrates that RGC axonal regeneration is possible. Further work is needed before this reaches the clinical setting, but the preliminary work from this thesis and other studies in the field is promising and provides hope for restoring vision loss from optic nerve disorders in the future.

References

[1] Al-Ali, H., Ding, Y., Slepak, T., Wu, W., Sun, Y., Martinez, Y., Xu, X. M., Lemmon, V., and Bixby, J. (2017). The mTOR Substrate S6 Kinase 1 (S6K1) Is a Negative Regulator of Axon Regeneration and a Potential Drug Target for Central Nervous System Injury. *J Neurosci*, 37(30):7079 – 7095.

[2] Andrews, M. R., Czvitkovich, S., Dassie, E., Vogelaar, C. F., Faissner, A., Blits, B., Gage, F. H., Ffrench-Constant, C., and Fawcett, J. W. (2009). Alpha9 integrin promotes neurite outgrowth on tenascin-C and enhances sensory axon regeneration. *J Neurosci*, 29(17):5546 – 5557.

[3] Andrews, M. R., Soleman, S., Cheah, M., Tumbarello, D. A., Mason, M. R. J., Moloney, E., Verhaagen, J., Bensadoun, J. C., Schneider, B., Aebischer, P., and Fawcett, J. W. (2016). Axonal Localization of Integrins in the CNS Is Neuronal Type and Age Dependent. *eNeuro*, 3(4).

[4] Arlotta, P., Molyneaus, B. J., Chen, J., Inoue, J., Kominami, R., and Macklis, J. D. (2005). Neuronal subtype-specific genes that control corticospinal motor neuron development in vivo. *Neuron*, 45(2):207 – 221.

[5] Barber, A. C., Evans, R. S., Nieuwenhuis, B., Pearson, C. S., Fuchs, J., MacQueen, A. R., van Erp, S., Hänzi, B., Hulshof, L.-A., Osborne, A., Conceição, R., Deshpande, S. S., Cave, J., Ffrench-Constant, C., Smith, P. D., Okkenhaug, K., Eickholt, B. J., Martin, K. R., Fawcett, J. W., and Eva, R. (2020). PI3 kinase delta enhances axonal PIP3 to support axon regeneration in the adult CNS. *not yet published*.

[6] Bardeesy, N., Sinha, M., Hezel, A. F., Signoretti, S., Hathaway, N. A., Sharpless, N. E., Loda, M., Carrasco, D. R., and DePinho, R. A. (2002). Loss of the Lkb1 tumour suppressor provokes intestinal polyposis but resistance to transformation. *Nature*, 419(6903):162 – 167.

[7] Benson, M. D., Romero, M. I., Lush, M. E., Lu, Q. R., Henkemeyer, M., and Parada, L. F. (2005). Ephrin-B3 is a myelin-based inhibitor of neurite outgrowth. *Proc Natl Acad Sci USA*, 102(30):10694 – 10699.

[8] Bilanges, B., Posor, Y., and Vanhaesebroeck, B. (2019). PI3K isoforms in cell signalling and vesicle trafficking. *Nat Rev Mol Cell Biol*, 20(9):515 – 534.

[9] Borrás, T., Buie, L. K., and Spiga, M. G. (2016). Inducible scAAV2.GRE.MMP1 lowers IOP long-term in a large animal model for steroid-induced glaucoma gene therapy. *Gene Ther*, 23(5):438 – 449.

[10] Bourne, R. R. A., Flaxman, S. R., Braithwaite, T., Cicinelli, M. V., Das, A., Jonas, J. B., Keeffe, J., Kempen, J. H., Leasher, J., Limburg, H., Naidoo, K., Pesudovs, K., Resnikoff, S., Silvester, A., Stevens, G. A., Tahhan, N., Wong, T. Y., Taylor, H. R., and VisionLossExpertGroup (2017). Magnitude, temporal trends, and projections of the global prevalence of blindness and distance and near vision impairment: a systematic review and meta-analysis. *Lancet Glob Health*, 5(9):888 – 897.

[11] Bringmann, A., Pannicke, T., Grosche, J., Francke, M., Wiedemann, P., Skatchkov, S. N., Osborne, N. N., and Reichenbach, A. (2006). Müller cells in the healthy and diseased retina. *Prog Retin Eye Res*, 25(4):397 – 424.

[12] Cheah, M., Andrews, M. R., Chew, D. J., Moloney, E. B., Verhaagen, J., Fässler, R., and Fawcett, J. W. (2016). Expression of an Activated Integrin Promotes Long-Distance Sensory Axon Regeneration in the Spinal Cord. *J Neurosci*, 36(27):7283 – 7297.

[13] Chiba, T., Yamada, M., Sasabe, J., Terashita, K., Shimoda, M., Matsuoka, M., and Aiso, S. (2009). Amyloid-beta causes memory impairment by distrupting the JAK2/STAT3 axis in hippocampal neurons. *Molecular psychiatry*, 14:206 – 222.

[14] CollaborativeNormal-TensionGlaucomaStudyGroup (1998). The effectiveness of intraocular pressure reduction in the treatment of normal-tension glaucoma. *Am J Ophthalmol*, 126(4):498 – 505.

[15] Conceição, R., Evans, R. S., Pearson, C. S., Hänzi, B., Osborne, A., Deshpande, S. S., Martin, K. R., and Barber, A. C. (2019). Expression of developmentally important axon guidance cues in the adult optic chiasm. *Invest Ophthalmol Vis Sci*, 60(14):4727 – 4739.

[16] Cosker, K. E. and Eickholt, B. J. (2007). Phosphoinositide 3-kinase signalling events controlling axonal morphogenesis. *Biochem Soc Trans*, 35(Pt 2):207 – 210.

[17] Daniel, S., Clark, A. F., and McDowell, C. M. (2018). Subtype-specific response of retinal ganglion cells to optic nerve crush. *Cell Death Discov*, 4(67).

[18] De-Fraja, C., Conti, L., Govoni, S., Battaini, F., and Cattaneo, E. (2000). STAT signalling in the mature and aging brain. *Int J Dev Neurosci*, 18:439 – 446.

[19] de Lima, S., Koriyama, Y., Kurimoto, T., Oliveira, J. T., Yin, Y., Li, Y., Gilbert, H. Y., Fagiolini, M., Martinez, A. M., and Benowitz, L. (2012). Full-length axon regeneration in the adult mouse optic nerve and partial recovery of simple visual behaviors. *Proc Natl Acad Sci USA*, 109(23):9149 – 9154.

[20] Dergham, P., Ellezam, B., Essagian, C., Avedissian, H., Lubell, W. D., and McKerracher, L. (2002). Rho signaling pathway targeted to promote spinal cord repair. *J Neurosci*, 22:6570 – 6577.

[21] D'Onofrio, P. M., Shabanzadeh, A. P., Choi, B. K., Bähr, M., and Koeberle, P. D. (2019). MMP Inhibition Preserves Integrin Ligation and FAK Activation to Induce Survival and Regeneration in RGCs Following Optic Nerve Damage. *Invest Ophthalmol Vis Sci*, 60(2):634 – 649.

[22] Dooley, M. C. and Foroozan, R. (2010). Optic Neuritis. *J Opthalmic Vis Res*, 5(3):182 – 187.

[23] Duan, X., Qiao, M., Bei, F., Kim, I. J., He, Z., and Sanes, J. R. (2015). Subtype-specific regeneration of retinal ganglion cells following axotomy: effects of osteopontin and mTOR signaling. *Neuron*, 85(6):1244 – 1256.

[24] Dupraz, S., Grassi, D., Karnas, D., Nieto Guil, A. F., Hicks, D., and Quiroga, S. (2013). The insulin-like growth factor 1 receptor is essential for axonal regeneration in adult central nervous system neurons. *PLoS One*, 8(1):e54462.

[25] Eickholt, B. J., Ahmed, A. I., Davies, M., Papakonstanti, E. A., Pearce, W., Starkey, M. L., Bilancio, A., Need, A. C., Smith, A. J., Hall, S. M., Hamers, F., Giese, K. P., Bradbury, E. J., and Vanhaesebroeck, B. (2007). Control of axonal growth and regeneration of sensory neurons by the p110delta PI3-kinase. *PLoS One*, 2(9):e869.

[26] Eva, R., Dassie, E., Caswell, P. T., Dick, G., Ffrench-Constant, C., Norman, J. C., and Fawcett, J. W. (2010). Rab11 and its effector Rab coupling protein contribute to the trafficking of beta 1 integrins during axon growth in adult dorsal root ganglion neurons and PC12 cells. *J. Neurosci.*, 30(35):11654 – 11669.

[27] Eva, R. and Fawcett, J. W. (2014). Integrin signalling and traffic during axon growth and regeneration. *Curr Opin Neurobiol*, 27:179 – 185.

[28] Faulkner, J. R., Herrmann, J. E., Woo, M. J., Tansey, K. E., Doan, N. B., and Sofroniew, M. V. (2004). Reactive astrocytes protect tissue and preserve function after spinal cord injury. *J Neurosci*, 24(9):2143 – 2155.

[29] Fischer, D., He, Z., and Benowitz, L. I. (2004). Counteracting the Nogo receptor enhances optic nerve regeneration if retinal ganglion cells are in an active growth state. *J Neurosci*, 24:1646 – 1651.

[30] Flaxman, S. R., Bourne, R. R. A., Resnikoff, S., Ackland, P., Braithwaite, T., Cicinelli, M. V., Das, A., Jonas, J. B., Keeffe, J., Kempen, J. H., Leasher, J., Limburg, H., Naidoo, K., Pesudovs, K., Silvester, A., Stevens, G. A., Tahhan, N., Wong, T. Y., Taylor, H. R., and VisionLossExpertGroupoftheGlobalBurdenofDisease (2017). Global causes of blindness and distance vision impairment 1990 - 2020: a systematic review and meta-analysis. *Lancet Glob Health*, 5(12):e1221 – e1234.

[31] Gardiner, N. J. (2011). Integrins and the extracellular matrix: key mediators of development and regeneration of the sensory nervous system. *Dev Neurobiol*, 71(11):1054 – 1072.

[32] Garway-Heath, D. F., Crabb, D. P., Bunce, C., Lascaratos, G., Amalfitano, F., Anand, N., Azuara-Blanco, A., Bourne, R. R., Broadway, D. C., Cunliffe, I. A., Diamond, J. P., Fraser, S. G., Ho, T. A., Martin, K. R., McNaught, A. I., Negi, A., Patel, K., Russell, R. A., Shah, A., Spry, P. G., Suzuki, K., White, E. T., Wormald, R. P., Xing, W., and Zeyen, T. G. (2015). Latanoprost for open-angle glaucoma (UKGTS): a randomised, multicentre, placebo-controlled trial. *Lancet*, 385(9975):1295 – 1304.

[33] Gedde, S. J., Herndon, L. W., Brandt, J. D., Budenz, D. L., Feuer, W. J., Schiffman, J. C., and TubeVersusTrabeculectomyStudyGroup (2012). Postoperative complications in the Tube Versus Trabeculectomy (TVT) study during five years of follow-up. *Am J Ophthalmol*, 153(5):804 – 814.

[34] Geoffroy, C. G., Hilton, B. J., Tetzlaff, W., and Zheng, B. (2016). Evidence for an age-dependent decline in axon regeneration in the adult mammalian central nervous system. *Cell Rep*, 15(2):238 – 246.

[35] Geoffroy, C. G., Meves, J. M., and Zheng, B. (2017). The age factor in axonal repair after spinal cord injury: a focus on neuron-intrinsic mechanisms. *Neurosci Lett*, 652:41 – 49.

[36] Gertig, U. and Hanisch, U. (2014). Microglial diversity by response and responders. *Front Cell Neurosci*, 8.

[37] GrandPre, T., Li, S., and Strittmatter, S. M. (2002). Nogo-66 receptor antagonist peptide promotes axonal regeneration. *Nature*, 417:547 – 551.

[38] GrandPre, T., Nakamura, F., Vartanian, T., and Strittmatter, S. M. (2000). Identification of the Nogo inhibitor of axon regeneration as a Reticulon protein. *Nature*, 403(6768):439 – 444.

[39] Groszer, M., Erickson, R., Scripture-Adams, D. D., Lesche, R., Trumpp, A., Zack, J. A., Kornblum, H. I., Liu, X., and Wu, H. (2001). Negative regulation of neural stem/progenitor cell proliferation by the Pten tumor suppressor gene in vivo. *Science*, 294(5549):2186 – 2189.

[40] Harfe, B. D., McManus, M. T., Mansfield, J. H., Hornstein, E., and Tabin, C. J. (2005). The RNaseIII enzyme Dicer is required for morphogenesis but not patterning of the vertebrate limb. *Proc Natl Acad Sci USA*, 102(31):10898 – 10903.

[41] Hawkins, P. T., Anderson, K. E., Davidson, K., and Stephens, L. R. (2006). Signalling through Class I PI3Ks in mammalian cells. *Biochem Soc Trans*, 34(Pt 5):647 – 662.

[42] Hawkins, P. T. and Stephens, L. R. (2015). PI3K signalling in inflammation. *Biochem Biophys Acta*, 1851(6):882 – 897.

[43] Hogan, M. J. and Feeney, L. (1963). The ultrastructure of the retinal vessels: III. Vascular-Glial relationships. *J Ultrastruct Res*, 49:47 – 64.

[44] Hollis, E. R., Lu, P., Blesch, A., and Tuszynski, M. H. (2009). IGF-I gene delivery promotes corticospinal neuronal survival but not regeneration after adult CNS injury. *Exp Neurol*, 215(1):53 – 59.

[45] Huang, J. K., Phillips, G. R., Roth, A. D., Pedraza, L., Shan, W., Belkaid, W., Mi, S., Fex-Svenningsen, A., Florens, L., Yates, J. R., and Colman, D. R. (2005). Glial membranes at the node of Ranvier prevent neurite outgrowth. *Science*, 310(5755):1813 – 1817.

[46] Huber, A. B., Weinmann, O., Brosamle, C., Oertle, T., and Schwab, M. E. (2002). Patterns of Nogo mRNA and protein expression in the developing and adult rat and after CNS lesions. *J Neurosci*, 22(9):3553 – 3567.

[47] Jeon, C. J., Strettoi, E., and Masland, R. H. (1998). The major cell populations of the mouse retina. *J Neurosci*, 18(21):8936 – 8946.

[48] Kang, H. and Lichtman, J. W. (2013). Motor axon regeneration and muscle reinnervation in young adult and aged animals. *J Neurosci*, 33:19480 – 19491.

[49] Kang, S., Denley, A., Vanhaesebroeck, B., and Vogt, P. K. (2006). Oncogenic transformation induced by the p110beta, -gamma, and -delta isoforms of class I phosphoinositide 3-kinase. *Proc Natl Acad Sci USA*, 103(5):1289 – 1294.

[50] Kirwan, J. F., Lockwood, A. J., Shah, P., Macleod, A., Broadway, D. C., King, A. J., McNaught, A. I., Agrawal, P., and GroupAuditStudyGroup, T. (2013). Trabeculectomy in the 21st century: a multicenter analysis. *Opthalmology*, 120(12):2532 – 2539.

[51] Kurimoto, T., Yin, Y., Omura, K., Gilbert, H. Y., Kim, D., Cen, L. P., Moko, L., Kügler, S., and Benowitz, L. I. (2010). Long-distance axon regeneration in the mature optic nerve: contributions of oncomodulin, cAMP, and pten gene deletion. *J Neurosci*, 30(46):15654 – 15663.

[52] Landers, J., Martin, K., Sarkies, N., Bourne, R., and Watson, P. (2012). A twenty-year follow-up study of trabeculectomy: risk factors and outcomes. *Ophthalmology*, 119(4):694 – 702.

[53] Lehmann, M., Fournier, A., Selles-Navarro, I., Dergham, P., Sebok, A., Leclerc, N., Tigyi, G., and McKerracher, L. (1999). Inactivation of Rho signaling pathway promotes CNS axon regeneration. *J Neurosci*, 19(17):7537 – 7547.

[54] Leon, S., Yin, Y., Nguyen, J., Irwin, N., and Benowitz, L. I. (2000). Lens injury stimulates axon regeneration in the mature rat optic nerve. *J Neurosci*, 20(12):4615 – 4626.

[55] Li, S., Kim, J. E., Budel, S., Hampton, T. G., and Strittmatter, S. M. (2005). Transgenic inhibition of Nogo-66 receptor function allows axonal sprouting and improved locomotion after spinal injury. *Mol Cell Neurosci*, 29:26 – 39.

[56] Liebl, D. J., Huang, W., Young, W., and Parada, L. F. (2001). Regulation of Trk receptors following contusion of the rat spinal cord. *Exp Neurol*, 167(1):15 – 26.

[57] Lim, J. H., Stafford, B. K., Nguyen, P. L., Lien, B. V., Wang, C., Zukor, K., He, Z., and Huberman, A. D. (2016). Neural activity promotes long-distance, target-specific regeneration of adult retinal axons. *Nat Neurosci*, 19(8):1073 – 1084.

[58] Liu, K., Lu, Y., Lee, J. K., Samara, R., Willenberg, R., Sears-Kraxberger, I., Tedeschi, A., Park, K. K., Jin, D., Cai, B., Xu, B., Connolly, L., Steward, O., Zheng, B., and He, Z. (2010). PTEN deletion enhances the regenerative ability of adult corticospinal neurons. *Nat Neurosci*, 13(9):1075 – 1081.

[59] Lu, P., Blesch, A., and Tuszynski, M. H. (2001). Neurotrophism without neurotropism: BDNF promotes survival but not growth of lesioned corticospinal neurons. *J Comp Neurol*, 436(4):456 – 470.

[60] Luo, X., Salgueiro, Y., Beckerman, S. R., Lemmon, V. P., Tsoulfas, P., and Park, K. K. (2013). Three-dimensional evaluation of retinal ganglion cell axon regeneration and pathfinding in whole mouse tissue after injury. *Exp Neurol*, 247:653 – 662.

[61] Mandelker, D., Gabelli, S. B., Schmidt-Kittler, O., Zhu, J., Cheong, I., Huang, C. H., Kinzler, K. W., Vogelstein, B., and Amzel, L. M. (2009). A frequent kinase domain mutation that changes the interaction between PI3Kalpha and the membrane. *Proc Natl Acad Sci USA*, 106(40):16996 – 17001.

[62] Mansour-Robaey, S., Clarke, D. B., Wang, Y. C., Bray, G. M., and Aguayo, A. J. (1994). Effects of ocular injury and administration of brain-derived neurotrophic factor on survival and regrowth of axotomized retinal ganglion cells. *Proc Natl Acad Sci USA*, 91(5):1632 – 1636.

[63] Marino, S., Vooijs, M., van Der Gulden, H., Jonkers, J., and Berns, A. (2000). Induction of medulloblastomas in p53-null mutant mice by somatic inactivation of Rb in the external granular layer cells of the cerebellum. *Genes Dev*, 14(8):994 – 1004.

[64] Martin, K. R., Quigley, H. A., Zack, D. J., Levkovitch-Verbin, H., Keilczewski, J., Valenta, D., Baumrind, L., Pease, M. E., Klein, R. L., and Hauswirth, W. W. (2003). Gene therapy with brain-derived neurotrophic factor as a protection: retinal ganglion cells in a rat glaucoma model. *Invest Ophthalmol Vis Sci*, 44(10):4357 – 4365.

[65] McKeon, R. J., Schreiber, R. C., Rudge, J. S., and Silver, J. (1991). Reduction of neurite outgrowth in a model of glial scarring following CNS injury is correlated with the expression of inhibitory molecules on reactive astrocytes. *J Neurosci*, 11:3398 – 3411.

[66] Ménager, C., Arimura, N., Fukata, Y., and Kaibuchi, K. (2004). PIP3 is involved in neuronal polarization and axon formation. *J Neurochem*, 89(1):109 – 118.

[67] Mokhles, P., Schouten, J. S., Beckers, H. J., Azuara-Blanco, A., Tuulonen, A., and Webers, C. A. (2016). A Systematic Review of End-of-Life Visual Impairment in Open-Angle Glaucoma: An Epidemiological Autopsy. *J Glaucoma*, 25(7):623 – 628.

[68] Moreau-Fauvarque, C., Kumanogoh, A., Camand, E., Jaillard, C., Barbin, G., Boquet, I., Love, C., Jones, E. Y., Kikutani, H., Lubetzki, C., Dusart, I., and Chedotal, A. (2003). The transmembrane semaphorin Sema4D/CD100, an inhibitor of axonal growth, is expressed on oligodendrocytes and upregulated after CNS lesion. *J Neurosci*, 23(27):9229 – 9239.

[69] Müller, A., Hauk, T. G., and Fischer, D. (2007). Astrocyte-derived CNTF switches mature RGCs to a regenerative state following inflammatory stimulation. *Brain*, 130(Pt 12):3308 – 3320.

[70] Nieuwenhuis, B., Haenzi, B., Andrews, M. R., Verhaagen, J., and Fawcett, J. W. (2018). Integrins promote axonal regeneration after injury of the nervous system. *Biol Rev Camb Philos Soc*, 93(3):1339 – 1362.

[71] Nordstrom, B. L., Friedman, D. S., Mozaffari, E., Quigley, H. A., and Walker, A. M. (2005). Persistence and adherence with topical glaucoma therapy. *Am J Ophthalmol*, 140(4):598 – 606.

[72] Nyabi, O., Naessens, M., Haigh, K., Gembarska, A., Goossens, S., Maetens, M., De Clercq, S., Drogat, B., Haenebalcke, L., Bartunkova, S., De Vos, I., De Craene, B., Karimi, M., Berx, G., Nagy, A., Hilson, P., Marine, J. C., and Haigh, J. J. (2009). Efficient mouse transgenesis using Gateway-compatible ROSA26 locus targeting vectors and F1 hybrid ES cells. *Nucleic Acids Res*, 37(7):e55.

[73] O'Callaghan, J., Crosbie, D. E., Cassidy, P. S., Sherwood, J. M., Flügel-Koch, C., Lütjen-Drecoll, E., Humphries, M. M., Reina-Torres, E., Wallace, D., Kiang, A. S., Campbell, M., Stamer, W. D., Overby, D. R., O'Brien, C., Tam, L. C. S., and Humphries, P. (2017). Therapeutic potential of AAV-mediated MMP-3 secretion from corneal endothelium in treating glaucoma. *Hum Mol Genet*, 26(7):1230 – 1246.

[74] O'Neill, E. C., Danesh-Meyer, H. V., Connell, P. P., Trounce, I. A., Coote, M. A., Mackey, D. A., and Crowston, J. G. (2010). The optic nerve head in acquired optic neuropathies. *Nat Rev Neurol*, 6(4):221 – 236.

[75] Orellana, A. M., Vasconcelos, A. R., Leite, J. A., de Sa Lima, L., Andreotti, D. Z., Munhoz, C. D., Kawamoto, E. M., and Scavone, C. (2015). Age-related neuroinflammation and changes in AKT-GSK-3beta and WNT/beta-CATENIN signaling in rat hippocampus. *Aging*, 7:1094 – 1111.

[76] Osborne, A., Khatib, T. Z., Songra, L., Barber, A. C., Hall, K., Kong, G. Y. X., Widdowson, P. S., and Martin, K. R. (2018). Neuroprotection of retinal ganglion cells by a novel gene therapy construct that achieves sustained enhancement of brain-derived neurotrophic factor/tropomyosin-related kinase receptor-B signaling. *Cell Death Dis*, 9(10):1007.

[77] Ozdinler, P. H. and Macklis, J. D. (2006). IGF-I specifically enhances axon outgrowth of corticospinal motor neurons. *Nat Neurosci*, 9(11):1371 – 1381.

[78] Painter, M. W., Brosius Lutz, A., Cheng, Y. C., Latremoliere, A., Duong, K., Miller, C. M., Posada, S., Cobos, E. J., Zhang, A. X., Wagers, A. J., Havton, L. A., Barres, B., Omura, T., and Woolf, C. J. (2014). Diminished Schwann cell repair responses underlie age-associated impaired axonal regeneration. *Neuron*, 83:331 – 343.

[79] Park, K. K., Liu, K., Hu, Y., Smith, P. D., Wang, C., Cai, B., Xu, B., Connolly, L., Kramvis, I., Sahin, M., and He, Z. (2008). Promoting axon regeneration in the adult CNS by modulation of the PTEN/mTOR pathway. *Science*, 322(5903):963 – 966.

[80] Pernet, V., Joly, S., Dalkara, D., Jordi, N., Schwarz, O., Christ, F., Schaffer, D. V., Flannery, J. G., and Schwab, M. E. (2013). Long-distance axonal regeneration induced by CNTF gene transfer is impaired by axonal misguidance in the injured adult optic nerve. *Neurobiol Dis*, 51:202 – 213.

[81] Pinkstaff, J. K., Detterich, J., Lynch, G., and Gall, C. (1999). Integrin subunit gene expression is regionally differentiated in adult brain. *J Neurosci*, 19(5):1541 – 1556.

[82] Purves, D., Augustine, G. J., Fitzpatrick, D., Katz, L. C., LaMantia, A. S., McNamara, J. O., and Williams, S. M. (2001). *Neuroscience, 2nd Edition*. Sinauer Associates, Sunderland (MA), 2nd edition.

[83] Puttagunta, R., Tedeschi, A., Sória, M. G., Hervera, A., Lindner, R., Rathore, K. I., Gaub, P., Joshi, Y., Nguyen, T., Schmandke, A., Laskowski, C. J., Boutillier, A. L., Bradke, F., and Di Giovanni, S. (2014). PCAF-dependent epigenetic changes promote axonal regeneration in the central nervous system. *Nat Commun*, 5:3527.

[84] Reichenbach, A., Siegel, A., Rickmann, M., Wolff, J. R., Noone, D., and Robinson, S. R. (1995). Distribution of Bergmann glial somata and processes: implications for function. *J Hirnforsh*, 36:509 – 517.

[85] Reichenbach, A., Stolzenburg, J. U., Eberhardt, W., Chao, T. I., Dettmer, D., and Hertz, L. (1993). What do retinal muller (glial) cells do for their neuronal 'small siblings'? *J Chem Neuroanat*, 6:201 – 213.

[86] Rheaume, B. A., Jereen, A., Bolisetty, M., Sajid, M. S., Yang, Y., Renna, K., Sun, L., Robson, P., and Trakhtenberg, E. F. (2018). Single cell transcriptome profiling of retinal ganglion cells identifies cellular subtypes. *Nat Commun*, 9(1):2759.

[87] Richardson, P. M., Miao, T., Wu, D., Zhang, Y., Yeh, J., and Bo, X. (2009). Responses of the nerve cell body to axotomy. *Neurosurgery*, 65(4 Suppl):A74 – 79.

[88] Sapieha, P. S., Peltier, M., Rendahl, K. G., Manning, W. C., and Di Polo, A. (2003). Fibroblast growth factor-2 gene delivery stimulates axon growth by adult retinal ganglion cells after acute optic nerve injury. *Mol Cell Neurosci*, 24(3):656 – 672.

[89] Schachner, M. and Bartsch, U. (2000). Multiple functions of the myelin-associated glycoprotein MAG (siglec-4a) in formation and maintenance of myelin. *Glia*, 29(2):154 – 165.

[90] Schiapparelli, L. M., Shah, S. H., Ma, Y., McClatchy, D. B., Sharma, P., Li, J., Yates, J. R., Goldberg, J. L., and Cline, H. T. (2019). The Retinal Ganglion Cell Transportome Identifies Proteins Transported to Axons and Presynaptic Compartments in the Visual System In Vivo. *Cell Rep*, 28(7):1935 – 1947.

[91] Schwartz, G. F. and Quigley, H. A. (2008). Adherence and persistence with glaucoma therapy. *Surv Ophthalmol*, 53 Suppl1:S57 – 68.

[92] Smith, D. S. and Skene, J. H. (1997). A transcription-dependent switch controls competence of adult neurons for distinct modes of axon growth. *J Neurosci*, 17(2):646 – 658.

[93] Smith, P. D., Sun, F., Park, K. K., Cai, B., Wang, C., Kuwako, K., Martinez-Carrasco, I., Connolly, L., and He, Z. (2009). SOCS3 deletion promotes optic nerve regeneration in vivo. *Neuron*, 64(5):617 – 623.

[94] Stephen, L. and Hawkins, P. (2011). Signalling via class IA PI3Ks. *Adv Enzyme Regul*, 51(1):27 – 36.

[95] Sun, F., Park, K. K., Belin, S., Wang, D., Lu, T., Chen, G., Zhang, K., Yeung, C., Feng, G., Yankner, B. A., and He, Z. (2011). Sustained axon regeneration induced by co-deletion of PTEN and SOCS3. *Nature*, 480(7377):372 – 375.

[96] Tan, C. L., Andrews, M. R., Kwok, J. C., Heintz, T. G., Gumy, L. F., Fässler, R., and Fawcett, J. W. (2012). Kindlin-1 enhances axon growth on inhibitory chondroitin sulfate proteoglycans and promotes sensory axon regeneration. *J Neurosci*, 32(21):7325 – 7335.

[97] The Jackson Laboratory (2018). Mouse Strain Datasheet - 007908. https://www.jax.org/strain/007908. [online] Accessed: 2018-08.

[98] Unknown (2019). fMRI of Visual System.

[99] Vecino, E., Rodriguez, F. D., Ruzafa, N., Pereiro, X., and Sharma, S. C. (2016). Glia-neuron interactions in the mammalian retina. *Prog Retin Eye Res*, 51:1 – 40.

[100] Verdu, E., Ceballos, D., Vilches, J. J., and Navarro, X. (2000). Influence of aging on peripheral nerve function and regeneration. *J Peripher Nerv Syst*, 5:191 – 208.

[101] Weinreb, R. N., Aung, T., and Medeiros, F. A. (2014). The pathophysiology and treatment of glaucoma: a review. *JAMA*, 311(18):1901 – 1911.

[102] Weinreb, R. N. and Khaw, P. T. (2004). Primary open-angle glaucoma. *Lancet*, 363(9422):1711 – 1720.

[103] Williams, R. W., Strom, R. C., Rice, D. S., and Goldowitz, D. (1996). Genetic and environmental control of variation in retinal ganglion cell number in mice. *J Neurosci*, 16(22):7193 – 7205.

[104] Wu, J., Bell, O. H., Copland, D. A., Young, A., Pooley, J., Maswood, R., Evans, R. S., Khaw, P.-T., Ali, R. R., Dick, A. D., and Chu, C. J. (2020). Gene therapy for Glaucoma by Ciliary Body Aquaporin 1 disruption using CRISPR-Cas9. *Mol Therapy*, 28(3).

[105] Yan, Q., Radeke, M. J. Matheson, C. R. Talvenheimo, J. Welcher, A. A., and Feinstein, S. C. (1997). Immunocytochemical localization of TrkB in the central nervous system of the adult rat. *J Comp Neurol*, 378(1):135 – 157.

[106] Yang, I., Han, S. J., Kaur, G., Crane, C., and Parsa, A. T. (2010). The role of microglia in central nervous system immunity and glioma immunology. *J Clin Neurosci*, 17(1):6 – 10.

[107] Yang, X., Li, C., Herrera, P. L., and Deng, C. X. (2002). Generation of Smad4/Dpc4 conditional knockout mice. *Genesis*, 32(2):80 – 81.

[108] Yiu, G. and He, Z. (2006). Glial inhibition of CNS axon regeneration. *Nat Rev Neurosci*, 7(8):617 – 627.

[109] Zhou, F. Q., Zhou, J., Dedhar, S., Wu, Y. H., and Snider, W. D. (2004). NGF-induced axon growth is mediated by localized inactivation of GSK-3beta and functions of the microtubule plus end binding protein APC. *Neuron*, 42(6):897 – 912.

[110] Zukor, K., Belin, S., Wang, C., Keelan, N., Wang, X., and He, Z. (2013). Short hairpin RNA against PTEN enhances regenerative growth of corticospinal tract axons after spinal cord injury. *J Neurosci*, 33(39):15350 – 15361.